University of Stavanger

Faculty of Science and Technology

MASTER'S THESIS

Study program/Specialization: MSc Petroleum Geosciences Engineering	Spring semester, 2017 Open access
Writer: Øystein Storaas	…… (Writer's signature)
Faculty supervisor: Wiktor Waldemar Weibull, University of Stavanger	
Thesis title: Processing techniques to enhance imaging of ultra-high frequency seismic data acquired with P-Cable technology.	
Credits (ECTS): 30	
Keywords: - P-Cable - Seismic processing - Barents Sea - Vestnesa Ridge - Snøhvit field	Pages: …… + enclosure: …… Stavanger, 15th June, 2017 Date/year

Processing techniques to enhance imaging of ultra-high frequency seismic data acquired with P-Cable technology

By

Øystein Storaas

Master Thesis

Presented to the Faculty of Science and Technology

University of Stavanger

University of Stavanger

June 2017

Acknowledgment

First and foremost, I want to give special thanks to my supervisor, Wiktor Waldemar Weibull for letting me work on such an exciting and challenging thesis. He has given continuous support and guidance throughout the last semester, and I'm grateful for his commitment and the encouragement he has given me by weekly meetings and through constructive feedback. Further, big thanks to Andreas Habel at the Institute of petroleum technology for continuous help with technical issues throughout the semester.

Through the past five years, I have had the pleasure of studying at the University of Stavanger. In my time at UIS, I have been challenged in many ways both practical and theoretical to gain knowledge. I am very grateful for all the people at The Faculty of Science and Technology, and all the professors I had the pleasure of working with at the Institute of Petroleum Technology. They have shown commitment and encouragement by putting a tremendous amount of resources in up to date equipment, computer technology and providing great work environment.

Further, I would like to express my gratitude to my friends and colleagues for heated, and mostly constructive discussions, helping me out, and guidance throughout the past few years. I would also thank my family for always being there and inviting me out for dinner in busy times.

Finally, I want to give special thanks to my girlfriend, Alexandra, who have shown greater encouragement and given me unending love and support throughout my academic career.

Øystein Storaas,

Stavanger, 15th June 2017

Abstract

Processing techniques to enhance imaging of ultra-high frequency seismic data acquired with P-Cable technology

Øystein Storaas

University of Stavanger

Supervisor: Wiktor Waldemar Weibull

P-Cable seismic acquisition system is a rather new technology; developed through the past 20 years. Consequently, the use of P-Cable technology has been limited, although researchers still believe that further improvements can achieve better results with this type of data. Characteristics associated with P-Cable seismic data include broad frequency bandwidth, shot offset, and low fold.

The objectives of this thesis will be to provide a processing workflow with the main goal of enhancing imaging of ultrahigh resolution P-Cable 3D seismic, acquired at Vestnesa Ridge and Snøhvit Field. This has been done by testing various methods, corresponding parameters, and through constructing a synthetic model to confirm whether improvements have been reached or not. This project differs from previous studies dealing with P-Cable 3D seismic data as it will also focus on analyzing the behavior of the synthetic model to compare the different migration techniques. The processing steps will also be considered with emphasis to aspects such as time-efficiency, resolution and geological reasoning. However, the result should ideally present images of higher resolution than previously possible to obtain with published workflows.

This work has revealed how different approaches can lead to completely different results regarding signal-to-noise ratio with similar resolution, precision in presenting accurate imaging of the subsurface, and cost-efficiency. The results have shown that noise filtered Stolt migrated data including pre-migration operation such as brute stack, F-XY deconvolution, missing data interpolation, and automatic gain control obtains good imaging with high spatial resolution and improved signal-to-noise ratio. Stolt migration also presented images with more continuous reflectors, and resolution sufficient to confidently separate features. Compared, prestack time

migration constructed images of less diffraction imprint, but contained more extensive acoustic blanking and noise bursts.

The use of synthetic seismic data has shown to be useful in diagnosing properties of the different migration techniques, and for eliminating uncertainties related to velocity variation. However, results also point to independence between imaging quality of P-Cable seismic data and the input velocity model, as prestack- and reverse- time migration did not show any significant changes after applying it with constant versus actual velocity model.

Table of Content

List of Tables

List of Figures

List of Equations

1. Introduction

In the past 30 years, crucial steps have been taken to improve data integrity and data quality by promoting advances in seismic acquisition, processing, and interpretation techniques. This has led to a reduction in uncertainties associated with exploration, evaluation of plays and prospects, as well as in field development (Games and Self, 2017; Sheriff and Geldart, 1995). Essentially, making the decision analyzer able to create shareholder value by a stream of value-maximizing decisions. This is accomplished by estimating the value of an exploration opportunity by clearly defining alternatives, and consistent comparison among alternatives to increase projects effectiveness. As a result, oil companies are more confident in making a decision of discarding projects that create negative expected net present value and invests in those that have a positive value (Bratvold et al., 2010).

However, Games and Shelf (2017), argue even though the industry in the past few years have established high standards and up-to-date guideline for conducting drilling hazard site surveys, it appears that our ability to unambiguously identify the presence of geohazards such as shallow gas has not improved at the same rate. The existence of shallow gas is one of the more severe complications that influence top-hole drilling condition and consequently could force drilling operations to move to another location (Games and Self, 2017). According to Ostanin et al (2013), recognition of active or paleo- hydrocarbon seepage in sedimentary basins are critical as it provides evidence concerning the present-day risks associated with the petroleum system.

High-resolution P-Cable 3D seismic is a new seismic acquisition technology first used in 2004, which has shown to be cost-efficient and well suitable for sub-surface imaging near scientific boreholes (Planke et al., 2013). This new technology has also been applied to investigate geohazards, such as seabed fluid features that not only includes shallow gas but also slope instabilities that might obstruct successful seabed installations (Ostanin et al., 2013). The main advantage, besides being cost-efficient is that it presents an image of the subsurface with a spatial resolution of a couple of meters. However, as this technology is still rather new, and the use of it has been limited, scientists still believes that there is potential in exploring new ways of dealing with this kind of data. Moreover, as mentioned by Games and Self (2017), a dataset with high resolution would be helpful for better identifying potential geohazards.

1.1 Objectives

The focus of this project is to experiment with different processing methods with the aim of establishing a processing workflow that enhances imaging of ultrahigh resolution P-Cable 3D seismic data. This is done by investigating the nature of acquisition setup, limitations, and by constructing a synthetic model to examine the behavior of the various processing techniques applied. However, the processing steps will also be considered with emphasis to aspects such as time-efficiency, resolution and geological reasoning (Figure 2), and the results will be discussed and compared with emphasis on image quality improvement (signal to noise ratio), cost efficiency in time, and the ability to present accurate imaging of the geological setting. However, the final goal is to enhance imaging, as the product of this work should ideally be images of higher resolution than previously been possible to obtain with published workflows. Finally, the workflow should be cost effective while at the same time allow the extraction of as much geological information from the images as possible.

The data available for this project was acquired by the Artic University of Norway, Tromsø at Vestnesa Ridge, the western continental margin of Svalbard in 2013, and in the southwestern part of the Barents Sea, Snøhvit Field, Hammerfest Basin in 2011. An overview map of the area of interest with the study area marked out is shown in Figure 1.

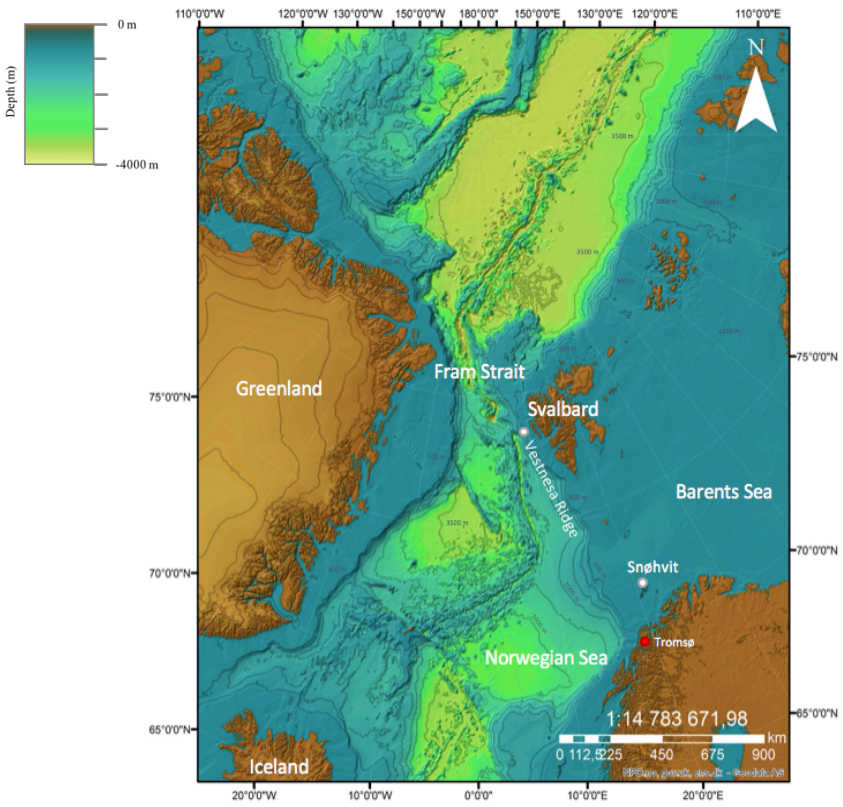

Figure 1 - Overview map of the study area with counter line every 500m. (ArcMap)

Data typically acquired by P-Cable technology contain a broad frequency range (20 – 500 Hz), with relatively small offset (range of 84 – 159 m), and high sampling rate (25 ms) that allows high vertical and horizontal resolution. However, this kind of data also contains certain limitations such as limited investigation (penetration) depth. This is typically around twice the water depth, depending on frequency attenuation within the strata. The limited offset range in the data does not provide sufficient information about the velocity field within the medium of the investigation, although previous studies has assumed that computing with constant velocity gives similar results. These factors (cost-efficiency, geological reasoning, and resolution) is considered as result defining aspects, and the combination of them are very important when quantifying the results. Figure 2 show these three factors and the main processes considered in this research.

However, as P-Cable 3D seismic comes with its certain limitation, the investigation of seismic imaging will focus on processes that take those into account. For instance, there is no available data regarding the velocities through the geological record, which means that normal moveout and different migration technique (Prestack time migration, poststack Stolt and reverse time migration) will be accomplished by certain approximation based on our best guess. In addition, events such as multiples will not be accounted for in this project as P-Cable seismic data usually do not contain such events. The synthetic model will be built on the available data at Vestnesa Ridge to investigate the impact of the different techniques as mentioned above, to compare, for example, the result of applying migration with a predefined constant velocity in relation to doing the same with the actual velocity model.

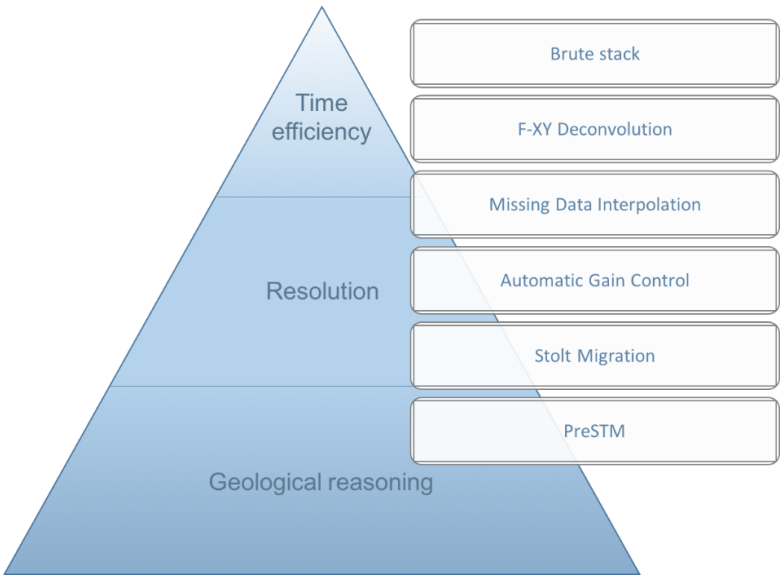

Figure 2 - The three main aspect that will be considered in relation to the processing techniques performed.

1.2 The importance

Since the opening of southwestern Barents Sea for exploration in 1980 several discoveries have proven to contain excellent hydrocarbon potentials. However, this region is still considered as immature as there are only a few producing fields such as Snøhvit and Goliat (Ostanin et al., 2013). The focus has mainly been exploring the hydrocarbon potentials in the western part of Loppa High and Hammerfest Basin, with emphasis on the Triassic and Jurassic stratigraphic units. More specifically, the Stø Formation, which is one of the most prolific reservoir units so far. However, the attention to petroleum exploration in this area is increasing as recent work has resulted in discoveries, such as Johan Castberg (2011), Havis (2012), Wisting (2013), and Alta (2014) that contain proven reserves. Interesting enough, Wisting field is a very shallow discovery with the top reservoir unit (Stø Formation) at 662 m, only 237 m below the subsurface, making it one of the most shallow reservoir with proven potential (Directorate, 2016). If the use of P-Cable technology can reduce uncertainties related to hydrocarbon potential, understanding of pathways and mechanics of fluid flow, safety in a drilling operation and general efficiency in the development of current licenses, it would add significant value in doing so. Further, high-resolution 3D seismic (an example of it in Figure 3) in shallow depth could increase the value as it could possibly make a better correlation with well data, and consequently result in more accurate knowledge of the time-depth relation.

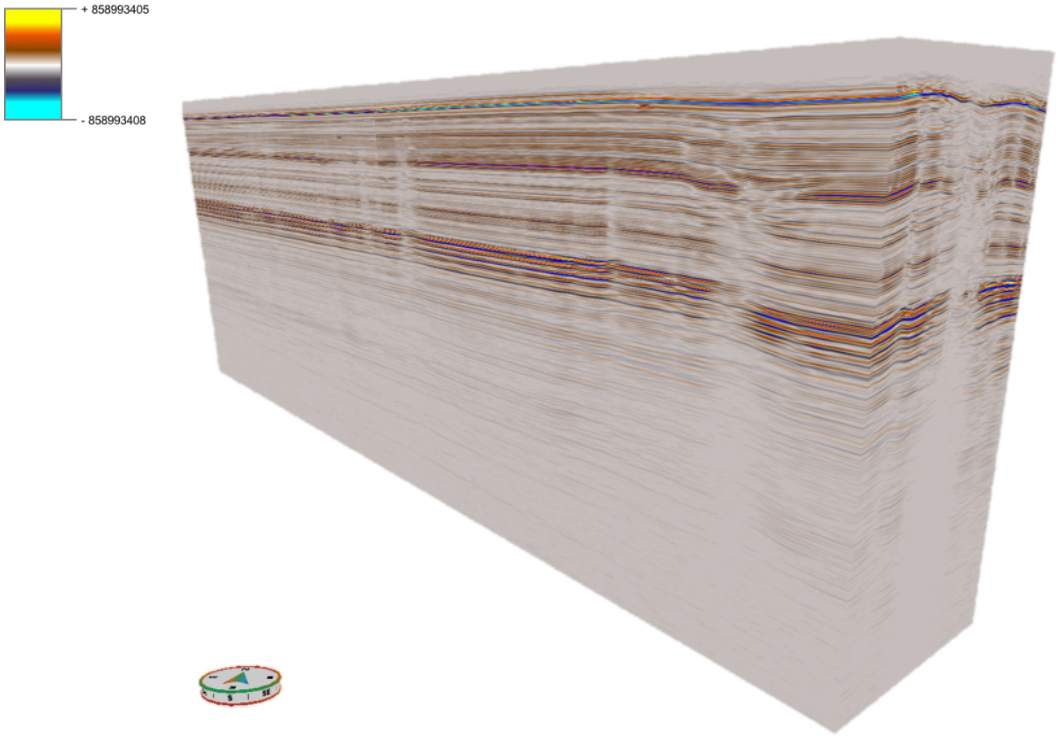

Figure 3 - Example of P-Cable 3D seismic data from Vestnesa Ridge, x: 8.35 km, y: 1.46 km, z: [0,2400] ms.

2. Literature review

This section will address key concepts and some historical events important for the objectives of the project. It will elaborate on theories and thoughts made by scientists in the recent past.

2.1 Previous work

Since 2004, more than 50 high-resolution P-Cable 3D seismic cubes have been acquired at different locations, such as in the Gulf of Mexico, the Barents Sea, the southern part of California, etc. The P-Cable system is a cost-efficient, lightweight, high-resolution 3D seismic acquisition technology that was developed in collaboration between the University of Tromsø, Volcanic Basin Petroleum Research (VBPR, Oslo), and National Oceanographic Centre, Southampton. It was designed for studies of the shallow subsurface with high resolution. Dimensions of the seismic cubes vary in size from 5 to 200 km^2. This new technology was developed with the purpose of studying landslide dynamics, gas hydrates and shallow gas migration, and shallow gas exploration. However, it is also useful for doing scientific research, core-log data integration, as well as for studying possible geohazards regarding drilling safety (Planke et al., 2013). The primary consideration during the development of P-Cable technology was to improve operational reliability, depth control of the streamers, seismic processing data flow, and efficiency associated with the operation. A conceptual illustration of P-Cable acquisition can be seen in Figure 4. A more detailed description of the acquisition system can be seen in Figure 20.

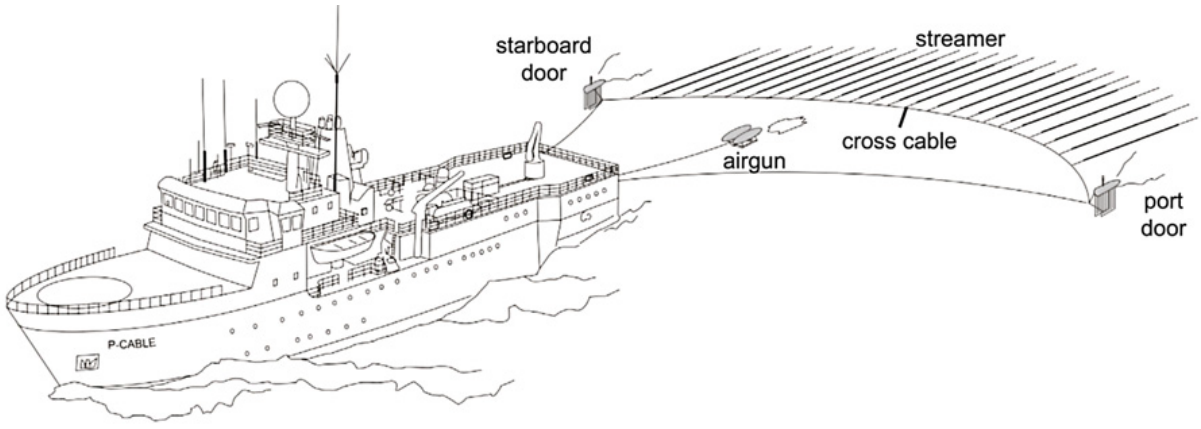

Figure 4 - Schematic drawing of the P-Cable system, modified by (Petersen et al., 2010)

Previous studies working with P-Cable data have done imaging by using different software such as RadExPro 3.96, Shell scripts, Seismic Unix and SeisSpace Promax. Methods applied include navigational correction, binning, static and tidal correction, bandpass filtering (35-350 Hz), amplitude correction, trace editing, normal move out, 3D stack and 3D Stolt migration with a constant velocity of 1500 m/s (Rajan et al., 2011). Figure 5 shows an overview of the processing workflow that was used by one of the P-Cable pioneers, Petersen et al, (2010).

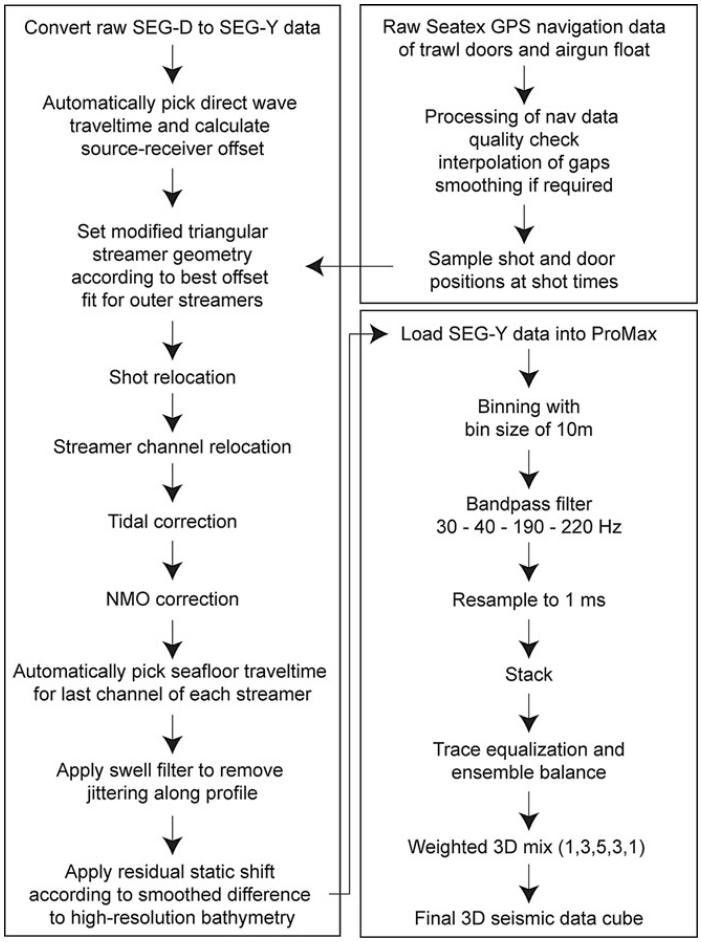

Figure 5 – Processing workflow from previous research, by (Petersen et al., 2010)

2.2 Factors affecting the quality of seismic data

A seismic interpreter would ideally like to have seismic sections that allow an unambiguous geological interpretation of the subsurface and to obtain as many details as possible (maximum resolution). Including idealized sections where bedding contacts are sharply imaged at their correct locations, without noise to confuse or distort the image. To achieve short, and sharp events require a broad wavelength spectrum with high frequency, which helps compress the seismic signature. To display features at their correct locations one need to apply migration, accurate knowledge of the seismic velocities and understanding of the embedded wave. Finally, to preserve the contrasts at the different geological boundaries, amplitude values must be authentically preserved (Sheriff and Geldart, 1995).

In seismic imaging, the image reliability is strongly dependent upon the quality of the seismic records, and also on the employed velocity model. However, the quality of seismic data can vary extremely. For example, excellent reflections at one location, while at another site the data can be useless, even though the same equipment, field techniques, and data processing are applied to acquire it. These two examples are both extreme cases, with most of the data acquired lying in between these two extremes (Sheriff and Geldart, 1995).

In seismology, a signal is a term often used to imply any event on the seismic record from which useful information can be obtained. Everything else is classified as noise as seen in Figure 6, which include incoherent, and coherent events that interfere with the observations and measurement of the signal. Diffraction and primary reflection is highlighted in Figure 6 as they represent the record portion classified as a signal.

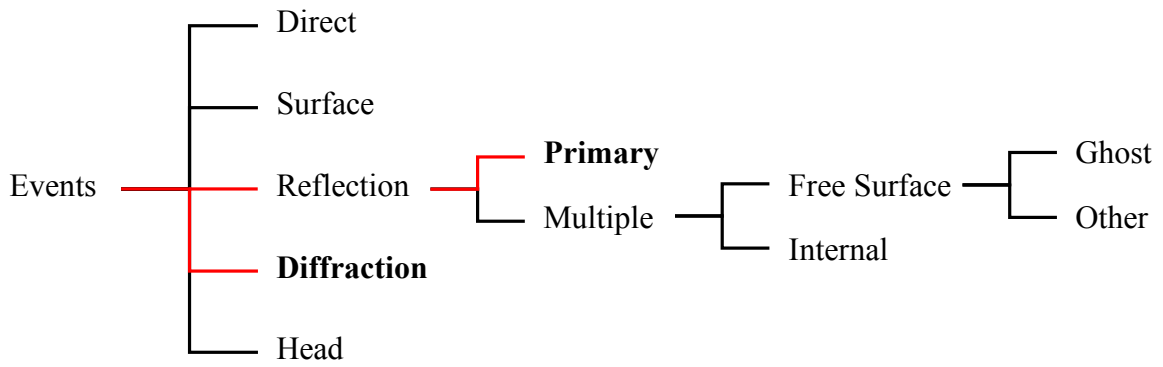

Figure 6 – A classification scheme of the different events that is likely to be seen on the seismic record, with diffraction and primary highlighted as they represent the main (raw) input used in migration for seismic imaging. All the other events are generally considered as noise. Modified after (Christopher, 2003; Liner, 2003).

The signal-to-noise ratio is a ratio of the total amount of signal in a particular portion of the record to the total noise in the same portion. Whenever the signal-to-noise ratio is small, the result is poor records. Although, the definition of low signal-to-noise ratio is to some extent a measure of subjective judgement, in general when the signal-to-noise ratio is less than unity, the quality of the record is usually marginal with a deteriorated effect as the ratio decreases (Sheriff and Geldart, 1995).

As mentioned above, noise in the seismic record may be either coherent or incoherent. The coherent noise can be observed in at least a few traces, while incoherent noise is more randomly distributed, and unrelated on all traces making it difficult to predict the nature of it based on knowledge of nearby traces. Incoherent noise is often called spatially random noise which not only implies unpredictable character but also that it contains certain statistical properties. However, the general behavior of incoherent noise is not actually random as spatial and time randomness may be independent. It may be caused by scattering from near-surface irregularities and inhomogeneities as a result of boulders and scale faulting. Other none repeatable noise may be ambient generated by action in the acquisition environment such as the wind, wave, vehicle, vessel, or cultural interferences. The main difference between coherent and incoherent noise in many cases breaks down to a subject of scale, as the acquisition of data with even smaller receiver spacing would have the effect of outlining incoherent noise as coherent. However, incoherent noise is defined without considering what the effect of closer spacing would reveal, but instead on the records available.

Coherent noise includes events such as surface-waves, multiple reflections, refraction, or reflected refractions as the response of near-surface structures, fault planes, buried channels, in addition to high-velocity stringers, multiples, and so on. It can be subdivided into energy that travels horizontally or energy that spreads vertically. Further, it is also important to separate noise that is repeatable, and noise that is not. The three properties, coherence, travel direction, and repeatability form the basis of most methods of improving record quality.

2.3 Seismic resolution

The ability to image sedimentary features in seismic data is dependent on the seismic resolution. High seismic resolution is a relative term that has evolved with new technology. However, the seismic resolution is referred to as the smallest distance between structures possible to distinguish, whereas the ability to detect is determined by the minimum size of features detected by slight interference in the seismic record. It is highly dependent on signal to noise ratio, frequency spectrum, and bandwidth, as well as interval velocity within the rock units. In Figure 7, one can see the relationship between vertical and lateral resolution, as it changes as a function of depth (Liner, 2003). According to Sheriff and Geldart, (1995) resolution can be enhanced by expanding the frequency passband. The factors limiting resolution are: 1) limitations in the source, 2) processing within the earth that discriminate against high frequencies, 3) conditions at or near the surface, including array effects, and occasionally, 4) recording instruments. As depth increases, high frequencies tend to be attenuated by absorption, with the wavelength approximately linearly increasing with distance. At the same time peg-leg multiples that cause a reduction in the spectral resolution (Sheriff and Geldart, 1995).

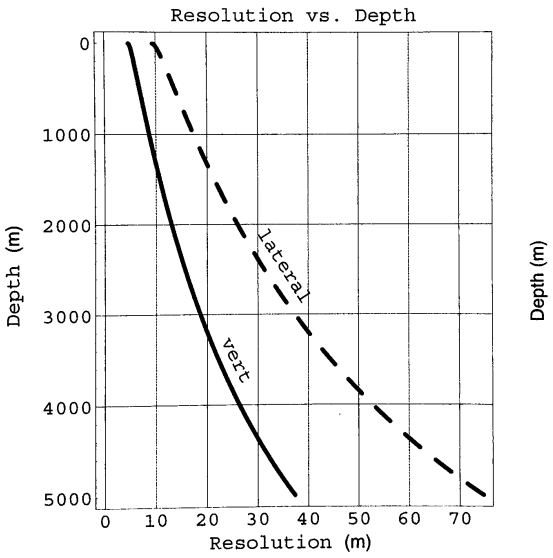

Figure 7 - Textbook example of the decrease in vertical, and lateral resolution as a function of depth with linear v(z) at Gulf of Mexico (Liner, 2003).

2.3.1 Horizontal resolution

The spatial resolution is highly dependent on the factors such as trace spacing, migration, and the Fresnel zone. It is defined as the minimum lateral distance between two reflectors necessary to distinguish and identify the different structures. In seismology, a fundamental concept that is important to keep in mind is that a reflection does not actually arise from a single point on a reflector, but it arises from the Fresnel zone, which is the lateral resolution limit of seismic data. This means that two closely spaced features in the subsurface enclosed within the Fresnel zone, cannot be individually distinguished. The Fresnel zone is defined mathematically by Equation 1 and can be seen in 2- and 3-dimensional space in Figure 8.

Equation 1 – Fresnel zone

$$F = \sqrt{2\lambda z + \lambda^2/(2v)^2}$$

F : Fresnel diameter (m), v : average velocity (m/s), λ : wavelength (m), z : depth of reflector

With depth, the horizontal resolution is decreasing consequently as high frequencies are being attenuated while wavelength and internal velocity are increasing. However, migration of seismic data enhances the spatial resolution as the Fresnel zone collapses by an increase in inline sampling density and increase in crossline spacing (3D migration). The result of this is called focusing effect, essentially making the horizontal resolution in 3D migrated data correspond to the bin size given that the bin size is larger than $\lambda/4$ (Rafaelsen, 2006; Sheriff and Geldart, 1995).

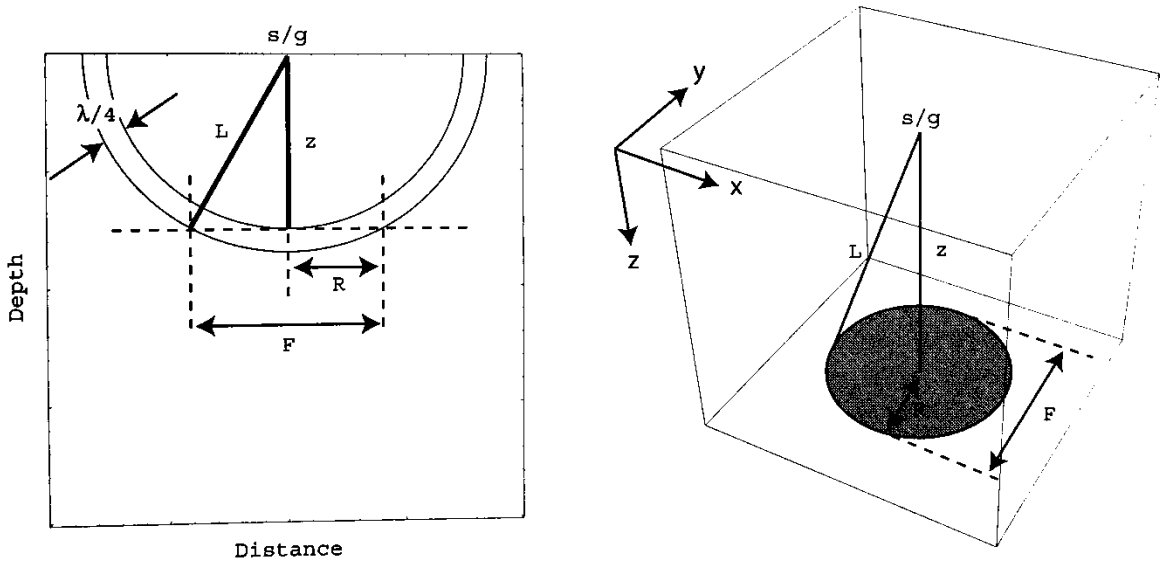

Figure 8 - Fresnel zone geometry, 2D (left) and 3D (right) for zero dip, and offset data (Liner, 2003).

Figure 9 below illustrate the concept of how bin size with appropriate fold will affect the horizontal resolution depending on how it is set. It shows an overview satellite image of the Kjølv Egelands hus at the University of Stavanger, and within the narrowed down, red square display the parking space. A, B, C and D are all the same section, but show relative resolution depending on bin size. Section A represent bin size of 12.5 x 12.5 m, B equal to 6.25 x 6.25 m, C is gridded by 3.125 x 3.125 m, and D illustrate the effect of using conventional bin size of 25 x 25 m.

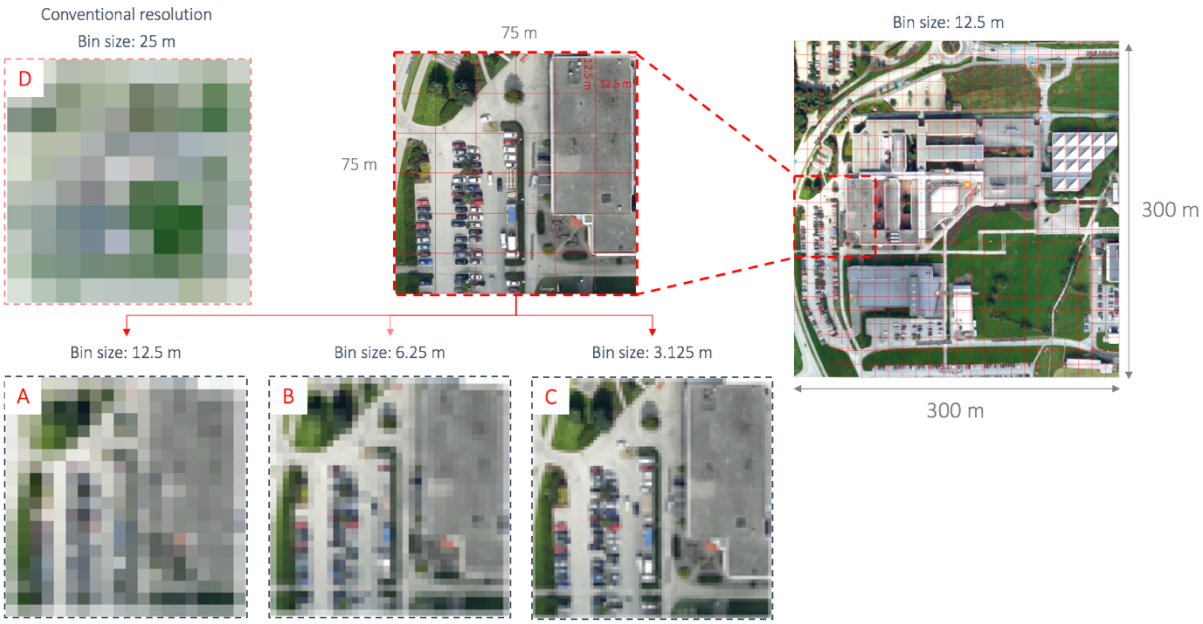

Figure 9 – Satellite image of Kjølv Egelands hus at the University of Stavanger with grid size of ~ 12.5 x 12.5 meters. A, B, and C represents relative resolution associated with bin size of ~~12.5 m, ~~6.25 m, and ~3.125 m and can be compared to conventional resolution as seen in D.

2.3.2 Vertical resolution

As the sedimentary profiles usually includes horizontal beds, the vertical resolution is referred to as the least spacing between two layers, creating adequate acoustic impedance contrast to generate two distinguishable seismic reflections. In situations where the spacing is less than the vertical resolution, overlapping of seismic traces is generated, which consequently either result in enhancing or canceling interference. This means that the net response of very thin beds is a single peak, whereas for beds with a thickness of more than λ/4 (tuning thickness) separates into two peaks as seen in Figure 10. Similarly, as with horizontal resolution, the vertical resolution is lost as a function of depth, due to high-frequency attenuation in addition to the increasing internal velocity (Liner, 2003).

Equation 2 – Vertical resolution

$$r_v = \frac{\lambda}{4} = \frac{v}{4f}$$

r_v : vertical resolution, λ : wavelength (m), v : interval velocity (m/s), f : dominant frequency

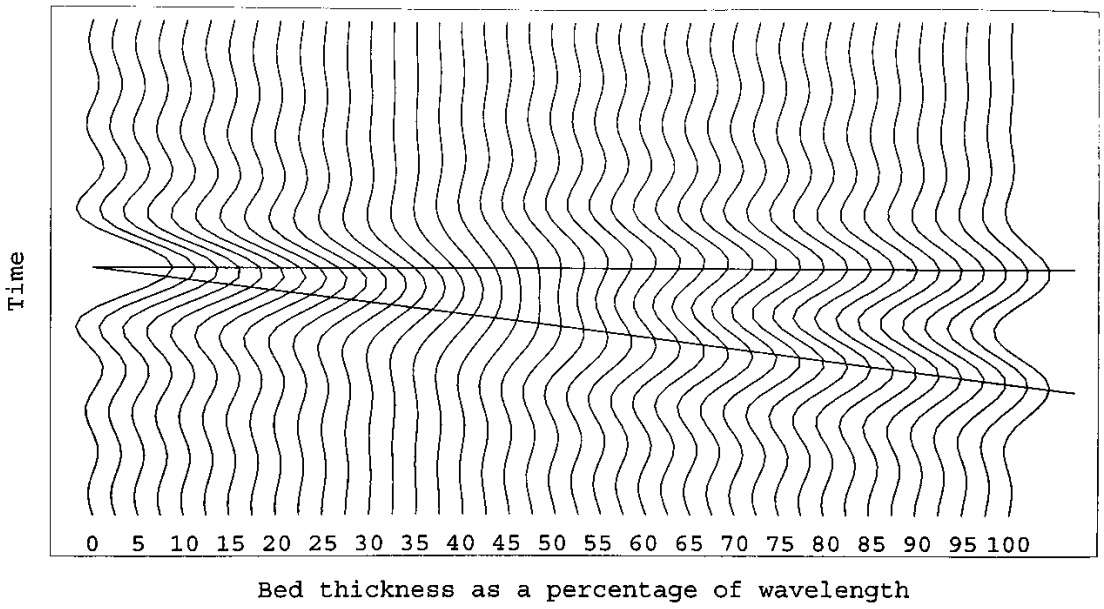

Figure 10 - Vertical resolution wedge model showing resolution limit occur at one quarter wavelength thickness. (Liner, 2003).

2.4 Towed receiver systems

In a marine acquisition of seismic data, the most common method is towed streamer systems. This kind of setup includes streamers of various length containing acoustic receivers that are sweeping the elastic waves propagating in all directions from the subsurface as it is towed in shallow depth below the sea surface, illustrated in Figure 11 (Robein, 2010).

Airguns are typically used in offshore acquisition. This source produces waves by volume injection. Consequently, as water is an acoustic medium, and airguns are a pressure source, the elastic waves generated purely pressure waves (P-wave). Furthermore, as the reflected energy travels back up to the sea surface, the receivers or hydrophones record the signature of the seismic signal (Parkes and Hatton, 2013).

This technique has shown a good result for several applications within the industry, for example, in exploration seismology. However, compared to land acquisition, external factors such as wave, wind, and tide might affect, consequently generating noise, and other unwanted positioning issues such as feathering. Feathering is known as an angle deviation of the streamers towing direction that can cause misalignments of several hundred meters depending on the angle (Liner, 2003).

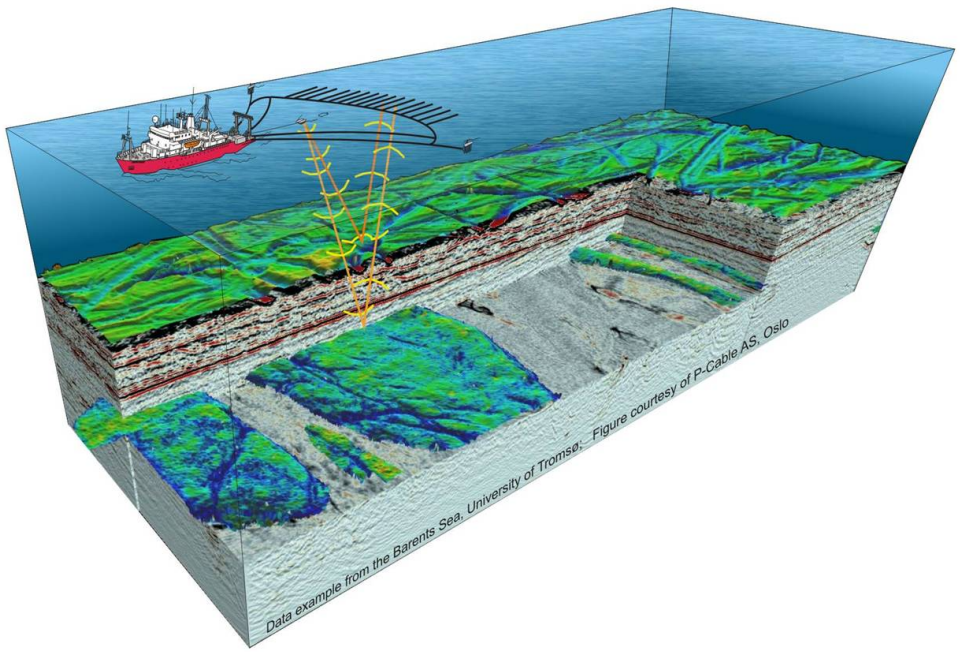

Figure 11 - A conventional drawing of P-Cable 3D seismic acquisition system, marine shooting with up to 24 streamers from (P-Cable, 2017).

2.5 2D and 3D surveying

Given the number of streamers, and the distance between them in the setup, 2D or 3D seismic can be acquired (Figure 12). The main difference between 2D and 3D seismic data lies in that 2D essentially is limited to a vertical cross-section, unlike 3D that allow the data to be displayed in time-slices (Bahorich and Farmer, 1995). 2D grid is considered dense with line spacing less than 400m. 3D seismic data is defined as a volume of data, with grid size referred to (nt,nx,ny) containing millions, up to billions of individual samples. Some advantages of 3D seismic data are that a 3D volume dataset honors true structural dip versus apparent and, include more and better stratigraphic information in time and horizontal slices. In addition, 3D data allow the interpreter to have an optimum lateral resolution, and mapping of faults in map view. Since 1970s as computer technology started to be integrated in the industry, 3D acquisition, processing, and interpretation advanced dramatically (Liner, 2003).

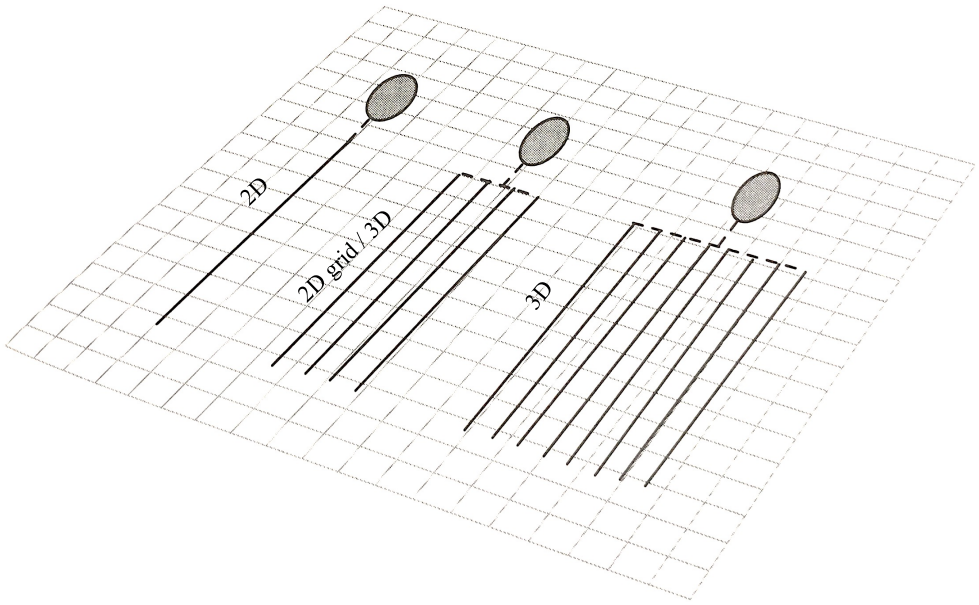

Figure 12 - Schematic of selected multiple cable marine acquisition configuration. The gray oval represents the towing ship, which is also the source ship, modified by (Liner, 2003).

2.6 Conventional versus P-Cable 3D seismic

Research conducted in recent time has shown that 3D seismic data is an important tool for studying geofluids. However, 3D seismic data are often limited to areas with prolific hydrocarbon systems, acquired with the aim of exploration. Conventional 3D seismic systems are not intended to image shallow subsurface structures, but rather targets at great depth typically including mapping of hydrocarbon reservoirs. In the field of scientific marine geology and geophysics, the available data is mainly conventional 3D seismic data that is outside areas of interest, such as the Artic region. The data itself generally leaves scientists with many questions unresolved as the resolution is limited. Typically, conventional 3D seismic technology comprises of very long streamers that are commonly varies from several to 10 km in length, with a frequency spectrum of 5-100 Hz. This relies on a relatively large source that ultimately comes with a high operation cost. In comparison to the P-Cable system, the contrast is quite evident, as P-Cable technology is a light-weight system that is fast to deploy from relatively small vessels. It only requires a small source that is made for imaging of shallow depth with high resolution as the frequency bandwidth range from 20-350 Hz (Petersen et al., 2010). A comparison of conventional (left) and P-Cable (right) 3D seismic can be seen in Figure 13, as the image on the right-side images features with higher spatial resolution than seen in the left image.

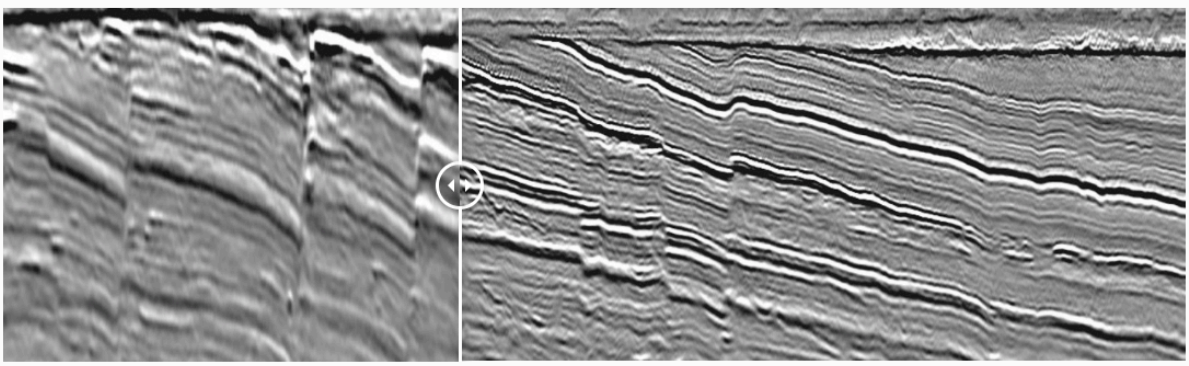

Figure 13 - Comparison of conventional (left) and P-Cable (right) 3D seismic data processed in the same manner. The image cover faulted Jurassic sandstone in the Barents Sea, by (VBPR AS, 2017)

2.7 Synthetic seismic modeling

Synthetic models have shown to be of high value in the sense of quality check a wide range of application within geophysics. It was first applied to simulate normal incident reflectivity of the horizontal stratified medium, while in recent years it has been used to obtain the response of increasingly complex subsurface structures and other stratigraphic features to construct a geological model (Kelly et al., 1976). In general, the purpose of using a synthetic model is to compare it with the actual seismic data, with the aim of identifying the behavior of primary reflection, multiples and other events with known predefined physical properties. It can also be used to study interference, but the strength of modeling is to gain knowledge of how defined boundaries and parameters affect the behavior of different wavefronts. A frequently used method utilized to compute numerical simulation of seismic wave propagation finite difference modeling. This method is based on the approximation of an exact derivative $\partial_x f(x_i)$ were x_i represent a specific grid position (nodes with given property), in relation to the function f computed by a finite number of neighboring grid points. Elastic parameters are predefined, fixed for each network node (x, y, z) and the finite difference simulation is done step-by-step at each space and time node. The wave equation used to construct seismic data can be seen below:

Equation 3 – The wave equation for P-waves in terms of the potential function:

$$\nabla^2\phi = \left(\frac{1}{\alpha^2}\right)\partial^2\phi/\partial t^2$$

∇: generic function, ϕ: scalar coefficient, α: P-wave velocity, t:traction vector.

There are many applications of this algorithm, but the breakthrough of finite difference modeling started off with staggered grid approach, modeling of the free surface, incorporation of anisotropy, and later discontinuities in the medium (Liner, 2003). Which today makes this approachable to compute full waveform data, simulation of wave propagation through a random medium, and studies of seismic ground motion in densely populated areas (Fichtner, 2010). In this project, synthetic data created with finite difference modeling is used to investigate the impact of the various processing and migration methods on the seismic data. The advantage of using synthetic data for this purpose is that the data is originally noise free and subsurface velocities model is fully known.

3. Geological setting and Background

3.1 Geological background of the study area

Two P-Cable 3D seismic surveys acquired at The Vestnesa Ridge and Snøhvit, Hammerfest Basin, are the two main research areas for this study (Figure 14). The available 3D seismic for this thesis at Vestnesa is covering mainly the eastern segments of the ridge, and the Snøhvit cube is located south of the main Snøhvit field. These two study areas have quite different geology. This subsurface condition needs to be taken in into account when processing. Further description of the two different areas can be seen in the following subchapter.

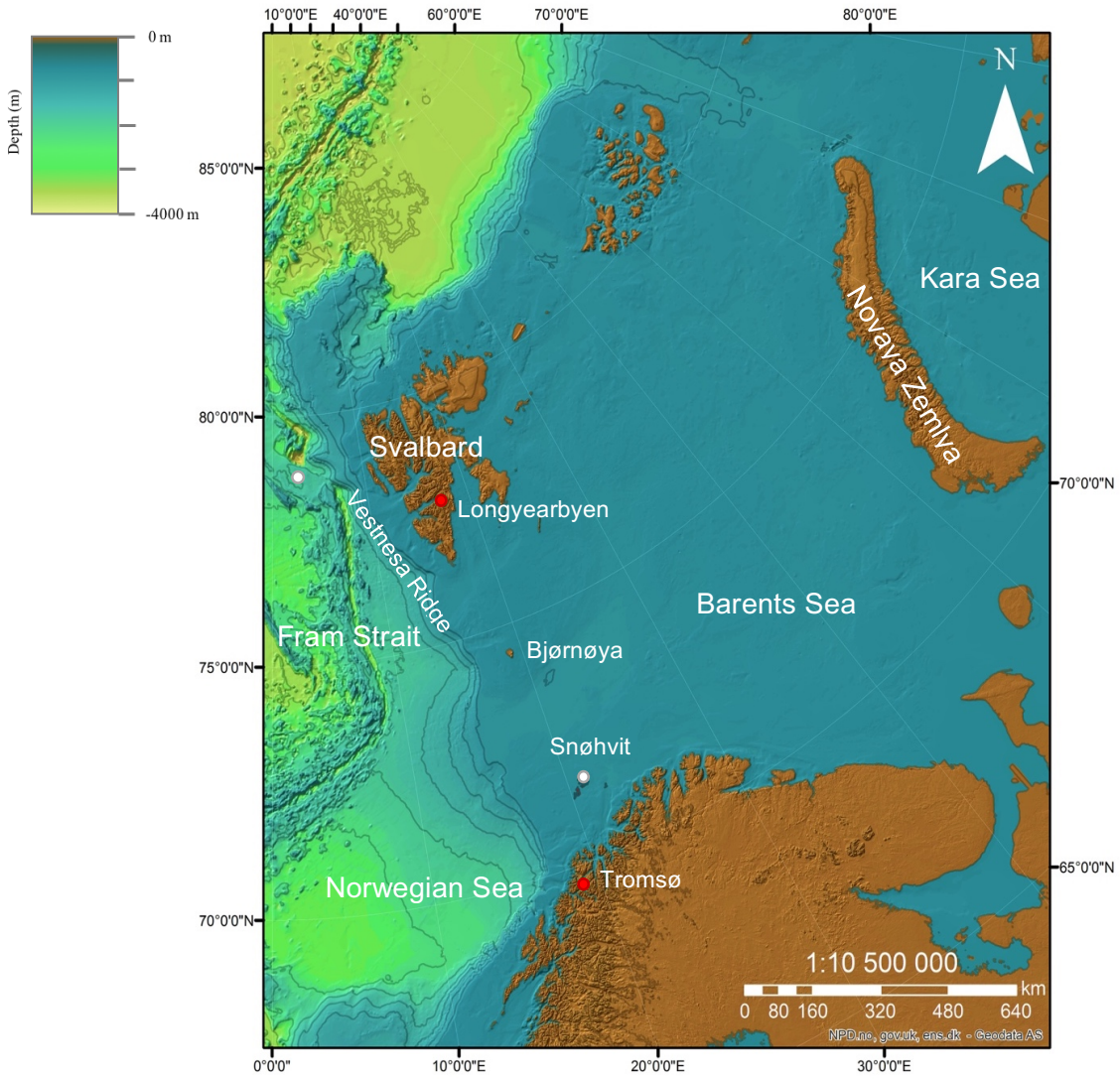

Figure 14 - Overview map of the Barents Sea and the two study areas; Vestnesa Ridge and Snøhvit (ArcMap)

3.1.1 Vestnesa Ridge; Geological Evolution

Vestnesa Ridge is situated in the Fram Strait passage at the NW part of the Svalbard continental margin, 78° – 79° N and 06° - 07° E, in proximity to the North Atlantic Ridge. More specifically, it is an SE-NW to E-W bending elongated sediment drift that lies north of the Molley transform fault and east of Molly Ridge, which is part of the North Atlantic Ridge systems, as seen in Figure 15 (Bünz et al., 2012; Howe et al., 2008).

According to Eiken and Hinz (1993), the geomorphological grows of the sediment drift is a result of bottom-current controlled sediment dynamics. The ridge lies at a water depth between 1200 and 1300m and comprises of approximately 2km thick contourite, turbidite, and hemipelagic deposits. By analyzing gravity and multicores from the crest, and ^{14}C dating the turbidite and contourite there is an approximate age of Early Holocene to Weichselian (8287 – 26900 years BP). In addition, it is suggested that there are several hundred meters of sediments that are lying in a relatively close distance (40 km) to the 20 Ma younger W-Svalbard margin, which is an area influenced by the northward directed W-Spitsbergen current affecting the morphology of Vestnesa Ridge (Eiken and Hinz, 1993).

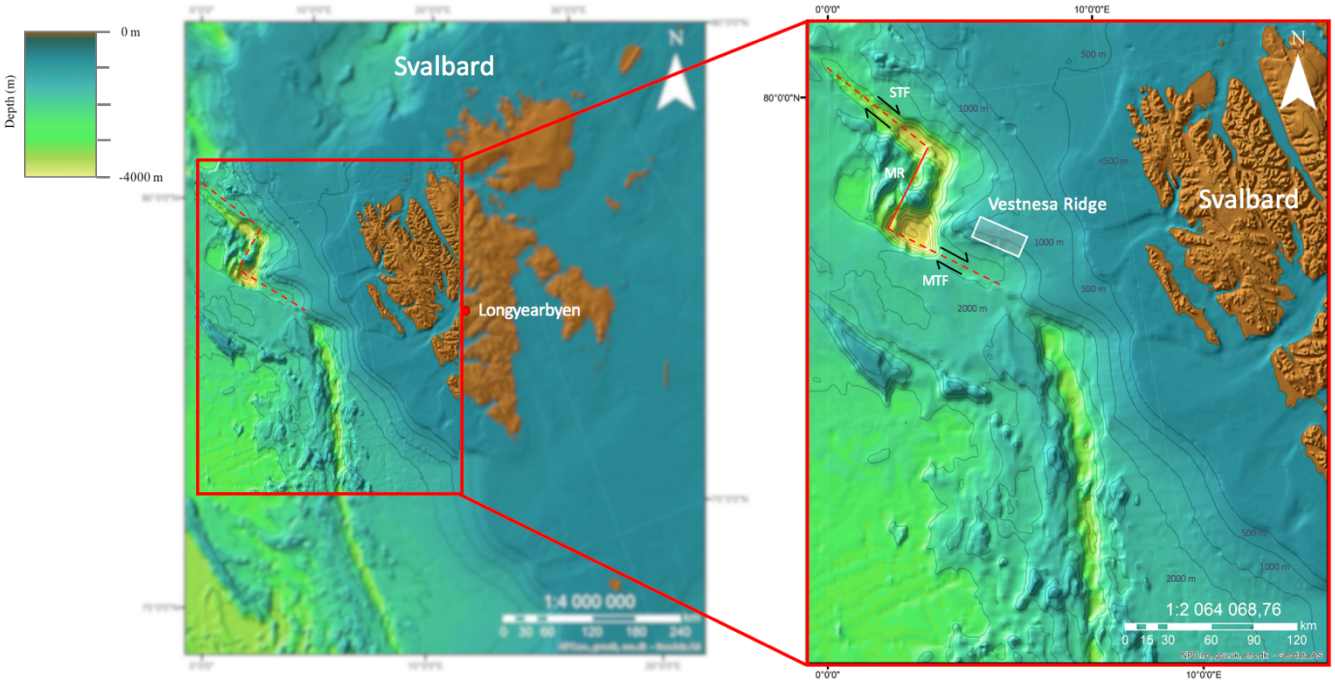

Figure 15 - Overview map of: Vestnesa Ridge at the western margin of Svalbard. MTS: Molloy Transfrom Fault, MR: Molloy Ridge, STF: Spitsbergen Transfrom Fault, after (ArcGIS, 2017; Plaza-Faverola et al., 2015).

This area is known to be one of the northernmost well-studied gas hydrate provinces, fluid flow systems with continuous fluid and gas migration (venting) that was first discovered

in 2008, and are creating pockmarks with varying size up to 700 m in diameter. The pockmarks are internally connected vertical features of fluid flows, which are called chimneys (Bünz et al., 2012). An example of this kind of feature from Vøring Basin can be seen in Figure 16. The driving force is thought to be gas overpressure beneath the gas hydrate stability zone, with a possible decrease in thickness of the gas hydrate stability zone as the bottom water temperature changed. It is also believed that the thickness change of gas hydrate stability zone caused a shift in the lateral position that ultimately led to higher amount of gas seepage on the western margin of Svalbard (Westbrook et al., 2009). There is a general trend as the pockmarks are larger in size, and they are more active at the at the eastern segment compared to western edge (Bünz et al., 2012). On seismic profiles gas hydrates are evident, and are shown as high amplitude bottom-simulating reflector (BSR), covering a vast area of the western side of Svalbard passive margin, including Vestnesa Ridge. These bottom-simulating reflectors are generally following the seafloor topography, with a phase reversed expression because of the negative acoustic impedance as it is representing the boundary between gas hydrates and free gas. (Hustoft et al., 2009). However, gas chimneys are characterized as low amplitude, low coherency, with changing dip and pull-up and pull-down effect on the seismic record (Berndt et al., 2003).

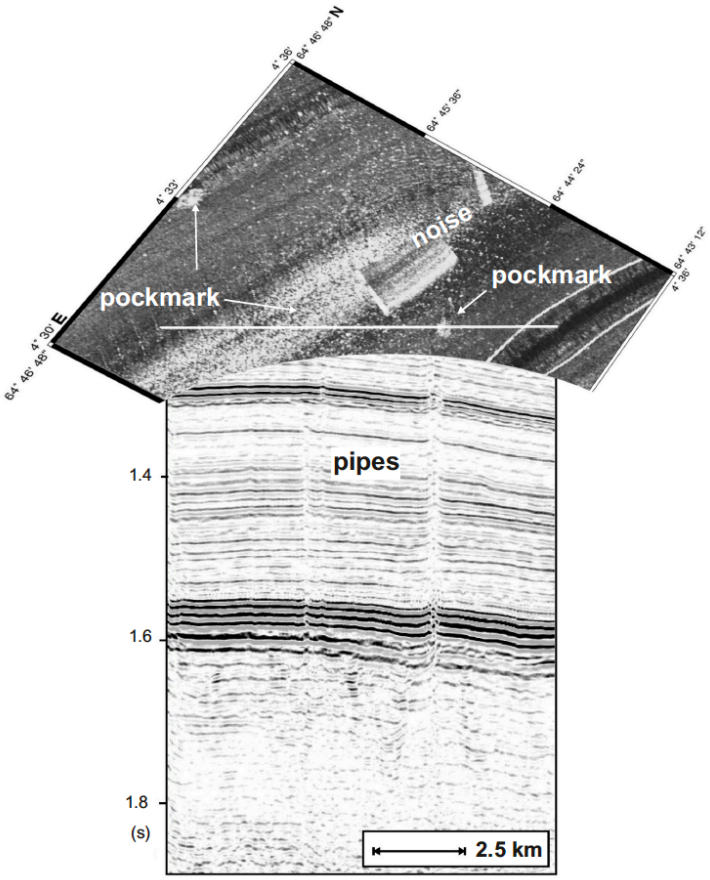

Figure 16 – Sonar side scan floor backscattering image with marked seismic section from the Vøring Basin showing pipes, terminate in circular pockmarks as a pull-up effect after (Berndt et al., 2003).

Even though Vestnesa Ridge is part of west Svalbard passive margin, it is situated in a highly complex and tectonically active area in between the dextral-slip Spitsbergen (Ritzmann et al., 2004) and subparallel Molley (Engen et al., 2008) transform faults. As a result, it is believed that the spreading of the Atlantic ridge plays a major controlling factor of the gas seepage (Plaza-Faverola et al., 2015). Previous research by Engen et a, 2008 have shown by using Bouger gravity map that the north facing edge of Vestnesa Ridge lies approximately 20 km from the continental-oceanic transition (COT). According to Plaza-Faverola et al, 2015, earthquake focal mechanisms have shown dextral strike-slip deformation to the north and the south, and extension to the west and the southeast. The location of Vestnesa Ridge is thought to be within the paleo-Spitsbergen shear zone, that is possibly linked to the orientation and distribution of the extensional faults related to rifting along the northern Knipovich Ridge (Crane et al., 1991).

The geology at Vestnesa Ridge can be subdivided into three different stratigraphic sequences, starting off with the oldest YP1 with Miocene age, which consists of synrift deposits, lying on a less than 20 Ma old oceanic crust. The second unit is the YP2 that is a product of migrating contour currents, and sediment flux with a depocenter striking similar to the western margin of Svalbard. Lastly the third sequence, YP3 which is also a result of contour currents, but with two main depocenter separated by a thin sedimentary sequence. Based on drilling operations in the area, the boundary between YP2 and YP3 has been dated to be ~2.7 Ma (Eiken and Hinz, 1993).

3.1.2 Snøhvit, Hammerfest Basin: Geological evolution

The Snøhvit field is located in the Hammerfest Basin, on the SW margin of Barents Sea (Figure 17). This is one of many basins in the epicontinental Barents Sea separated by structural highs (Faleide et al., 2008).

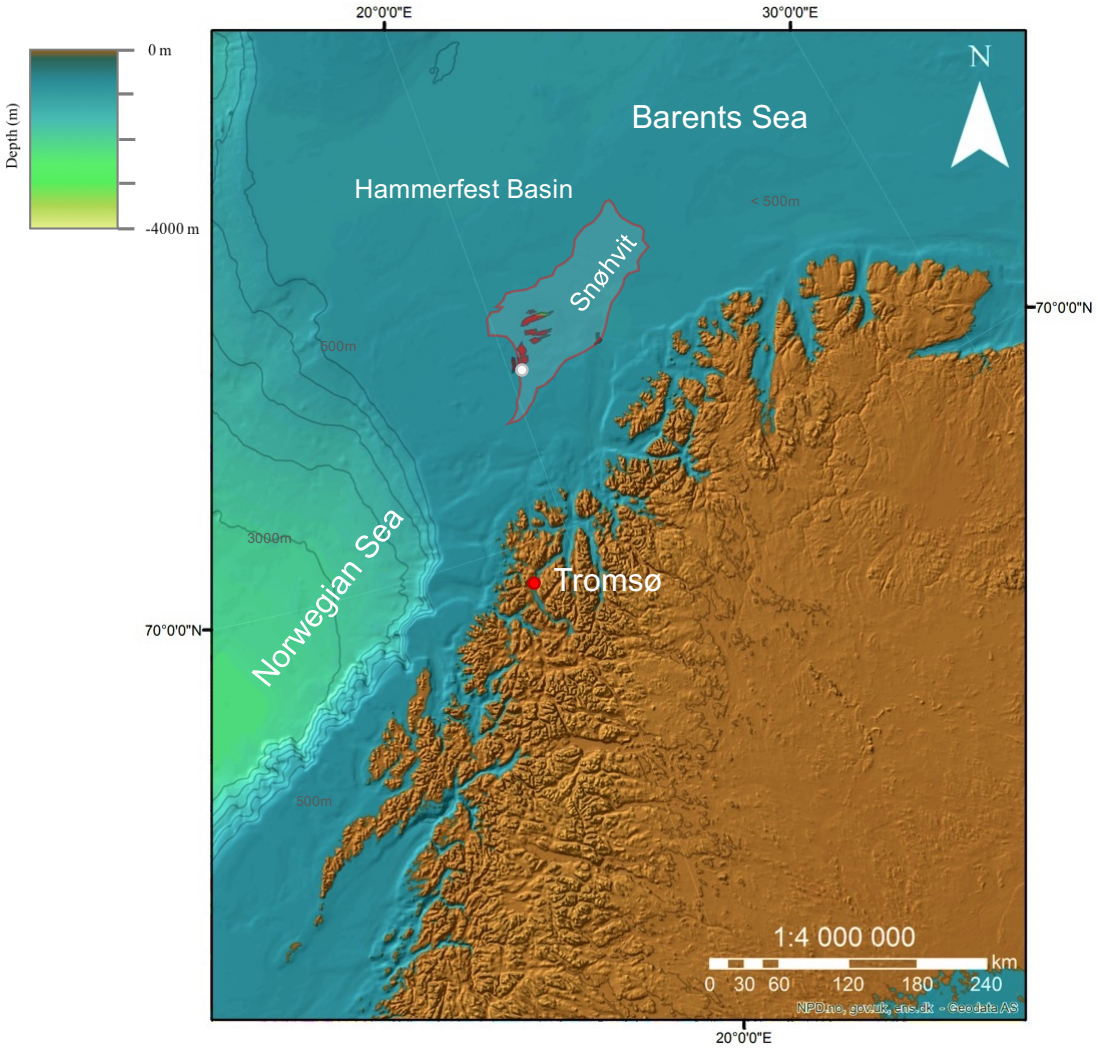

Figure 17 - Overview map of the western margin of Barents Sea: including the study area; Hammerfest Basin - Snøhvit gas field. (ArcMap)

The opening of Norwegian-Greenland Sea had a significant impact on the tectonic and depositional evolution throughout the Cenozoic development. In details, the Cenozoic development includes discontinuous uplift causing three exhumation events that took place in Paleocene (~ 60-55 Ma), then in Late Eocene (~ 36-35 Ma), and lastly in Late Miocene (~ 7-5 Ma) (Green and Duddy, 2010). Sedimentary structures such as prograding clinoforms are widespread in the Hammerfest Basin and were deposited due to the uplift of local highs that changed the tectonic and sedimentation regime (Faleide et al., 2008). In the Miocene, the Hammerfest basin experienced uplift that consequently eroded in the range of 800-1000m of

sediments, completely removing strata from Late Eocene to Pliocene, leaving the Neogene stratigraphic column incomplete. (Cavanagh et al., 2006; Green and Duddy, 2010). Later, in Pliocene – Pleistocene the area was influenced by ice sheets that covered significant parts of the Northern Hemisphere, that during last 2.7 Ma advanced and readvanced caused erosion of approximately 1 km of sediments. Some scientists speculate that in half of erosion took place around 0.7 Ma as erosion beneath fast moving ice streams with depocenter at the western margin, such as the Bear Island Through mouth fan (Faleide et al., 2008; Ostanin et al., 2013).

The present-day morphology of the Barents Sea is characterized by generally shallow seabed, with water depth less than 500m. Paleo ice streams that incised during the glaciation created throughs that represent the deepest part of the shelf. Plough marks and glacial lineation are commonly observed at seafloor due to movement of icebergs (Andreassen et al., 2008; Mohammedyasin et al., 2016). The lithology at Snøhvit area shows significant influence of glacial sediment setting, with massive, hard package of glacial deposits that appears as strong reflectors in the seismic records (Elverhøi et al., 1985). As the main sequences and boundaries of interest for this project can be seen in Figure 18, within the interval of 0 to 800 ms as the present sea-floor (Top Nordland), the Upper Regional Unconformity (URU), and Torsk Formation.

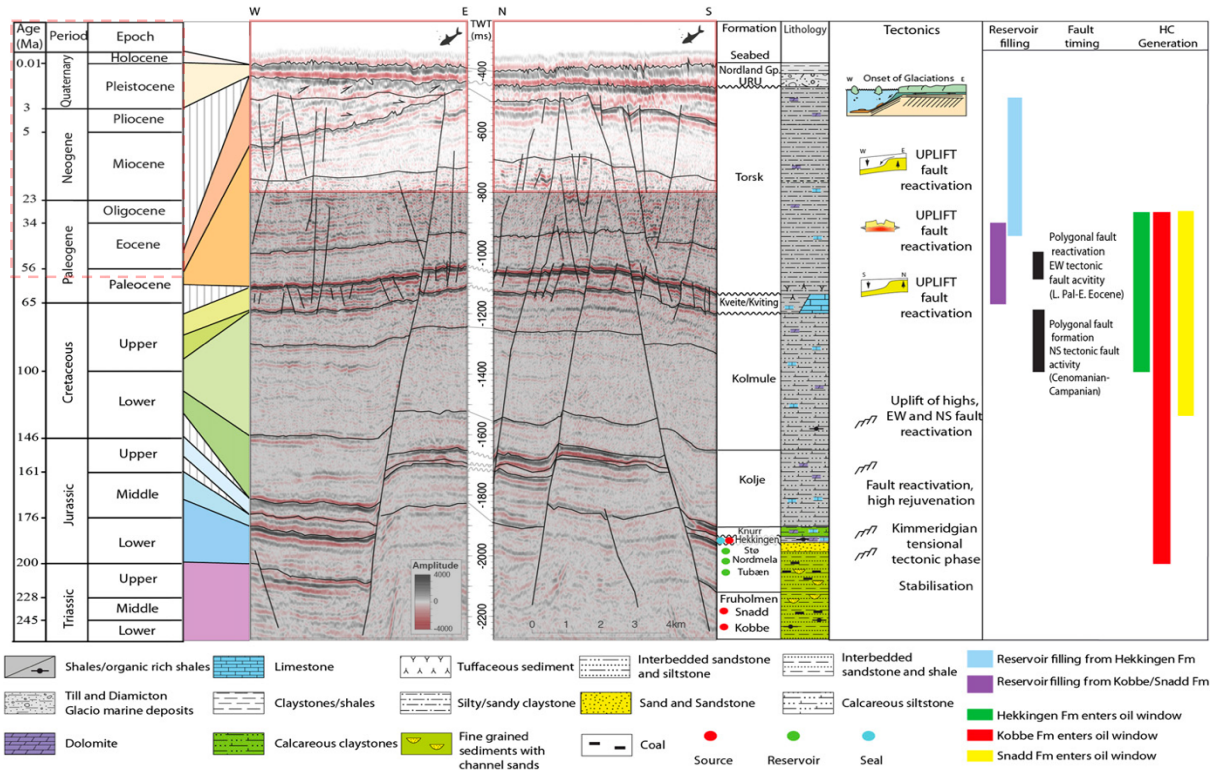

Figure 18 - Tectono-stratigraphic chart included with corresponding formations, lithology, petroleum system elements and the timing at the Hammerfest Basin. Area of interest marked with red squares, modified from (Ostanin et al., 2012; Ostanin et al., 2013; Rodrigues et al., 2011).

The quaternary glaciogenic sediments are separated from the dipping, preglacial bedrock below by the angular Upper Regional Unconformity, erosion surface associated with uplift. In general, the quaternary deposits compose mainly of muddy diamictites with varying thickness of 0 - 300m. It is also the oldest glaciogenic deposits on the continental shelf that marks the transition between glacial erosion to the aggradational regime (Faleide et al., 2008; Ostanin et al., 2013).

There has been a significant amount of attention to this region as it is an active area for hydrocarbon exploration, with complex geological evolution for scientists to study (Ostanin et al., 2013). Previous studies have reported hydrocarbon leakage from fields such as: Snøhvit, Albatross, and Askeladd, all situated in the Hammerfest Basin. Evidence of this seen as acoustic wipe-out zones, the result of large gas anomalies (Ostanin et al., 2012). In addition, paleo oil-water contact has been encountered which points to a substantial leakage of hydrocarbons that once represented a greater volume of resources than today (Linjordet and Olsen, 1992). According to Linjordet and Olsen 1992, major tectonic faults have acted as linkage, making the hydrocarbon able to migrate throughout reservoir structures. Pockmarks have also been found in this region as acoustic flares, but according to Judd and Hovland 2007, this indicates even later fluid leakage. In Figure 19 one can see a P-Cable 3D and 2D seismic data displaying chimney structures with highlighted BSR interpreted in blue (Vadakkepuliyambatta et al., 2015).

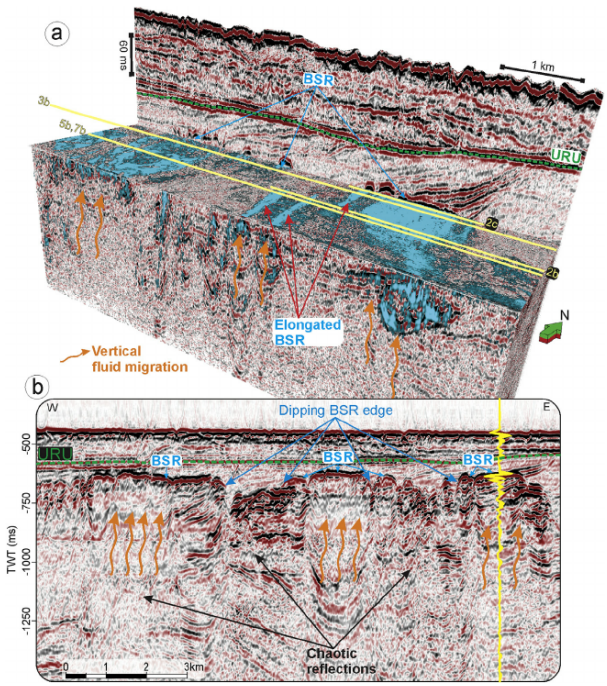

Figure 19 – a) P-Cable 3D seismic cube from Snøhvit with high amplitudes (seen in blue) that highlight the BSR, b) 2D section also displaying the BSR as dipping edges, after (Vadakkepuliyambatta et al., 2015)

4. Data and Methodology

To analyze and process the data, powerful processing tools such as SeisSpace® ProMAX 2D/3D software by Halliburton (Landmark Solution), and open-source Madagascar software has been used. Furthermore, Petrel 2016 interpretation and visualization platform by Schlumberger was utilized to compare the results step by step. Computer hardware available for this thesis was an HP workstation with 12 core processor and 32 Gb of ram, in addition to super-computers managed by Sigma2 Uninett AS, called Vilje and Stallo. The following chapter will elaborate on a detailed description of each of the processing steps, and their flows, which can also be seen in Appendix B.

4.1 P-Cable technology

P-Cable acquisition system in contrast to conventional 3D acquisition geometry consists of two trawl doors (port doors) each on both sides of a cross-cable perpendicular to the acquisition vessels towing direction. Attached to the cross-cable parallel to the towing direction is up to 24 multi-channel streamers with a typical length of 25 m. In figure 20, a conceptual drawing of acquisition setup is illustrated. Streamer spacing of 6.25 m to 12.5 m contribute to obtain high spatial resolution in the shallow subsea, with a frequency range of 20 – 500 Hz. The coverage of one single shot array with single channel streamers (10m apart) is approximately 240m wide, subdivided into 24 individual seismic lines (Petersen et al., 2010).

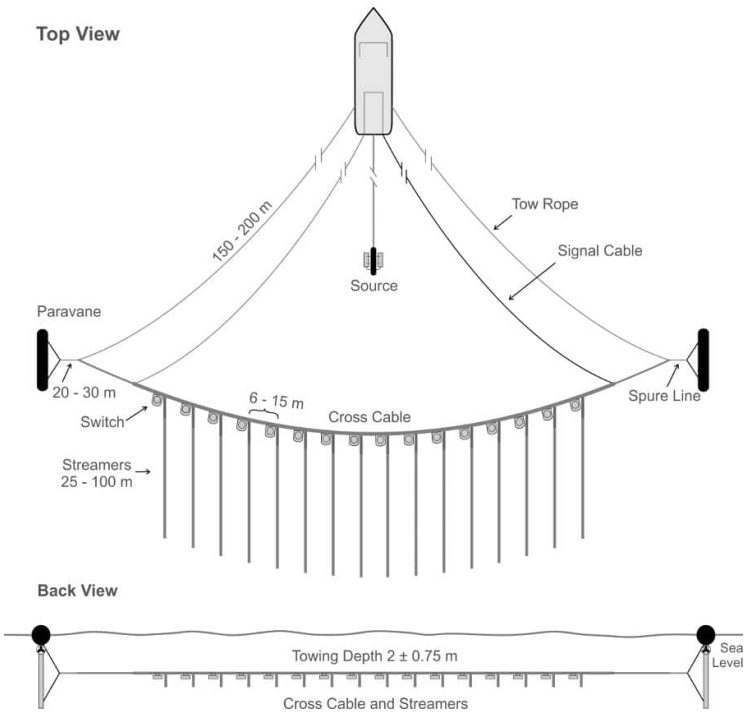

Figure 20 – Conceptual drawing of the P-Cable spread setup from (P-Cable, 2017)

As the P-Cable system is intended for near surface 3D acquisition, it is operated with a relatively small source that generates acoustic waves imaging the sub-seabed, down to a depth of approximately twice the water depth. To ensure high navigational accuracy, GPS antennas on both side of the trawl doors, in addition to the gun float, are added to limit uncertainties of the position down to 1m. In Figure 21, a top view of the streamer and shot position after relocation and CMP coverage are illustrated. This system can obtain a spatial resolution of at least one order of magnitude higher than conventional 3D seismic, with temporal resolution improved 3-5 times. This leads to more accurate imaging and more accurate target identification when compared to conventional seismic data. However, the downside with this type of acquisition system is that it will also record noise with very high frequencies, which is a challenge to remove. Typical characteristics associated with P-Cable systems are that the cube-size vary from 5 – 300 km2, operate at a water depth of 200m and greater, the vertical resolution of 1.5 m (depending on the interval velocities and attenuation), and a sampling interval of 25 ms (Petersen et al., 2010).

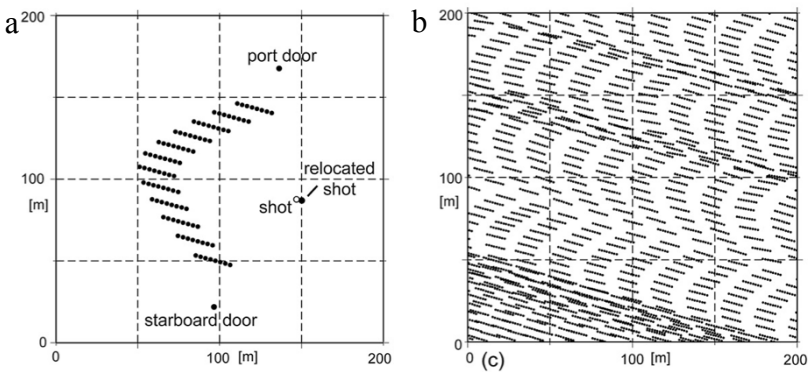

Figure 21 - Acquisition geometry a) Streamer channel and shot point position after source and receiver relocation, b) CMP coverage, modified by (Petersen et al., 2010)

4.2 Survey Data

The database for this study comprises of high-resolution, pre-stacked P-Cable 3D seismic raw data from both Vestnesa Ridge and Snøhvit, acquired in 2013 and 2011 respectively. A detailed description of the acquisition parameters as listed below in Table 1 and 2 are from survey logs, made the P-Cable 3D seismic data were acquired. Helmer Hanssen contracted by the University of Tromsø was the vessel used to obtain the data at both Snøhvit and Vestnesa Ridge.

4.2.1 Vestnesa Ridge

The Vestnesa Ridge seismic data was acquired in July 2013 with a geometry of 14 streamers, each with a length of 25 m. In total 96 receivers, eight geophones per receiver line, and a streamer spacing of 12.5 m. The towing depth was ~ 1.5 m (+/- 0.5 m), and the spreading of the paravans was 166 – 170 m. 12 square kilometers of the subsurface with a water depth of 1200 – 1300 m was acquired by utilizing Mini-GI (15/15 in^3) capable of releasing shooting pressure of 170 bars. The shooting interval was one shot every 5 seconds (6 seconds from line 5), and a sampling interval of 25 milliseconds. Weather conditions at that time were relatively good with a wind speed of 1.4 – 7 m/s. Due to unknown reasons, some small areas within the 3D cube lacks data, possibly as a result of the 10 m featuring (deviation) during acquisition. The minimum and maximum offset recorded was 84 m and 159 m respectively.

Table 1 – Acquisition parameters for Vestnesa 2013 (Survey log)

Vestnesa Ridge, July 2013	
Water Depth	~ 1200 - 1300 m
Number of acquisition lines	25
Spread of paravans	166 – 170 m
Distance between gun and paravans	96 – 106 m
Streamers	14 streamers with 25 m length
Streamer depth	1.5 m (+/- 0.5 m)
Channels	8 per streamer (96 in total)
Streamer Separation	12.5 m
Minimum offset	84 m
Maximum offset	159 m
Source	Mini-GI (15/15 in^3)
Shooting pressure	170 bar
Shot Spacing/Interval	5 sec., 6 sec (from line 5)
Weather	1.4 – 7 m/s wind
Deviation	Up to 10 m
Bin Size	3.125/6.25 x 6.25 m
Dominant Frequency	175 Hz

4.2.2 Snøhvit field

The Snøhvit seismic data was acquired in July 2011 with a geometry of 16 streamers, each with a length of 25 m. In total 112 receivers, eight geophones per receiver line, and a streamer spacing of 12.5 m. The towing depth was ~ 1.5 m (+/- 0.5 m). 4 square kilometers of the subsurface with a water depth of 300 – 350 m was acquired with Mini-GI (15/15 in^3) capable of releasing shooting pressure of 170 bars. The shooting interval was one shot every 4 seconds, and a sampling interval of 25 milliseconds. Weather conditions at that time were also fairly good as the water temperature of 6-8 ^oC and wind speed of 1.3 – 7.5 m/s. Due to inconsistent streamer azimuth and deviation the minimum offset recorded was 103 m and a maximum of 135 m.

Table 2 – Acquisition parameters for Snøhvit, 2011 (Survey log)

Snøhvit, July 2011	
Water Depth	~ 340 m
Number of acquisition lines	30
Spread of paravans	No data
Distance between gun and paravans	No data
Streamers	16 streamers with 25 m length
Streamer depth	1.5 m (+/- 0.5 m)
Channels	8 per streamer (112 in total)
Streamer separation	12.5 m
Minimum offset	103 m
Maximum offset	135 m
Source	Mini-GI (15/15 in^3)
Shot Spacing/Interval	No data (assumed 160 bars)
Shooting interval	4 sec
Weather	1.3–7.5 m/s wind, 6-8 ^oC water temperature
Deviation	Up to 5 m
Bin Size	3.125/6.25 x 6.25 m
Dominant frequency	155 Hz

4.3 Seismic processing workflow

For both the Vestnesa Ridge and Snøhvit data, the same processing steps were applied in a very similar way and will, therefore, be described together. The different techniques, or methods that were used will be described in subchapters. Settings that are not mentioned in the workflow description were left as default, but can be seen in Appendix B. An overview of the different processing stages, and the arrangement can be seen in Figure 22. SeisSpace ProMAX 3D was the main software utilized for the imaging, but noise suppression operation was accomplished in the noise expression module, which is part of GeoTeric 2016 software. Results for each process will be discussed in chapter 5. As the morphology of the study areas, Vestnesa Ridge and Snøhvit are considerably different the result of various processing steps may not be coherent.

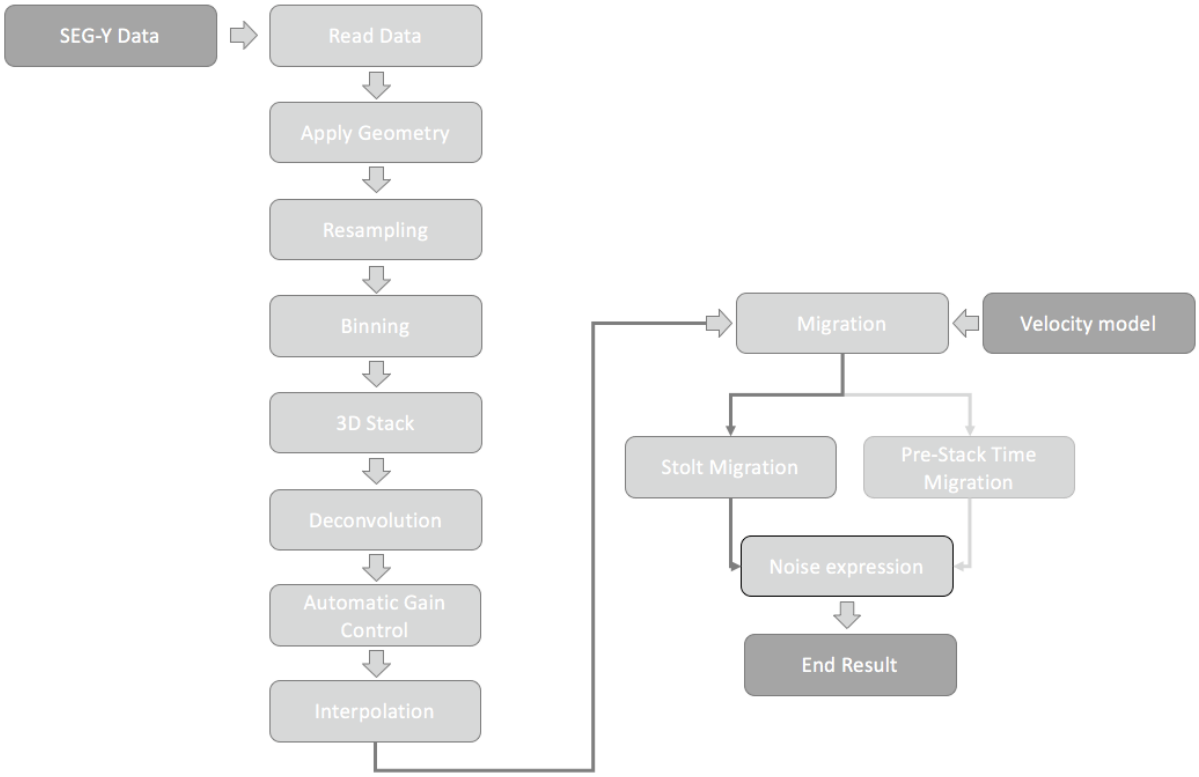

Figure 22 - Processing workflow

4.3.1 Data input and header assignment

The raw pre-stacked P-Cable 3D seismic data from Vestnesa Ridge and Snøhvit was 130.2 and 47.7 gigabytes (Gb) in size respectively. This data had to be corrected for the mismatch in the navigation header to be correctly imported it to SeisSpace ProMAX 3D. To correct the header, field recording number and source shot number were changed. When uploading the data

to SeisSpace ProMAX, the "disk data input" was set to upload "disk image" and "maximum traces per ensemble" were defined. To generate and load the database, "geometry header preparation" and "extract database file" needed to be included. The "geometry header preparation" mode was set to FFID (field file ID), and "maximum number of traces per source" to 96 and 112 for Vestnesa Ridge and Snøhvit respectively. Setting such as "data type" and "source index method" in the "extract data file" were defined as marine and FFID accordingly. This step creates the OPF database from geometry information existing in the incoming trace headers.

4.3.2 Geometry assignment and binning

To assign geometry and define bin size of the seismic data, a single flow with "3D Marine Geometry Spreadsheet" was created. The aim of this stage was to enter all the required field geometry information into the source spreadsheet, perform binning that honor the field data, and to finalize the database. By running this flow, one could define grid parameters such as azimuth, cell size along (dy) and across (dx) the azimuth (bin size), and number of cells in each direction (bin grid), with the aim of constructing a uniform grid that captures all the midpoints to form a 3D CDP gather grid (Christopher, 2003; Liner, 2003; Sheriff and Geldart, 1995). As part of this study includes trying out different bin sizes, two binning operations per data set needed to be completed. The minimum bin size should be half of geophone group interval, which for this data correspond to a 3.125 m and 6.25 m in crossline and inline direction accordingly. Optimally, the bin size should be small enough to capture resolution, but large enough to avoid bins turning out empty. However, the sampling should be dense enough (bin size small enough), to prevent aliasing during processing and interpretation. Based on this, a bin size of 3.125 x 6.25 and 6.25 x 6.25 were chosen as binning grids. The binning type was set to "bin midpoints," which later were staked by constructed a CMP gather by summing all the captured traces to create a single stack trace. An illustration of this process can be seen in Figure 23, as midpoints are gathered in their respective bins and grids, then assigned a common mid-point in each bin. The number of live traces within each bin correspond to the fold with assigned a number often described with terms like high or low. P-Cable seismic, in comparison to conventional seismic data contain a very low fold coverage, 6 – 30 in each bin, but considered high given the limited offset range and short shooting interval.

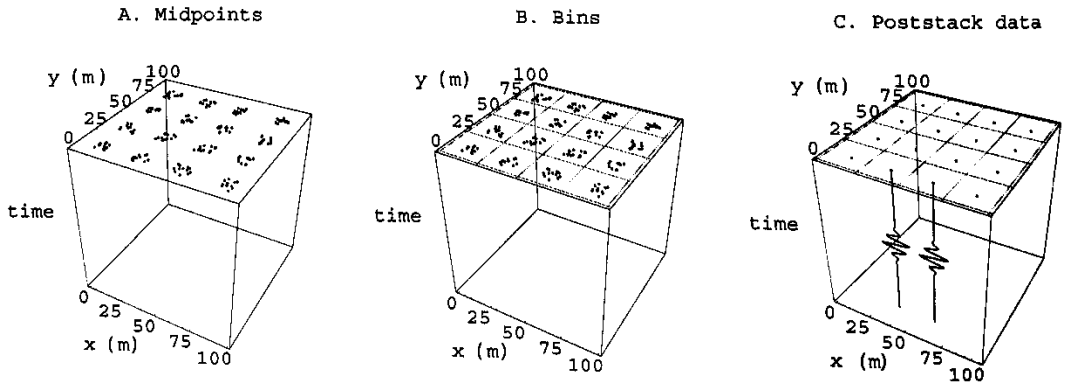

Figure 23 – Illustration of binning and CMP stack; A) each trace displayed as the midpoint, B) The bin grid is superimposed on the midpoint, and all prestack trace in a bin are captured, C) CMP gather where each bin contains one poststack trace (Liner, 2003).

The last step before the data could be further processed was to upload the geometry information from the database to the trace headers. This was done by creating a flow including "Inline Geometry Header Load". After binning as one could display the fold coverage (midpoint density) as fold map, as seen in Figure 24 and Figure 25.

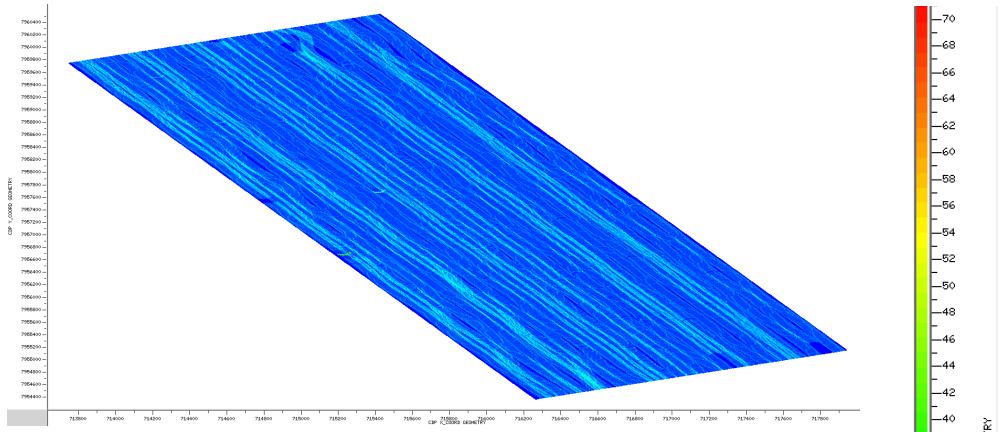

Figure 24 Fold map of Snøhvit seismic data, bin size of 6.25 x 6.25 m.

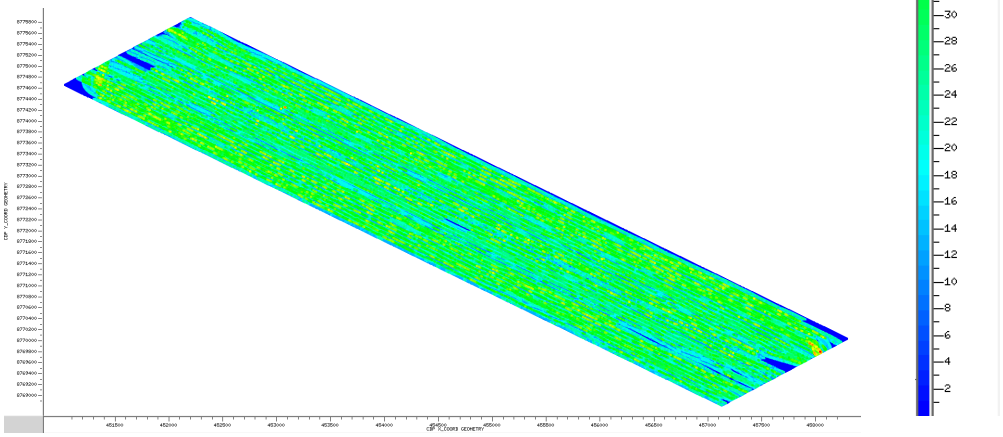

Figure 25 - Fold map of the Vestnesa Ridge seismic data, bin size of 6.25 x 6.25 m

An overview of the both surveys can be seen as all the source points with its coordinates in Figure 26 and 27, for Vestnesa Ridge and Snøhvit respectively. They both show some navigational problems during acquisition seen as curvy pattern and discontinuity that represent holes with zero data that correlates well with the low fold areas seen in the two previous Figures (24 and 25).

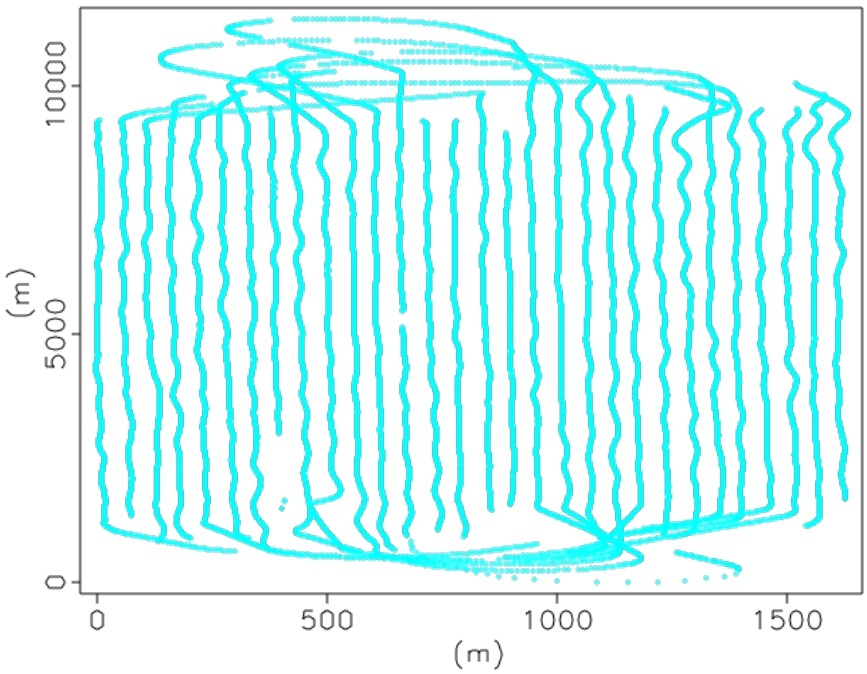

Figure 26 - Overview of source points with its coordinates acquired for Vestnesa Ridge, north is 46.2 degrees clockwise in relation to Y axis.

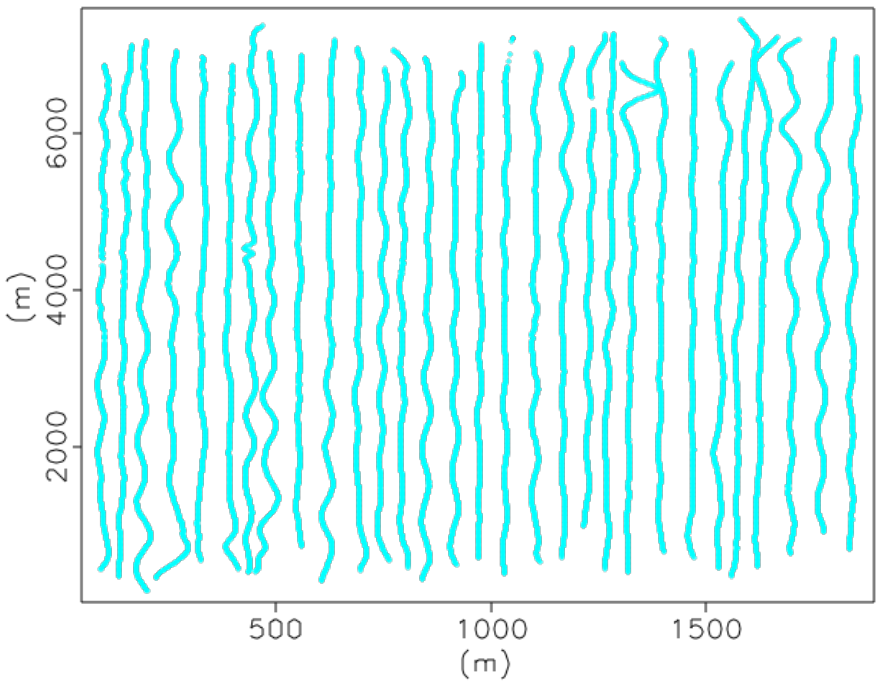

Figure 27 - Overview of source points with its coordinates acquired for Snøhvit, north is 25.25 degrees clockwise in relation to Y axis.

4.3.3 Resampling

Resampling is generally done either by making the sample rate finer or coarser. A process like this would not affect the quality of the data unless a significant amount of the frequency spectrum is not accounted for. The frequency bandwidth for both the Vestnesa Ridge and Snøhvit show similar trends with peak frequencies up to 350 Hz. As most of the frequency (Figure 28 and 29) lies between 20 to 250 Hz, notch at 100 Hz with a dominant frequency of 175 and 155 Hz for Vestnesa Ridge and Snøhvit respectively. Resampling of the data from 0.25 to 1 millisecond (Nyquist frequency of 500 Hz) does not affect the data quality, but decreases the amount of disk space required to store the data and makes the data processing quicker.

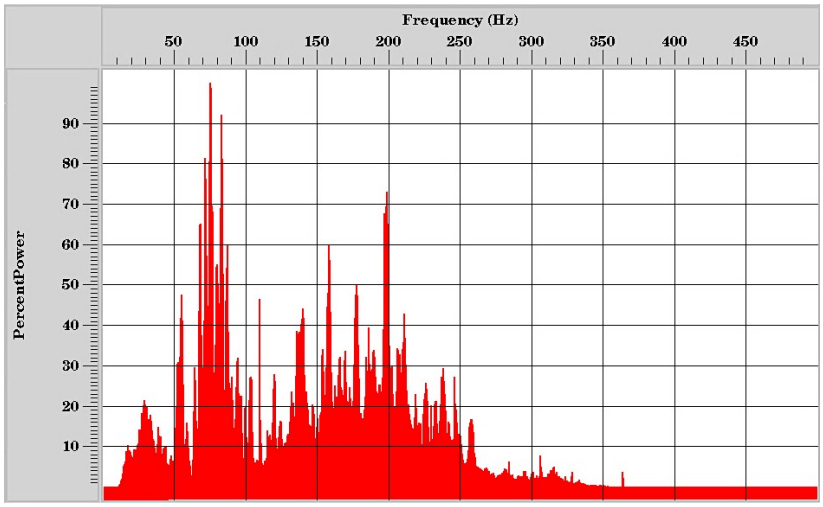

Figure 28 - Frequency spectrum of Vestnesa Ridge with corresponding percent power.

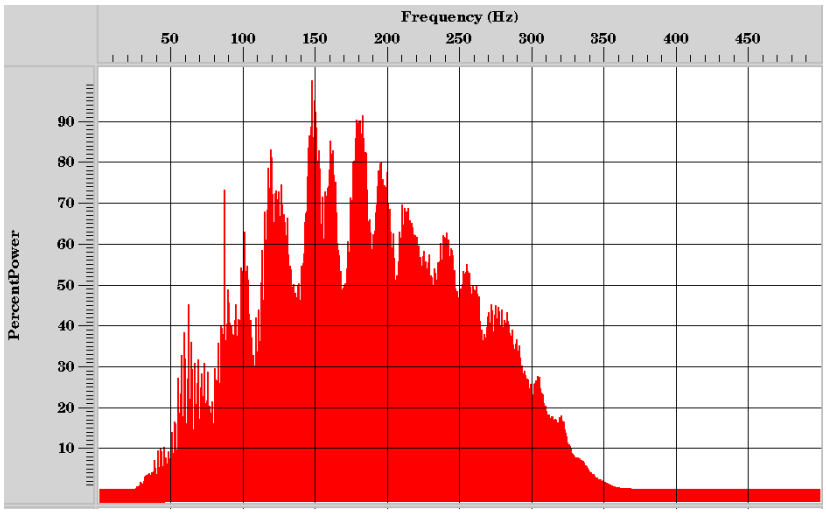

Figure 29 - Frequency spectrum of Snøhvit seismic data with corresponding percent power.

4.3.4 Top-mute

Noise associated with pre-signal arrivals was identified in both Vestnesa Ridge and Snøhvit pre-stacked data. This was seen as strong amplitudes related to shot generated noise that were considered unwanted noise and therefore muted. To accomplish this, a top-mute filter was set with a taper of 20 ms to avoid any artifacts such as ringing.

4.3.5 3D Stacking and NMO correction

The stacking of the data was accomplished by using "Stack 3D" in SeisSpace ProMAX 3D, which is a vertical stacking method based on the straight mean stack, which sums the sample values contributing to each CMP and divides them by the square root of the number of samples summed. It stacks the input traces into correct CDP bin location in the vertical domain. One upside to choosing coarser bin size is that the signal-to-noise ratio improves as the fold coverage increases after CMP stacking. However, by defining larger bin size usually involves lower resolution as less data are dealt with separately (Halliburton, 2017).

Before the data could be stacked, correction for normal moveout (NMO) needed to be applied. This was accomplished by specifying a constant velocity of 1480 m/s, stretch mute percent of 30, and in the forward direction of NMO and no long offset correction. The NMO correction was required as the data contained variation in arrival time as the geophones were spread out and moved away from the source. This is a very common operation, which is thought to be the most important criterion for identifying reflections and determining velocity. As for this project, velocities were not estimated because of the low offset and nature of the data (Halliburton, 2017).

4.3.6 F-XY Deconvolution

Seismic records usually contain events that may be considered as a convolution of several filters such as the source wavelet, the receiver impulse response, or the response generated by the Earth. Prestack processes such as zero-phase spectral enhancement or trace-by-trace spiking deconvolution might not always improve the signal to noise ratio, rather add noise content to the data. This type of noise typically is at the high end of the spectrum, and commonly dealt with by applying a bandpass filter to remove it. However, bandpass filter operates on the summed amplitude of the signal and noise content, consequently attenuating a portion of the signal as well. Seismic data with low fold, typically show stacked data as noisy sections which would benefit from separating the signal and noise to efficiently remove the random noise content (Gülünay, 2000).

F-XY deconvolution is based on F-X linear prediction filtering (Canales, 1984), only for 3D instead of 2D, in which seismic image is thought to compose of linearly-coherent reflectors. The use of prediction filter in the spatial direction is therefore justified as it extracts linear features and attenuates random noise (Gülünay, 2000). This is done by applying Fourier

transform to each input trace, which includes complex least-mean-square (LMS) adaptive unit prediction rectangular filter in x, y space for each frequency plane in the specified range. Lastly, each resulting frequency trace is inverse transformed back to the time domain. The output trace of this operation should have less random noise than the input. An example of the effect of applying F-XY predictive filter can be seen in Figure 30 as the input to the left, and the filtered output to the right.

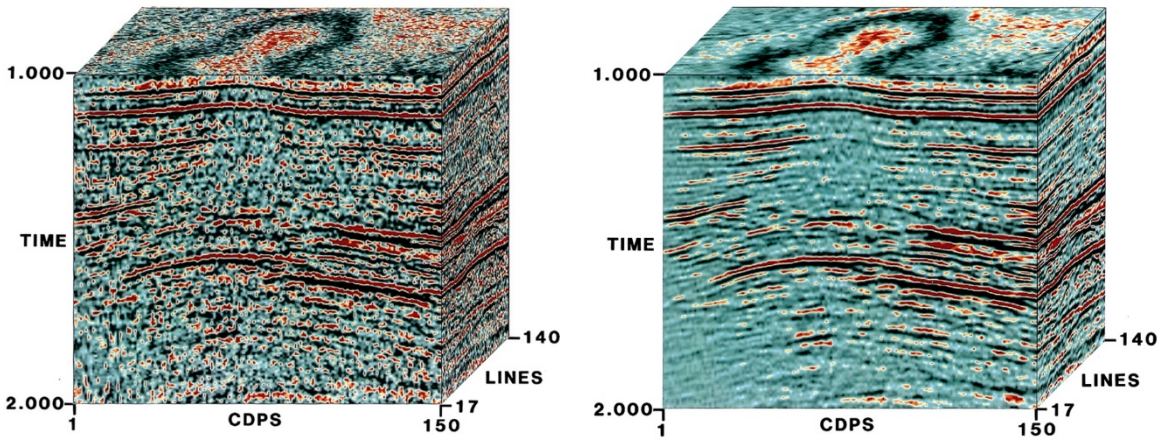

Figure 30 – Before (left) and after (right) F-XY prediction filter of noisy 3D land survey (Gülünay, 2000).

Consequently, when the data is transformed from time and space (x,y) to frequency (f) and space (x,y), a time slice is converted to a frequency slice. Each sample in the transformed data has both real and imaginary components. Events with similar spatial dips appear as a sinusoidally complex signal along a given frequency slice, which makes the signal predictable. Any difference between predicted complex value and the actual one can be classified as noise and removed. The time volume is divided into small windows to better approximate the assumption of regular spatial dips (Halliburton, 2017).

For this project, F-XY deconvolution was applied to suppress random noise and enhance the continuity of the reflectors in the initial stack. The input had to be sorted by primary trace header “3D inline number” and secondary trace header “3D crossline number”. In the setting menu, the maximum frequency was set to 250 Hz, and all other parameters as default. The result of this process will be elaborated in the next chapter.

4.3.7 Automatic Gain Control

Automatic gain control (AGC) is a common scaling type operator typically used to equalize the amplitudes of stacked data. It does so by automatically varying the gain applied to the traces as a function of the sample amplitude with an automatic gain control time window, which computes the average amplitude within a window (Lavergne, 1989). The AGC operator length defines the length of the AGC window used for gain computations. One could keep in mind that by applying AGC with too short operator length may result in boosting noise, and change the character of the section as the relation between high and low amplitudes reflections will be lost. Similarly, by defining to long operator length some weak amplitudes may be lost as the scaling is insufficient (Cahill, 1992). Furthermore, the calculation of scale factor is done at a different location as the AGC window is moved along the trace sample-by-sample. Depending on the operator setting, a factor is equal to the inverse of the mean, median, or RMS amplitude in the window. The scalar is applied to the sample at the beginning, middle, or end of the AGC window. To preserve harsh scaling of very weak or anomalously strong zones the AGC gain can be limited to a specified factor of the median gain (Halliburton, 2017).

The aim of using AGC is to improve the relative amplitude scaling as the reflector of subseafloor, and the Upper Regional Unconformity in the Snøhvit data is adamant compared to deeper down. As defined in the previous chapter, the resolution is defined as the ability to distinguish different features of the subsurface as separate events, AGC scaling will not improve the resolution as it is independent of the amplitude of these events. This type of operator should only be used if necessary. For this data application mode was set to “Apply (trailing)” and the type of AGC scalar to “Mean (Median),” and a basis for scalar application to “centered”. The automatic gain control operator length was tested out for a range of values, but was set to 100 ms, which gave the best result.

4.3.8 Interpolation

The interpolation method applied for this project was the 3-D missing data interpolation introduced by Sergey Fomel, 2013 done with local 3D plane-wave prediction, based on recursive filter preconditioning. The theory of plane-waves prediction was initially formed in one dimension (Fomel et al., 1997), which includes predicting a local plane wave accomplished by a T-X filters to interpolate based on recursive filter preconditioning efficiently. However, the 3D missing data interpolation utilized for this project can be constructed from a pair of two-dimensional filters, accomplished using helix transform and a one-dimensional spectral factorization algorithm. This technique has shown promising results as it fills empty and dead traces with interpolated data (Fomel, 2001) as seen in Figure 31 below. This Figure show how this interpolation technique restores most of the original signal, except for some high-curvature areas. The aim of this operation was to restore the coverage and enhance the geological imaging by preserving the local dips of the reflectors in the 3D seismic data available. The actual processing was completed in Madagascar software (Madagascar, 2017) and the run time varied between 17 and 24 hours.

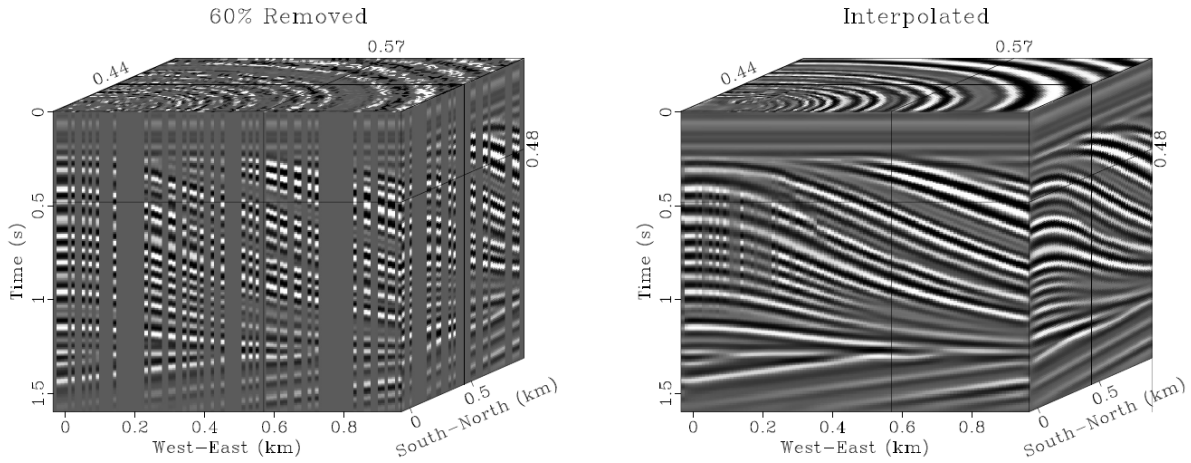

Figure 31 – Synthetic models after 60% of input traces are randomly removed (left), compared with the result of missing data interpolation with a 3D local plane-wave prediction filter (Fomel, 2001).

4.3.9 Migration

Migration is a general term for a collection of different methods based on mathematical algorithms with the objective of repositioning events in seismic data to their true locations of origin. This process is necessary, but also an expensive process that is done before accurate seismic interpretation can be completed. In many cases, migration is one of the last steps that are applied and therefore likely to be blamed for the lack of structure details, or inconsistent amplitude response, even though these problems likely were caused by processing issues or other acquisition problems. Seismic records often contain non-geological events such as coherent and incoherent noise associated with point-diffracted, sharp or dipping signature that can cause bow-tie effect, hyperbola that may be corrected by migration (Sheriff and Geldart, 1995). Diffraction creates and enlarges hyperboloids and is often considered as a natural process. However, migration does the reverse by computer processing to remove the effect of it (Claerbout et al., 1985).

Migration in detail is defined as an inversion operation that involves rearrangement of elements in seismic information with aims of locating reflections and diffraction at their actual position. This is based on using wave equation to back trace the wavefield to determine the real spatial position on section (x,t). The main types migration methods utilized are: 1) based on an integral solution called Kirchhoff, or diffraction stack migration, 2) solution in frequency domain associated with Stolt or Gadzag migration, and lastly, 3) finite difference solution in the time domain (Sheriff and Geldart, 1995). The advantage of applying finite difference method is that it is not limited to a simplified model of the subsurface. On the other hand, it is considered more expensive than most methods, for example, Stolt migration (F-K) which migrate the seismic data in frequency/wavenumber domain. However, Stolt migration also present some drawbacks as it does not account for lateral velocity variation. Finally, Kirchhoff time migration is a purely analytical process that sums amplitudes along diffraction curves, which is of high value in areas associated with steep dipping features, but present difficulties dealing with lateral velocity variation, and produce more migration artifacts. The incident angle is limited by spatial aliasing, which determines the amount of dip that can be migrated. The cost of migration is highly dependent on the amount of data, and the amount of physics put into it (Lavergne, 1989).

4.3.9.1 Time/depth migration

Essentially, any migration that is only accurate for constant velocity or v(z) is termed time migration. However, there are different methods of time migration that are exact arbitrary for v (z) (velocity through depth) and those that are actually constant velocity algorithms that can approximately incorporate vertical velocity variation. Time migration is considered as a relatively fast process that can be repeatedly done for easy velocity analysis, but is less accurate in areas with strong lateral velocity variation. In fact, the terms depth and time migration are used to distinguish those algorithms that do account for lateral velocity changes and appropriately bend rays (depth migration) and those that do not (time migration). According to Liner et al (2003), previous work has shown that there is growing evidence that for structurally complex areas, the standard processing flow that includes NMO, DMO, CMP stack, and poststack depth migration, is not the optimal approach in maximizing imaging. In figure 32, one can see what would be the appropriate method to use given variation in conditions such as lateral velocity and structural complexity.

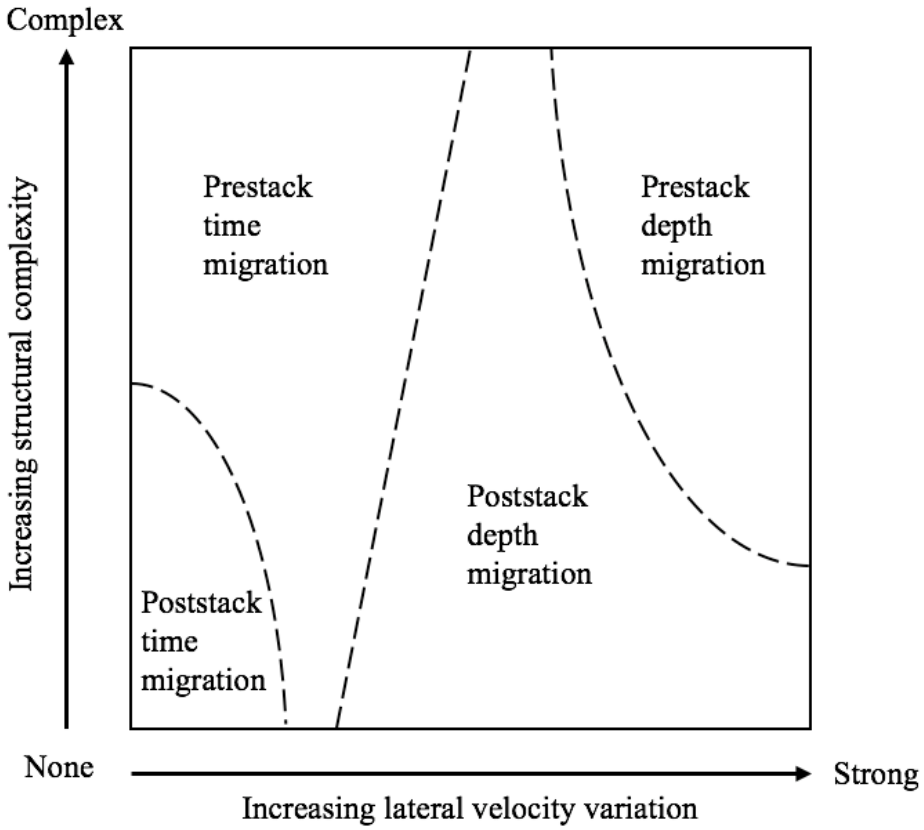

Figure 32 - Qualitative decision diagram for migration after (Liner, 2003).

This research will focus on prestack time migration based on Kirchhoff method, and poststack Stolt migration as the ability to obtain realistic velocity models cannot be accomplished only by the seismic record. Consequently, the migration performed on the available data for this project is done in the time domain, and by specifying constant velocity. However, with more available data, in example, with a significant amount of well data (sonic log: interval velocity), one could argue that the use of other methods would be more suitable. Several trials were done to determine the best possible migration technique for this P-Cable 3D seismic by changing different parameters, both for prestack and poststack migration. With that said, migration of the synthetic seismic data was however accomplished by using two velocity fields: one defined as constant, 1480 m/s, and the other one with the true synthetic velocity model. This allowed for a direct comparison of how sensitive the different migration technique depends on a realistic velocity model to present a realistic image of the synthetic model.

4.3.9.2 Prestack Time Migration

Prestack time migration (PSTM) performed on the available data from Vestnesa Ridge, and Snøhvit was tested in SeisSpace ProMAX and in open source Madagascar to compare the results. This process migrates the entire prestack data volume including every blip of amplitude impulse response on each trace. It can be seen as a combined flow that performs normal moveout (NMO), dip moveout (DMO), and poststack migration. Therefore, two velocity analysis steps are combined into one. If anything, deconvolution and static correction are typically the only steps that need to be considered before Prestack time migration. Compared to poststack migration, PreSTM is more expensive, but generally obtain more details in difficult areas. This method includes some assumptions, which limit the accuracy of the method, and zero phase Kirchhoff time migration assumes that the vertical axis is in time and that the Earth is horizontally layered with no changes in lateral velocity within the migration aperture. The concept of vertical time have been applied for many decades and is defined as the two-way travel time (TWT) that is computed along vertical trajectory without honoring Snell's law at velocity changes. Kirchhoff migration algorithm operates in the physical time-space domain and therefore suitable for irregular data. Typically, pitfalls associated are "pull-up effect" and false structures (Liner, 2003). The final product of PreSTM that was computed in the open source software, Madagascar only took 14 – 16 hours running in parallel, whereas the PreSTM performed in SeisSpace ProMAX took 16 days and 19 hours to complete even though the binning size was coarser and consequently require lower storage space.

4.3.9.3 Poststack Time Migration

Poststack time migration involves migration of the CMP stack data volume, which is usually considered to be zero offset data. This is significantly less expensive than PreSTM making it one of the fastest migrations available, and allowing processing on regular workstations. The poststack migration algorithm used in this project was the Stolt migration which is based on Fourier transform method, and valid for v(z) and naturally incorporate tuning waves. However, Stolt migration requires uniform trace spacing, that is corrected by interpolation (Sheriff and Geldart, 1995). This migration technique works by transforming the data to the FK domain by $\tan(\alpha) = \sin(\beta)$, which shifts the data vertically in the frequency axis with the aim of transforming the data to the migration dip. Followed by the final step, which is an inverse transformation to obtain the result in the time domain (Stolt, 1978).

4.3.10 Noise Expression (suppression)

The final products of both prestack time migration and poststack Stolt migration still contained some coherent and random noise in addition to migration artifacts such as migration smiles and frowns. To suppress image distburbing response with the aim of increase the data quality and to preserve the natural amplitude response at small scale, a software called GeoTeric was utilized. This software has a wide range of functions used for several applications, however, for this project the noise expression application made it possible to remove noise from poststack data in a visual and interactive manner. To do noise cancellation in an effective way, the algorithm applied should also ensure a minimum loss of information to represent the nature of geology. This flow included three different post stack noise cancelling algorithms, which is the TDiffusion, SO, and SO FMH that allowed the user to specify parameters such as "iteration", "filter size" and "dip azimuth filter size" with live update of any changes for easy comparison (Lee et al., 2013). Figure 33 show the affect of applying random noise (TDiffusion filter) attenuation and lastly, the aggressive noise (SO filter) compared to the original unfiltered data of Snøhvit.

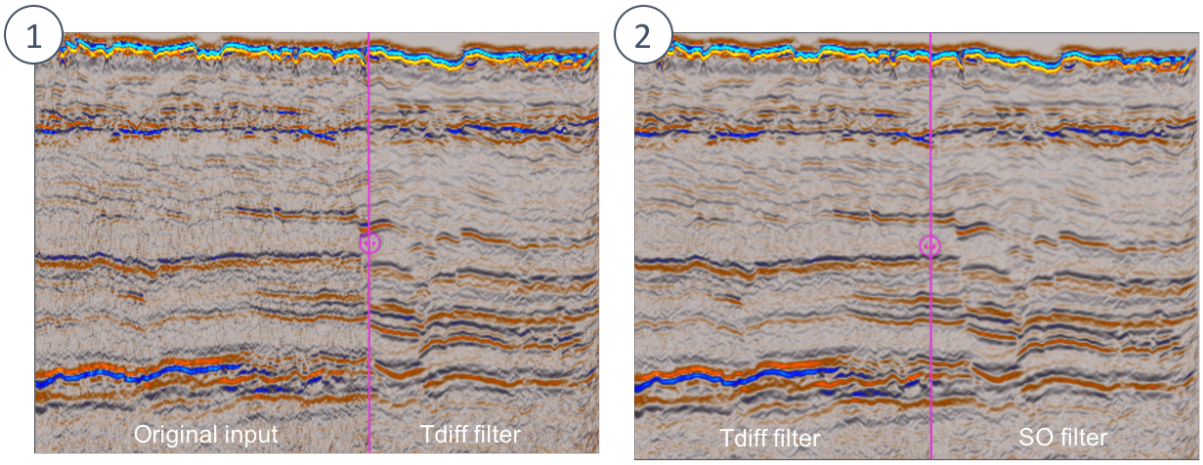

Figure 33 - Step-by-step improvements done in GeoTeric Noise Expression of Snøhvit seismic data, 1) show the difference between the unfiltered input with after TDiffusion filter, 2) comparison of TDiffusion and SO filter.

The TDiffusion filter allows the user to remove random noise in the data by applying a low-pass filter generated by a partial differential equation in time, consequently creating a series of smoother images. This filter is anisotropic and accounts for the orientation of local structures as it automatically orients the direction of the filter. The idea is that since this filter is sensitive to small scale discontinuities, making it highly suitable to remove random noise while preserving details of small scale structures. However, events that are coherent with consistent phase distribution in trace-to-trace, such as ground rolls and multiples, will still be preserved (Lee et al., 2013).

In comparison to SO FMH, the SO (structurally oriented) filter is less sophisticated as it does not remove coherent noise and may not preserve edges. However, this filter is intended to remove aggressive noise that in most cases are induced by sharp interfaces that absorb a significant amount of the seismic energy, for example, salt or basalt effect. The SO filter is applying smoothening along 2D plane restricted to points where dip and strike direction is specified. The first step is to calculate the dip azimuth volume, either by estimating the mean, or median in a 2D region (Lee et al., 2013).

SO FMH filter is an abbreviation for "structurally oriented finite media hybrid," and is typically applied to reduce noise by attenuate coherent energy such as multiples and acquisition artifacts. This is accomplished while preserving structures with sharp dips, corners, and edges. In many areas, high spatial frequency coherent noise may mask real representation of faults and local structures. As a result of this process, seismic sections showed a greater continuity of the reflectors and enhanced lateral and vertical resolution (Lee et al., 2013). An example of two-step filtering can be seen in Figure 34, as the seismic section of Vestnesa Ridge are filtered in noise expression by TDiffusion and SO filter.

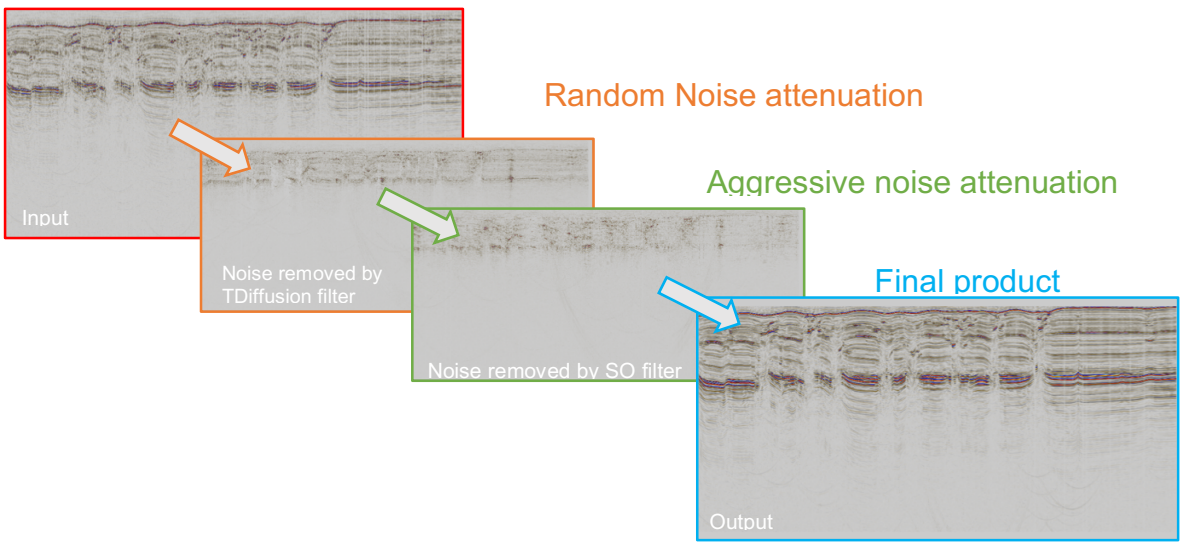

Figure 34 – Input and output of noise expression operation in GeoTeric, seismic section of Vestnesa Ridge.

Several different filters were tried out with varying parameters and arrangement, and the best result was obtained by applying random noise attenuation (TDiffusion) with ten iterations, and aggressive noise attenuation (SO noise) with a filter size of 3, and dip azimuth filter size of 15. When tested out, the SO FMH filter did not show as good of a result as the combination of applying TDiffusion and SO. This software showed excellent results, and a comparison of the input and the output of this procedure can be seen in Appendix B. The actual processing was done fairly quickly within minutes.

Figure 35 below show a 2D section with black and white attribute applied to highlight the noise, as section (a) shows lower signal to noise ration compared to section (c).

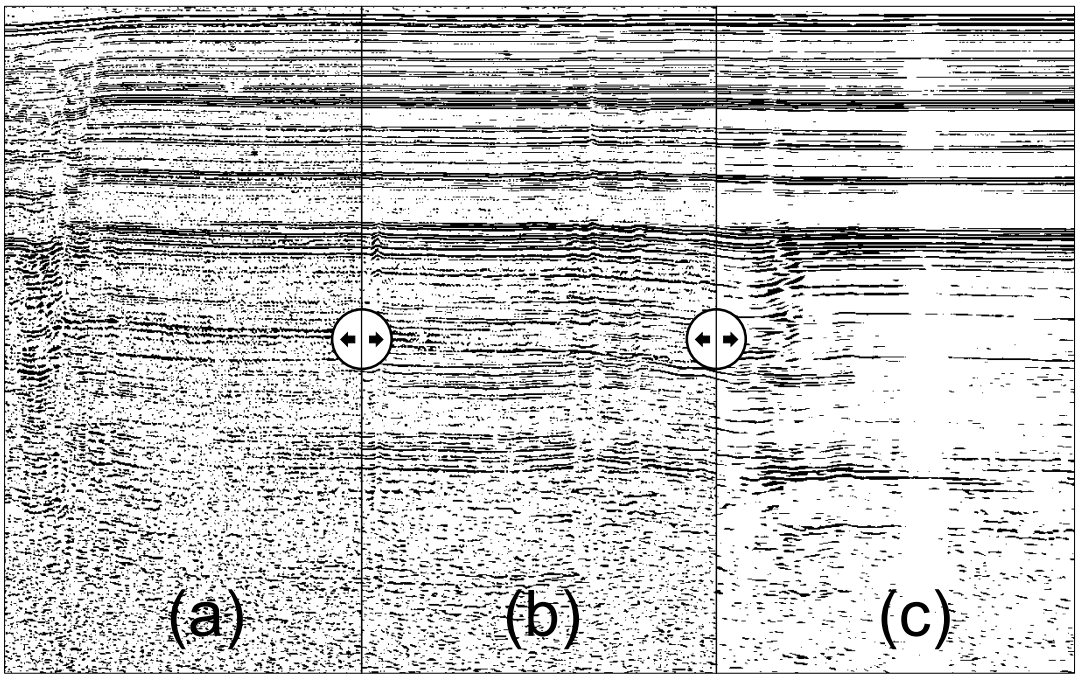

Figure 35 - Seismic section of Vestnesa Ridge displaying the effect of noise expression operation: a) Unfiltered stack, b) Random noise attenuated (TDiffusion), c) and aggressive noise attenuation (TDiffusion + SO).

4.4 Synthetic modeling

As mentioned earlier, the aim of constructing a 3D synthetic model is to generate 2D/3D seismic data that can be used to build confidence in determining whether the processes applied on the actual data show improvements or not. It was constructed by interpretation of poststack Stolt migrated 3D seismic data from Vestnesa Ridge and it is supposed to be a simple hypothetical geological model based on the knowledge brought up by earlier studies of the area. This was achieved by using the interpretation, and visualization software, Petrel, in addition to geophysical modeling in Madagascar. Lastly, GeoTeric 2016 and the newly launched GeoTeric 2D was utilized to improve the ability to interpret distinct features and remove artifacts associated with the modeling. A conceptual illustration of the three main steps in creating synthetic modeling can be seen in Figure 36.

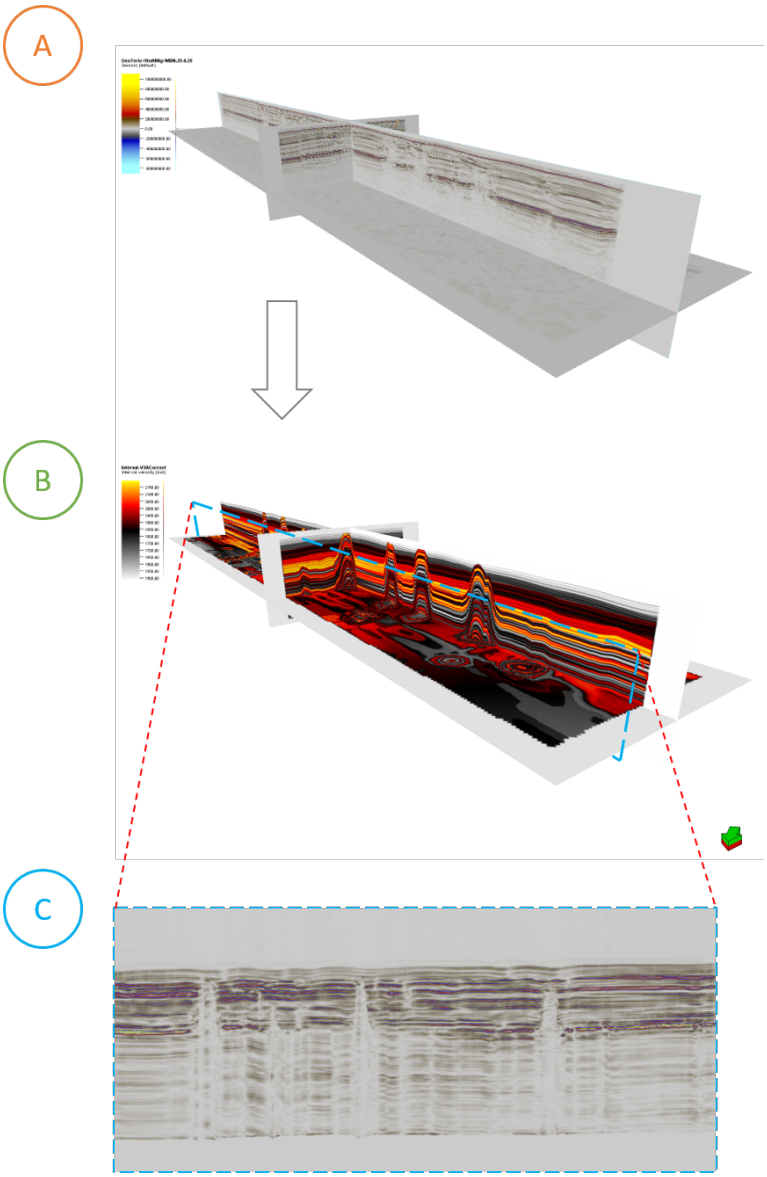

Figure 36 – Conceptual illustration of the tree main steps to construct synthetic model, and finally synthetic seismic, A) actual 3D seismic from Vestnesa Ridge, B) synthetic velocity model, C) Synthetic seismic inline (Not to scale).

4.4.1 Interpretation

The first step in constructing the synthetic model was to define the main boundaries and the level of detail that would be of importance to construct a realistic model. It was decided to manually interpret six different horizons covering the same area as the seismic data, which include the seafloor, some random well defined and continuous reflector, the bottom simulating reflector (BSR), in addition to mapping out the gas chimneys visible on the seismic data. As the geological record, mainly consistent of horizontally layered strata with minor structural features such as faults and folds, the interpretations of the horizons were easily accomplished by using seismic interpretation tools like 2D seeded tracking and some 3D auto-tracking. As the morphology at Vestnesa Ridge did not cover complex structural features, it was decided not to include faults. To correctly interpret the gas chimneys consistently, a module called high-definition frequency-decomposition in GeoTeric was utilized to highlight this kind of feature, typically as low frequencies matter (dark colors) as seen in figure 37 A, and B as both represent inline 117 with southeast – northwest trend. This filter applies an RGB blending on the input (3D seismic), which decomposes the frequency broadband spectrum into three frequency ranges that were manually defined. The specified frequency range for red color was 0 – 70 Hz, 71 – 120 Hz for green, and lastly 121 – 170 Hz for blue. It uses matching pursuit algorithm with constant bandwidth and scale filters, to create a frequency decomposed 3D cube that was later imported to Petrel for interpretation. The actual interpretations of gas chimneys was conducted in Petrel by using an operation called “Geobody interpretation,” which effectively made a geobody out of a picked frequency range. This was later converted to a horizon that had to be adjusted for some mismatch.

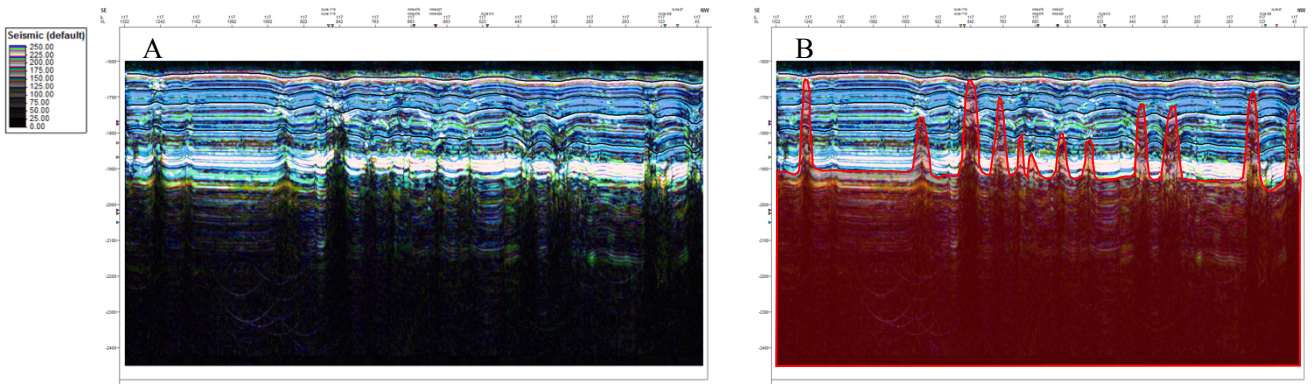

Figure 37 – High Definition frequency decomposition attribute made on Stolt migrated 3D seismic data from Vestnesa Ridge. A) low-frequency features displayed in black, B) Gas chimneys interpreted in red based on the low-frequency features seen in A.

All of the horizons that were interpreted had to be converted to surfaces, that was done in “make/edit surface” in Petrel. This step was accomplished by defining the horizons as input, specifying the grid increment, 6.25 m by 6.25 m in cross-line and inline directions and adding a polygon boundary. As many of gas chimneys were interpreted to intersect surfaces above, the area in between the chimneys had to be removed to obtain the correct body of all these structures as seen in Figure 38. The surfaces were named from top to base; Seabed, 1705 ms, 1730 ms, 1860 ms, BSR, and Chimneys respectively.

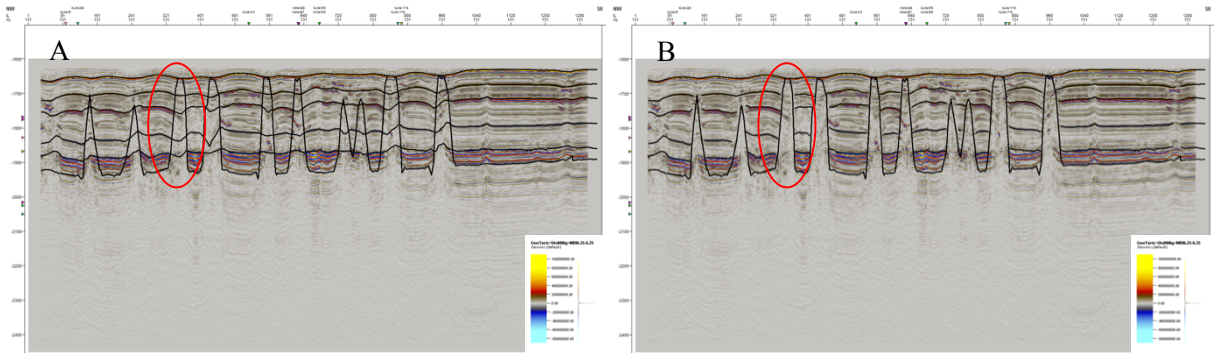

Figure 38 – Section A and B show inline 131 with all the interpreted surfaces that are utilized in the making of a hypothetical geological model of the Vestnesa Ridge. Within the red circle one can observe that in A) different surfaces are intersecting each other, whereas in B) it has been corrected to prevent problems related to the modeling.

The result of the interpretation can be seen in figure 39, Stolt migrated 3D seismic data in relation to the all the surfaces that form the basis for next modeling step.

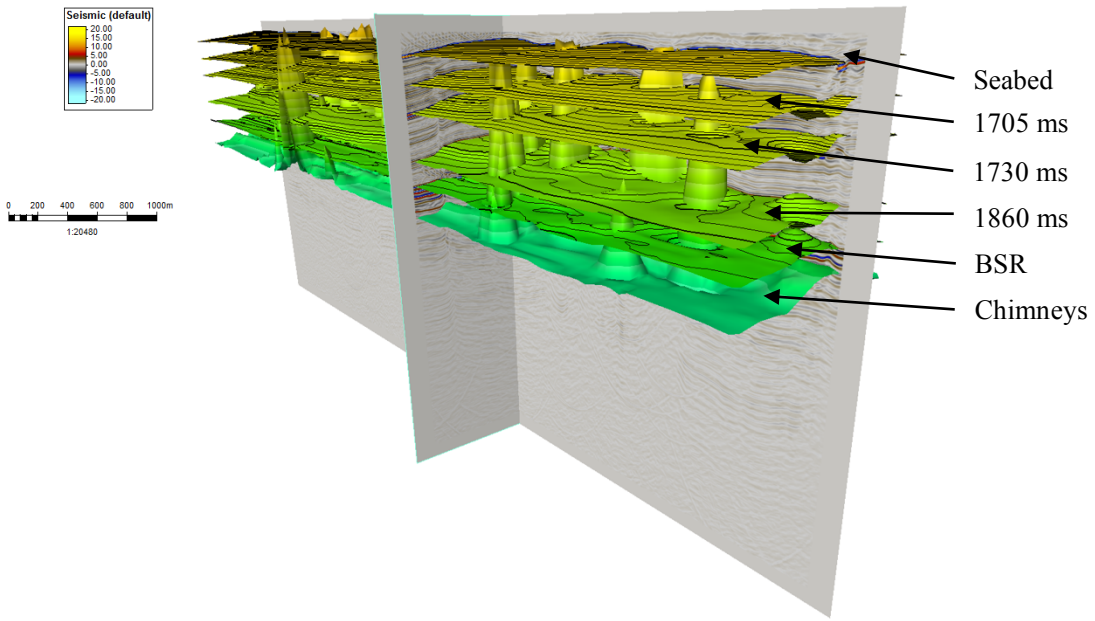

Figure 39 - Overview of all the interpreted surfaces in relation to the 3D seismic cube that will be the basis for the following modeling model, VE = 4 (Vertical exaggeration).

4.4.2 Structural modeling

A model project was defined in Petrel and followed by specifying the geometry in simple gridding. Two flat surfaces representing the top of the water column (set to -1550 ms) and the base of the gas chimneys (at -2400 ms) had to be added to obtain volumetric bodies of the water column and gas chimneys. In addition, the interpreted surfaces as seen in Figure 39, needed to be included in the modeling folder, which was done by using “make horizons”. This operation enables the user to define top and base and specify the type of horizon. The chimneys surface was set as the base, and all the others were defined as conformable horizon types. In figure 40, one can see the result of geometrical modeling of all the surfaces. The individual zone makes up a volumetric contribution without any properties.

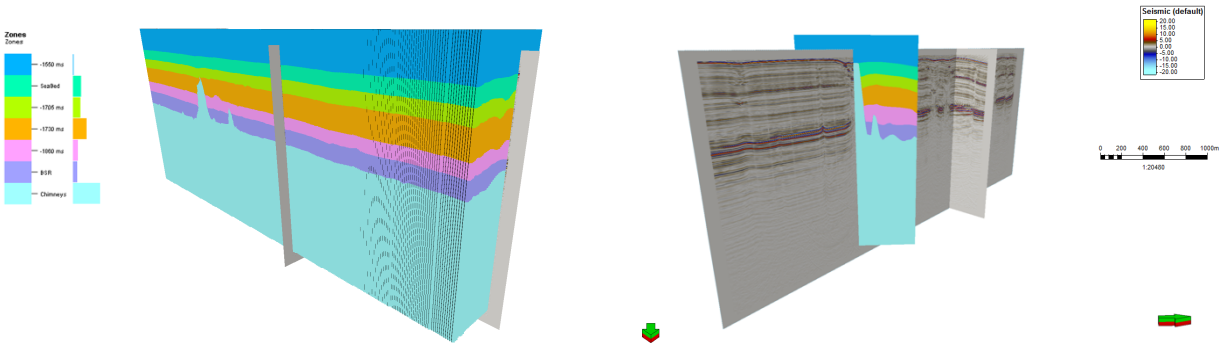

Figure 40 - Subdivision of the model in different zones between the surfaces model VE = 4 (Vertical exaggeration).

In Figure 41 one can see the result of adding layers in between each zone, done by utilizing the layering operation were the zone division was set to “follow base” with cell thickness ranging from 1 – 3. The correlation with the actual seismic data is surprisingly accurate and is the basis for the next step; adding elastic properties such as velocity and density.

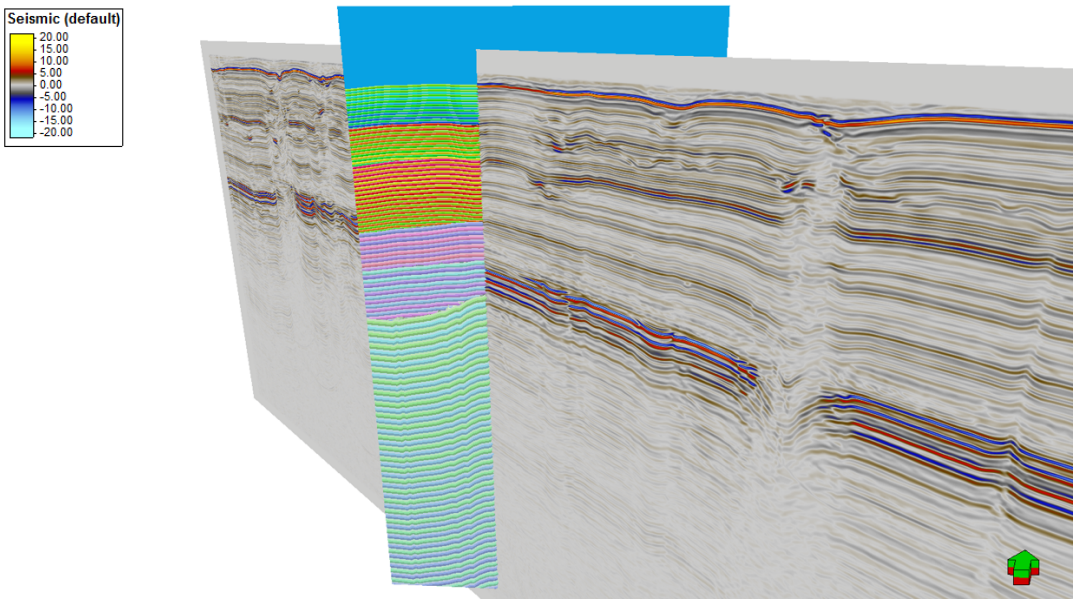

Figure 41 – Geological model with layers in comparison with the actual seismic data at Vestnesa Ridge, VE = 4.

4.4.3 Property modeling

To generate synthetic seismic data based on the constructed geological model, one needs to add elastic properties. For this project, it was decided to add interval velocity changes by Sequential Gaussian simulation to obtain the uniform normal distribution of lateral and vertical changes. This method is typically used when little to no data is available, which is the case for this project as no velocity data is given either by the seismic itself or well data. Another method such as the stochastic Gaussian random function simulation and deterministic Kriging were tried but provided an inappropriate representation. An important step in simulating the velocities include transforming the original distribution to Gaussian distribution by normal score transformation and giving a smooth cumulative detection probability (CDP) curve. Gaussian simulation is a pure stochastic method that is based on Kriging but is generally better at capturing and accounting for extreme values in heterogeneous medium (Bohling, 2005). The actual modeling of interval velocities was accomplished by simulating each zone step-by-step. The petrophysical module in Petrel allowed the data to be simulated in this manner and parameters such as seed number, output data range (minimum and maximum), the mean normal distribution value and the corresponding standard deviation were tested out for different values. As seismic data covers relatively shallow depth, it was decided to limit the velocities in the range of 1480 m/s, and up to 2200 m/s. The first zone below the seafloor was defined with seed number of 418, velocity range of 1480 m/s – 1625 m/s, mean of 1600 m/s and standard deviation of 90. The second zone was specified with a minimum velocity of 1625 m/s and maximum of 1815 m/s, mean of 1760 m/s and seed number of 6655. The following zone was defined similarly with increasing interval velocities, but a complete table of the settings can be seen in Appendix B. When all this was completed, a 3D cube of simulated interval velocities was constructed as seen in Figure 42 below.

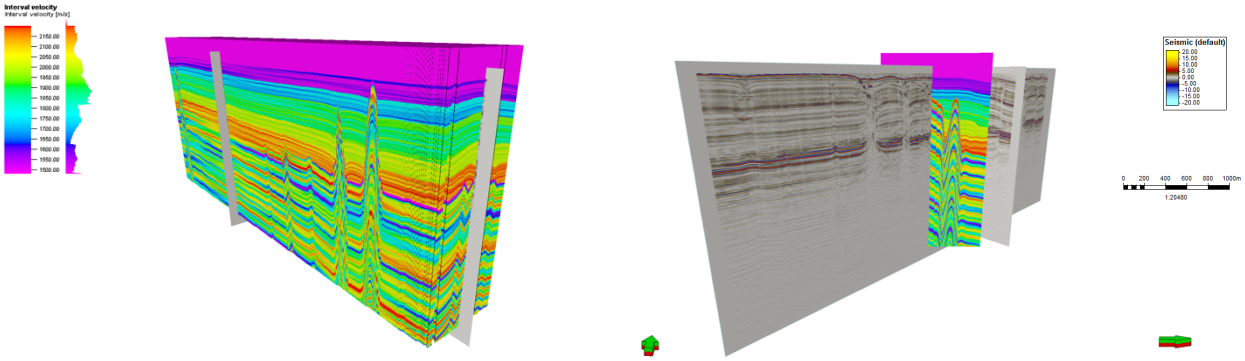

Figure 42 - Synthetic interval velocity 3D model constructed by Sequential Gaussian Simulation (left), and the same velocity model in relation to the actual seismic data (right), model VE = 4 (Vertical exaggeration).

4.4.4 Converting model to SEG-Y

To export the velocity field model, one had to convert it to SEG-Y file, which was done in Petrel. The tool utilized for this operation was “make seismic cube” in property operation, and the result can be seen in Figure 43. In the following Figure (44) one can see how the velocity field correlates with the real seismic data as inline 178 display a cross section of a gas chimney.

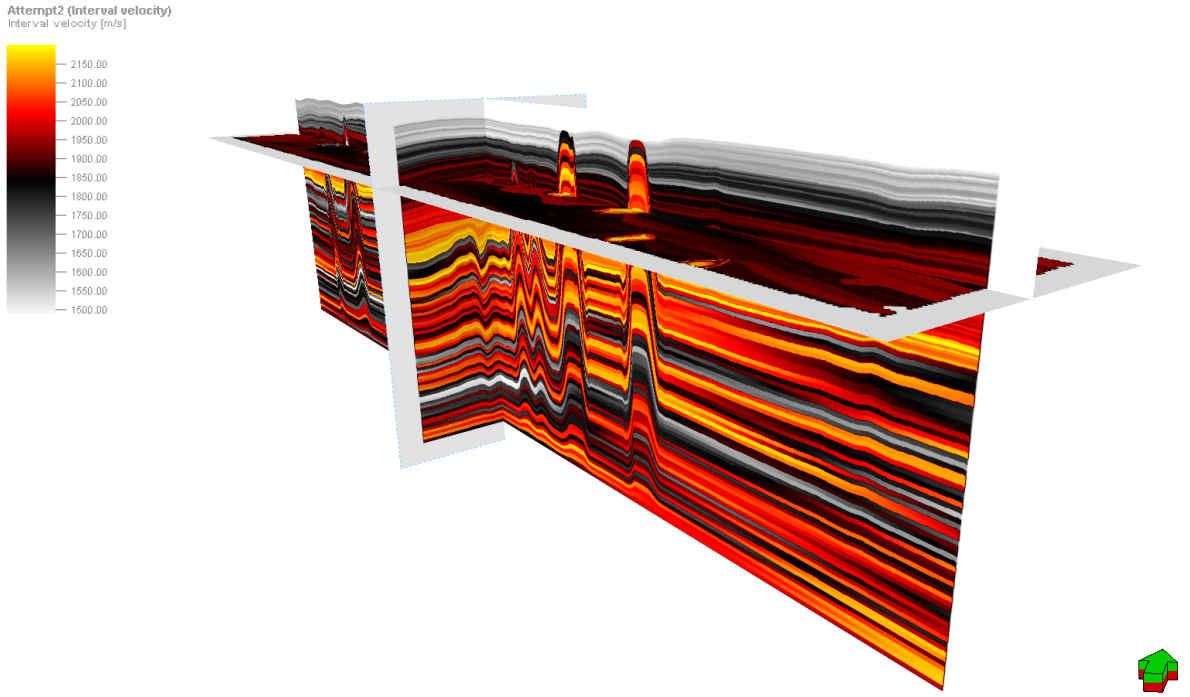

Figure 43 - Synthetic velocity field model that is converted to SEG-Y model VE = 4 (Vertical exaggeration).

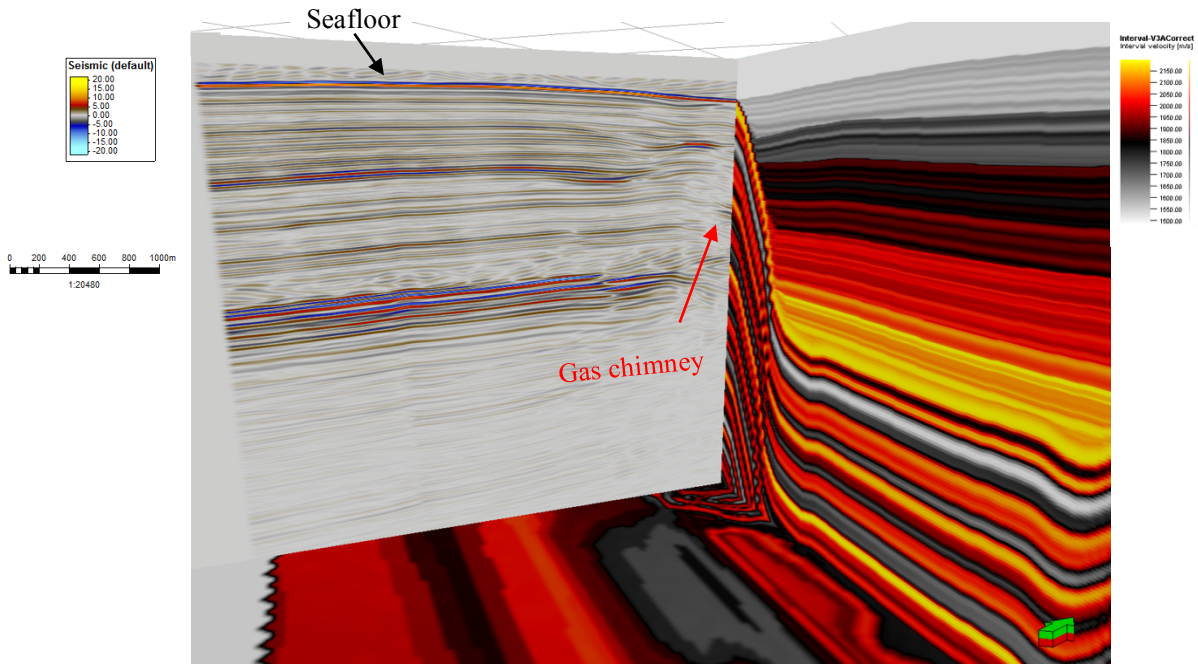

Figure 44 –Intersection of real seismic data in relation to the constructed synthetic velocity model VE = 4 (Vertical exaggeration).

4.4.5 Synthetic seismic data

Finally, with a 3D velocity field model, one can construct synthetic seismic data by finite difference modeling with a density normalized acoustic wave equation.

The main goal was to utilize supercomputer to create a synthetic 3D seismic cube. However, after several attempts of doing so in the powerful super-computer by spending more than 40,000 CPU hours in total, the computer crashed and resulted in failure. By investigating the process protocol, it was clear that amount of available memory per core needed to process this data was insufficient (2 Gb per CPU). Even by narrowing the size of the 3D cube, and reducing maximum frequency did not change the result, and it was decided to discard the 3D modeling as it would not add any additional scientific value compared to an only focus on 2D modeling. The 2D modeling was done by creating two inlines (number 141, and 167 as seen in Figure 45 and 46), which compared to 3D modeling was less expensive to compute, more time efficient and still gave a very similar result. This was done in Madagascar using 2D finite difference modeling program that solves the acoustic wave equation on a regular workflow. As necessary inputs to the model are the constructed velocity field, the acquisition geometry, and a source wavelet. The result will be further discussed in the following chapters. This is done with the aim of constructing synthetic seismic data to figure out which processing technique that constructs the most accurate representation of the input model (seen in Figure 45 and 46).

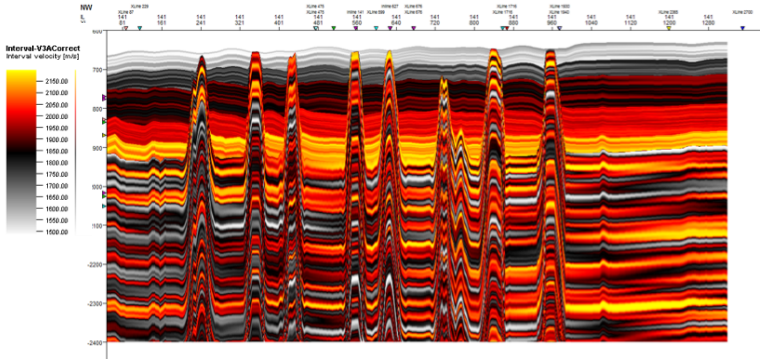

Figure 45 - Inline 141 of the velocity model (p-wave) used to create synthetic seismic data, X =8.04 km and Y = [0,2400] ms.

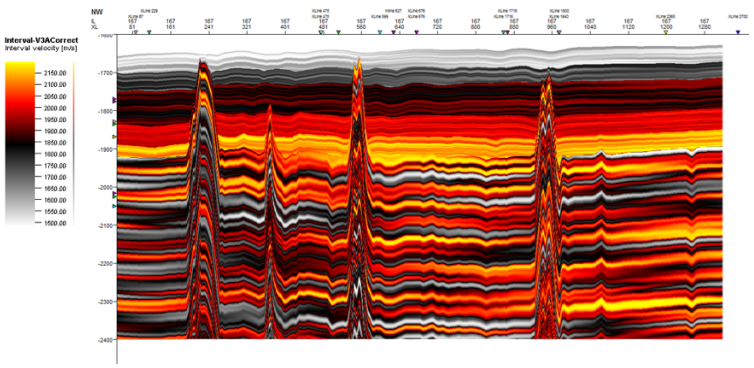

Figure 46 - Inline 167 of the velocity model (p-wave) used to create synthetic seismic data, X =8.04 km and Y = [0,2400] ms.

4.5 Processing of synthetic seismic data

This subchapter will discuss the imaging steps applied to the different synthetic 2D seismic inlines. The processing was done with the aim of applying similar processing steps as the actual seismic data. As this includes steps such as: geometry assignment, prestack time migration, brute stack (with NMO), poststack F-X (Y) deconvolution, and Stolt migration to be consistent, a detailed description is therefore not included to avoid repetition. However, synthetic data differs from the real seismic data as it contains information concerning interval velocity, which is an added value that allows the data to be migrated with even fewer uncertainties. Prestack time migration and reversed time migration were applied to the synthetic data in two steps corresponding to migration with constant velocity (wave propagation speed in water; 1480 m/s) or with the actual velocity field constructed for this model, and will be further discussed.

4.5.1 Reverse time migration

Reverse time migration that was performed on the synthetic seismic data is a depth migration method based on the acoustic wave equation. This method assumes that the acoustic medium has no shear modulus (μ) and the simplest wave equation that respects the kinematics of P-wave propagation through the subsurface are listed below (4):

Equation 4 – Simple wave equation

$$\left[\frac{1}{v_p^2(x)}\frac{\partial^2}{\partial t^2} - \nabla^2\right] p(x,t) = -\nabla \mathrm{F}(\mathrm{x},\mathrm{t})$$

∇: generic function, p: scalar coefficient, v_p: velocity, t:traction vector, F: arbitrary function , x: distance

It is solved either explicit or implicit by methods based on differential/spectral calculations. This method is one of the most commonly used approximations in seismic processing, explained by the fact that only the isotropic P-wave velocities need to be known to solve the equation (Weibull, 2014). Compared to Kirchhoff migration, reverse time migration computes numerical solutions to the wave equation in full extent, which makes it potentially more accurate (Yoon et al., 2003). Methods that are calculated by directly using wave equations often tend to have good amplitude control and result in very coherent images without losing resolution. However, the use of finite difference techniques also tends to be quite expensive and require the data to be interpolated to the regular grid before migration (Liner, 2003). Research of reverse time migration has shown good results handling steep dipping structures and strong velocity contrasts (Baysal et al., 1983). The reverse time migration was used to migrate two synthetic seismic inlines; 141, and 167, each with a constant velocity of 1480 m/s and with the actual 2D velocity model.

5. Results

This chapter will address the results of the main imaging steps, description and comparison of the data from Vestnesa Ridge and Snøhvit, with a separated subchapter examining the synthetic 2D seismic sections. The results will be listed in the same order as the processing steps were applied.

5.1 Bin size determination

In determination of bin size, many attempts both for Vestnesa Ridge and Snøhvit were conducted with bin size ranging from 12.5 x 12.5, 9.375 x 9.375, 6.25 x 6.25, 6.25 x 3.125, to 3.125 x 3.125 m (inline in meters, crossline in meters). After processing each data set, comparing them resulted in focusing on two bin sizes corresponding to 6.25 x 6.25 and 6.25 x 3.125. The bin gridding of 6.25 x 6.25 obtained higher resolution than the ones with coarser bin sizes and showed good signal-to-noise ratio without a significant amount of migration artifacts, noise bursts or blanking (empty traces). The decision of keeping 6.25 x 3.125 m bin size was based on the optimal theoretical bin size given by the acquisition geometry. By comparing the two bin sizes as seen in Figure 47 with 48, and 49 with 50, one can argue that 6.25 x 6.25 still provides a better result regarding imaging than 6.25 x 3.125 as it obtained the lower number of migration artifacts marked in red circles and higher signal-to-noise ratio. The lower signal-to-noise ratio in 6.25 x 3.125 m is even more evident in Figure 49 - 50, which displays stacked data with automatic gain control with an operator length of 100 m. Consequently, the result from here on will mainly be based on the binning size of 6.25 x 6.25 m.

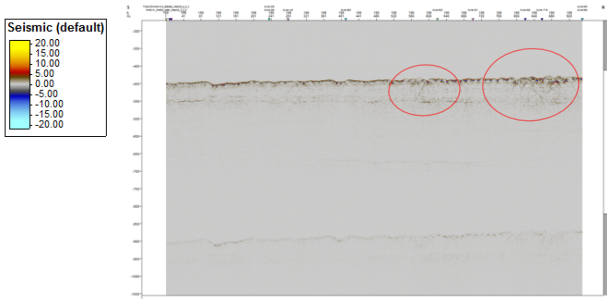

Figure 47 – Stacked; bin size of 6.25 x 6.25, Snøhvit

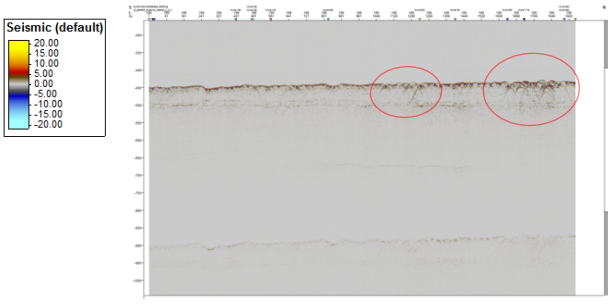

Figure 48 – Stacked; bin size of 6.25 x 3.125, Snøhvit

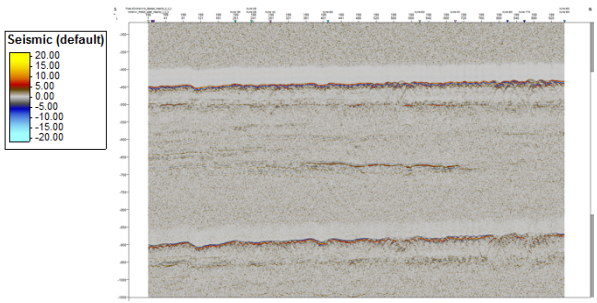

Figure 49 – Stacked, AGC: 100, 6.25 – 6.25 m

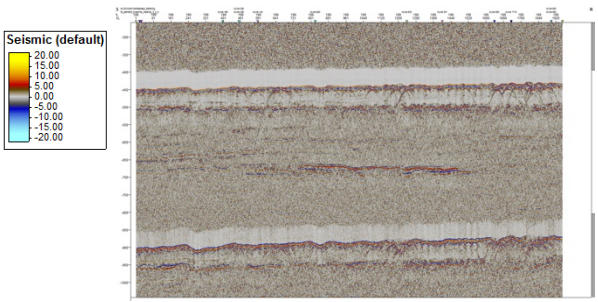

Figure 50 – Stacked, AGC: 100, 6.25 – 3.125 m

Peak frequency for both data set is ~250 Hz, which correspond to resolution (λ/2) of 2.96 m, but the dominant frequency for Vestnesa Ridge is 175 Hz correspond to (resolution) 4.22 m and Snøhvit 4.77 m. Bin size below this resolution limit given by (λ/2) will not contribute to any added value, and should be avoided based on the results of finer bin size.

5.2 Snøhvit

5.2.1 Brute Stack

The result of the initial brute stack of Snøhvit P-Cable 3D seismic data can be seen below in Figure 51. This process was completed in SeisSpace ProMAX and ran for approximately 25 minutes on the workstation. On the initial inspection of the seismic section, one can notice that the seafloor reflector is a tremendously brighter reflection, which leads to an abnormal distribution of the amplitude response below. Even other bright reflections such as the Upper Regional Unconformity (URU) at approximately 500 ms (milliseconds) are barely visible, and dipping beds or structures associated with Snøhvit field are basically invisible. Worth noticing is that the seafloor multiples are at ~900 ms and since P-Cable 3D seismic usually image structures at twice the water depth from sea-surface (~800 ms in this case) it was decided to focus the attention to the two-way travel time range of [0,800] ms. At the interval of 450 – 500 ms un-migrated events such as hyperbolas as a true expression of diffraction, which comes from points, tips, and edges. Discontinuities with high curvature possibly related to iceberg plough-marks cause bow-tie effect. These are all events, in addition to coherent and incoherent noise, beneficial to remove, thus improving overall imaging and signal-to-noise ratio.

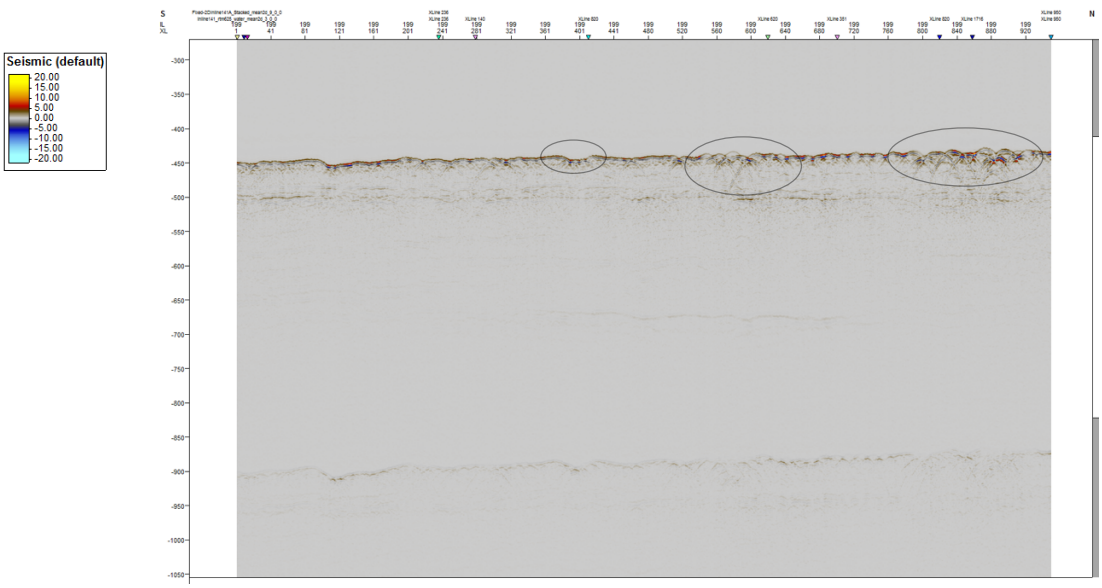

Figure 51 – Seismic inline 199; of brute stacked Snøhvit data with a bin size of 6.25 x 6.25, black circles are highlighting processing artifacts, x=5.94 km and y= [0,1050] ms (TWT) with an increment of 100 ms.

5.2.2 F-XY deconvolution

Next step was to apply F-XY deconvolution to improve the continuity of the reflections in the data and attenuate incoherent noise. This was also done in SeisSpace ProMAX on the available workstation with a running time of 35 minutes. By comparing the sections after F-XY deconvolution as seen in Figure 52, with the initial stacked data (Figure 51), one can clearly notice that the amplitude response of seafloor in a more continuous, slightly more detailed in shallow depths (450 – 500 ms), and generally less random noise. However, hyperbolas, bow-tie effect, and random noise are still distorting the image, marked with black circles. Due to adamant reflectors (sub-seafloor, and URU), Figure 52 still show skewed amplitude distribution.

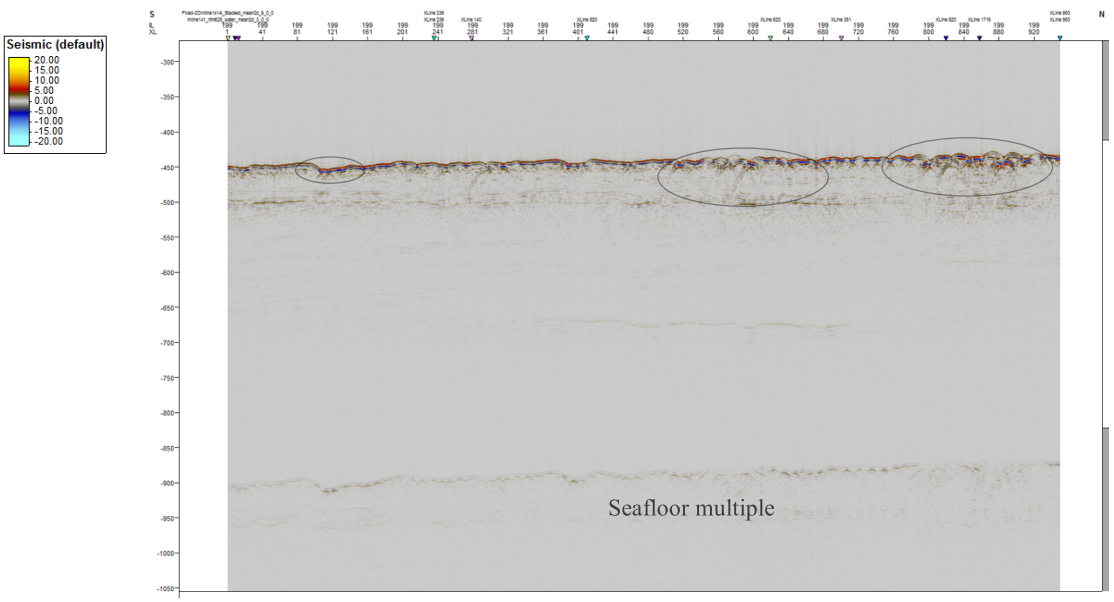

Figure 52 – Seismic section of post-stack F-XY deconvolution data, inline 199, bin size 6.25 x 6.25, x=5.94 km and y=[0,1050] ms (TWT) with an increment of 100 ms.

5.2.3 Missing data interpolation

Interpolation of Snøhvit 3D seismic data was accomplished by using the open source Madagascar software, by utilizing the missing data interpolation technique which was based on a Scons script (Appendix B). As the setup of this process was not parallelized, which meant that only one core was running simultaneously, consequently resulting in processing time of approximatly16 hours by running on 100% memory and single core. The result was not that different from the input as the data from Snøhvit did not have that many areas with dead or missing traces. Another interpolation method called inverse distance weighting was also tested by discarded as it did not account for dipping layers, shown as staircase effect.

5.2.4 Automatic gain control

The automatic gain control operation is a massively discussed technique that does not preserve the nature of the amplitude response. Even though it was still considered necessary in this case, as the seafloor reflector dominated the response distribution making underlying reflectors more or less invisible. This operation was accomplished in SeisSpace ProMAX software and was completed on the 3D seismic data within a few minutes. As mentioned in the previous chapter, several trials were conducted with various operator lengths, by trying coarser and finer gain operation, but an operator length of 100 ms showed the best relation between signal and noise. Important to notice is that this technique was only utilized purely for the purpose of visualizing the morphology with its structural features. It was decided to add this process in order, after interpolation to easily compare the result of migration processes that follows, even though this method can be applied at any stage. The result of this process can be seen in Figure 53, displaying inline 199, as underlying structures below seafloor such as dipping beds and faults are to some extent outlined. The image is still quite affected by artifacts as automatic gain control multiplies (power) both the signal and noise, e.g. seen as noise cloud above seafloor at a time interval of 0 – 400 ms. Worth noticing is the semi-continuous strong reflector at 650 – 700 ms that might be the result of captured gas generating strong impedance and the evident seafloor multiple at 900 ms.

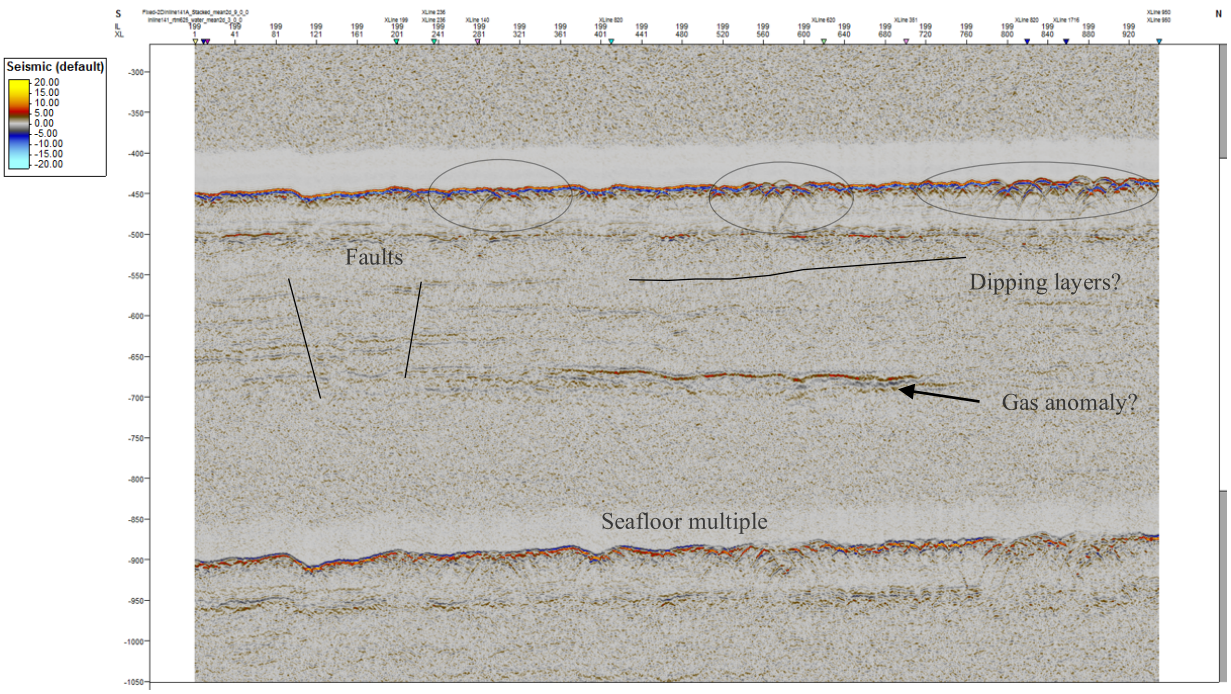

Figure 53 – Seismic section is displaying the effect of automatic gain control with operator length of 100 m applied on post stacked data, inline 199, 6.25 x 6.25 bin size, x=5.94 km and y=[0,1050] ms (TWT) with an increment of 100 ms.

5.2.5 Stolt migration

The Stolt migration with constant velocity (1480 m/s) was completed by using SeisSpace ProMAX on the available workstation. As mentioned previously, several trials were conducted with different parameters (Appendix B) with varying running time depending on bin size (~2-4 hours), although the optimal results without gain correction can be seen in Figure 54 and 55, migrated stack, and migrated stack filtered by F-XY deconvolution respectively. By comparing the before and after (input and output) of this process, one can easily see that migration relocate the amplitude response and remove most of the hyperbolas, as seen in the original stack and F-XY data (Figure 51, 52). However, migration artifacts such as noise bursts are generated, which is evident above the seafloor reflector. By comparing the Figure 51 with 52, the differences are not that obvious, but in small scale, one can notice that the main reflectors, including the Upper Regional Unconformity, are more continuous after applying F-XY deconvolution and Stolt migration. After migration hyperbolas and the bow-tie effect collapse to points. However, noise, which is not a true expression of wave phenomena are not correctly migrated and appears as smiles. Also, if the velocity is not accurate for migration, the hyperbolas will also not be fully collapsed.

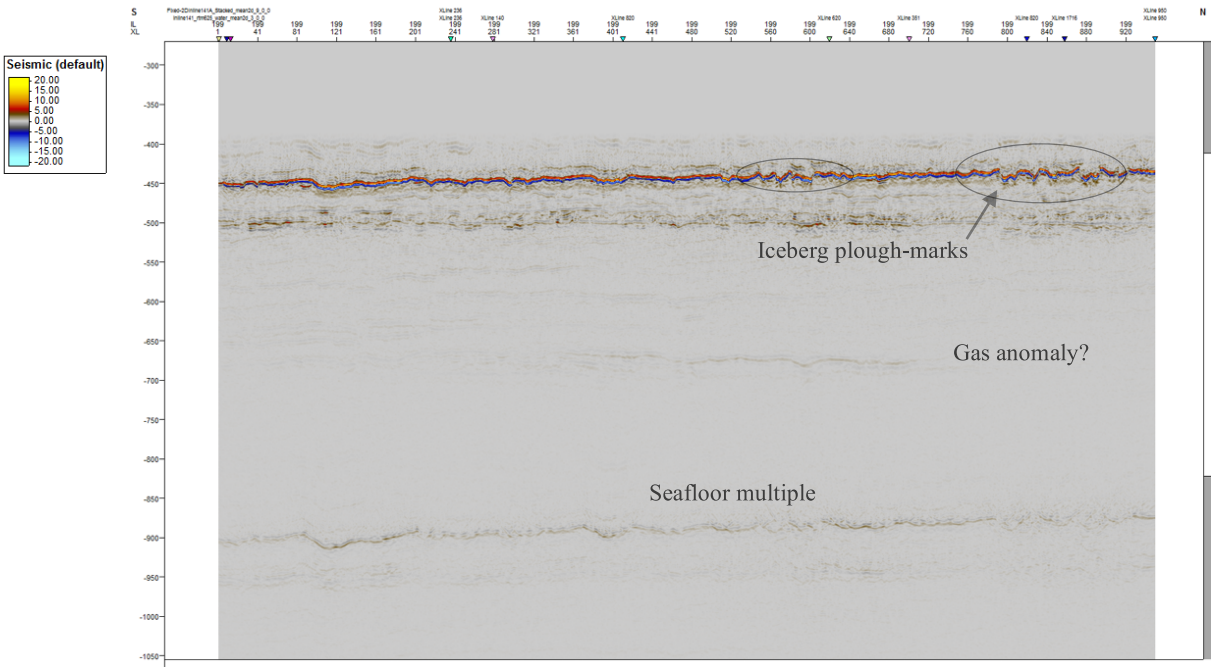

Figure 54 - Poststack Stolt migrated data, inline 199, 6.25 x 6.25 bin size, x=5.94 km and y=[0,1050] ms (TWT) with an increment of 100 ms.

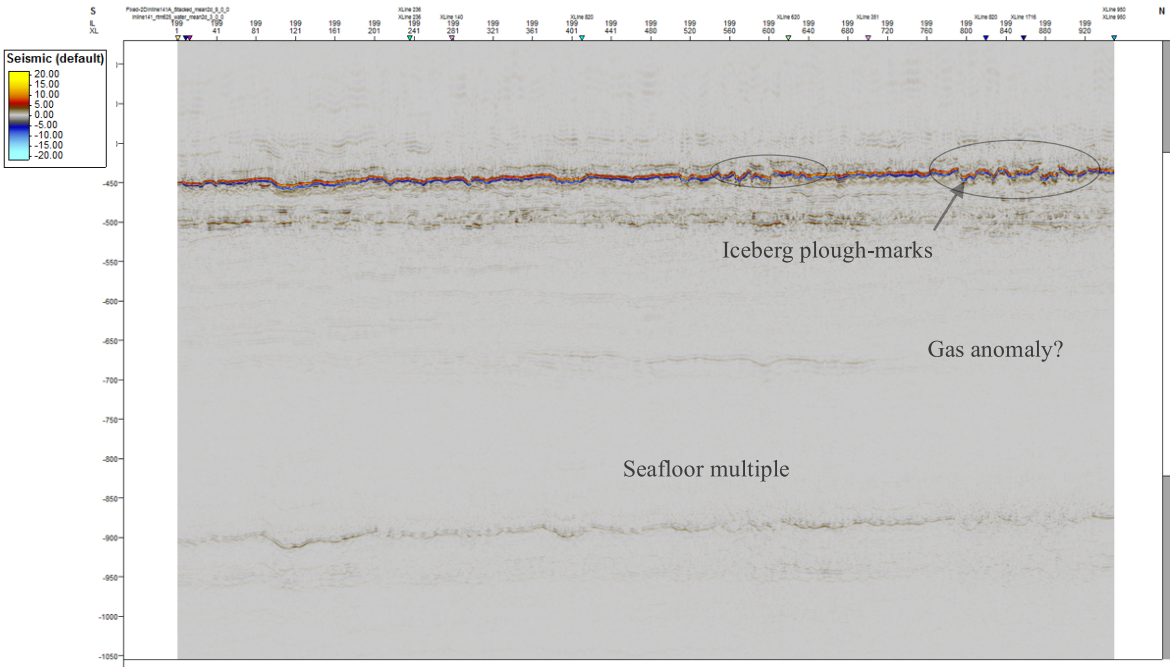

Figure 55 - Seismic section of Stolt migrated poststack F-XY deconvolved data, in line 199, 6,25 x 6.25 bin size, x=5.94 km and y=[0,1050] ms (TWT) with an increment of 100 ms.

5.2.5.1 Stolt migration: Automatic gain control

The result of applying automatic gain control with AGC scalar set to mean of the Stolt migrated data, seen in Figure 56 below. Similarly, as for stacked data, by adding the automatic gain control one get more details of the subsurface, even though the real amplitude relationship is distorted. Something worth noticing is that the seismic section in Figure 56 is carried out with a bin size of 6.25 x 3.125 m, which is quite clear as it shows bursts related to sharp edges of the seafloor. However, this section generally captures more details of the subsurface than in Figure 54 and 55.

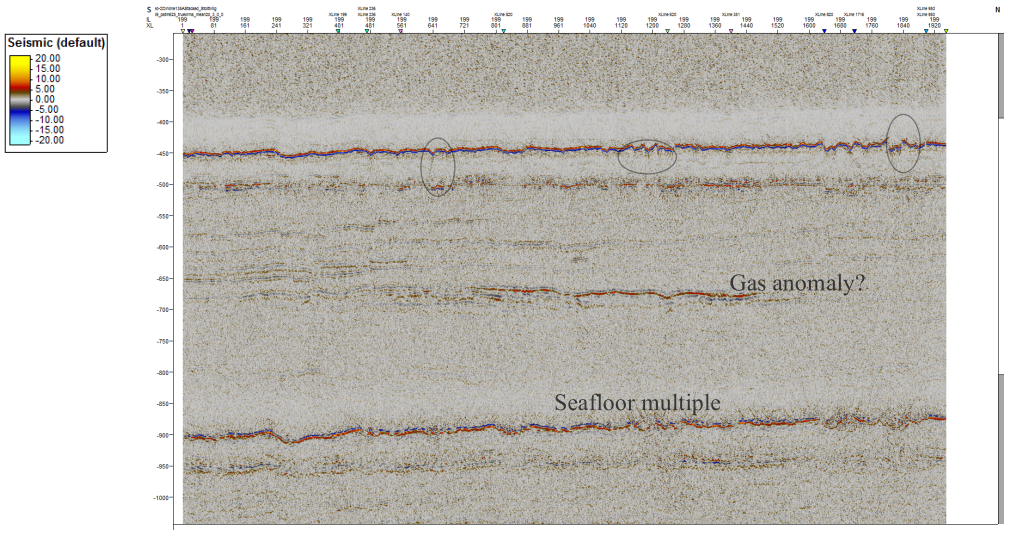

Figure 56 - Seismic section displaying the result of applying Stolt migration, poststack F-XY deconvolution, and automatic gain control, in line 199, 6,25 x 3.125 bin size, x=5.94 km and y=[0,1050] ms (TWT) with an increment of 100 ms.

5.2.5.2 Stolt migration: Noise expression

Furthermore, Figure 57 below consists of two Stolt migrated sections, Figure 57 A displays the southern part of Figure 55, while Figure 57 B shows the result of Stolt migration after applying automatic gain control (operator length of 100 ms) and noise attenuation in GeoTeric. The noise suppression is a two-stage process, starting with applying Random noise filter (TDiffusion; 15 iterations) and aggressive noise attenuation (SO filter; filter size of 3, and dip azimuth filter size of 15). By comparing those two, Figure 57 A and Figure 57 B, there is a significant difference in the vertical domain as dipping and tilted layers, fault blocks and structural features such as graben are now visible in the seismic record (B). Both sections shown are defined by top and base at 400 and 800 ms respectively. As for imaging quality in terms of highlighting the morphology, and structural features at Snøhvit, section B shows significantly better vertical and consequently lateral continuity and resolution, which for an interpreter would be beneficial in estimating volumes. The hand-lens corresponding to B shows a close-up view of fault interpretation of structures not easily seen in A. However, this detailed view also unveils incoherent random noise as small dots all over the image with some coherent noise.

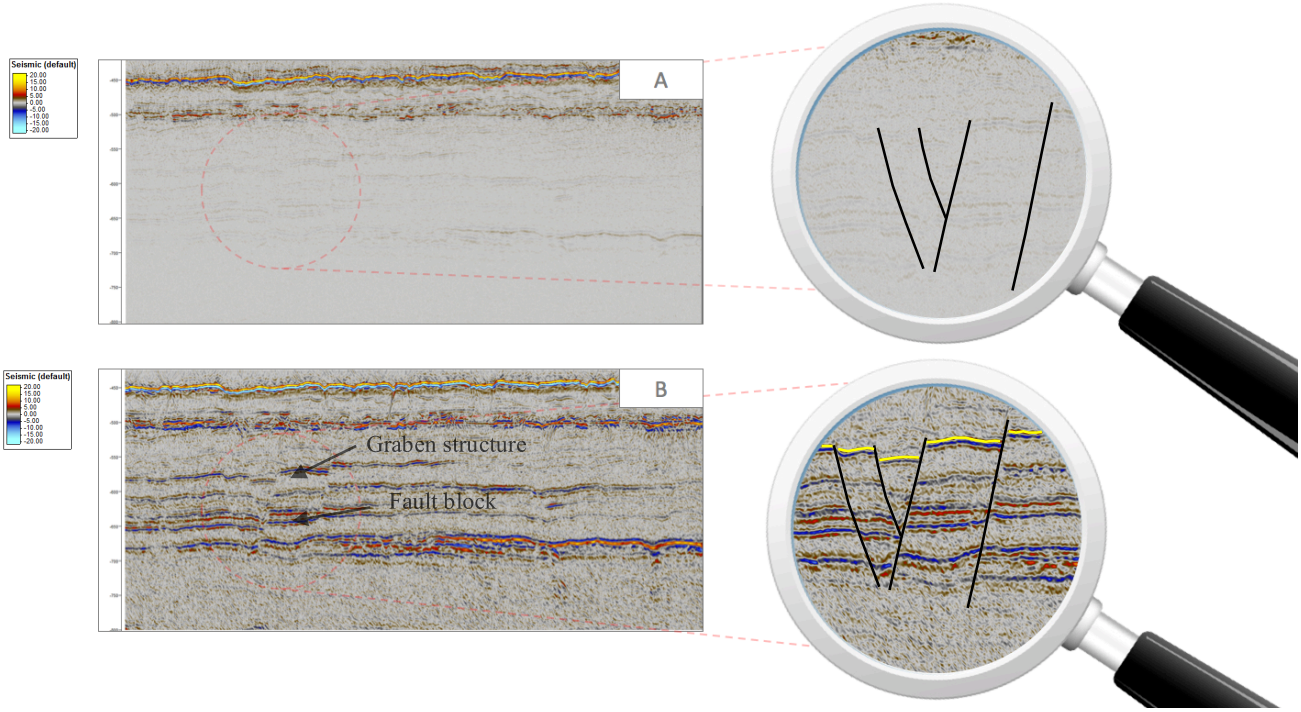

Figure 57 - Two seismic sections that display the result of automatic gain control; A) Stolt migration of poststack F-XY deconvolution data, B) Automatic gain control (100 m in operator length) applied on the same data as in A. Inline 199, 6.25 x 3.125 bin size, x=2.85 km and y= [350,800] ms (TWT) with an increment of 100 ms.

The final result of poststack F-XY deconvolution, Stolt migration, missing data interpolation, automatic gain control, and, noise expression can be seen in Figure 58 and 59, with a bin size of 6.25 x 3.135 m and 6.25 x 6.25 m respectively. By comparing those two, noise bursts in 6.25 x 3.125 are not as evident as in 6.25 x 6.25 m, seen in the highlighted black circle. The signal-to-noise ratio is therefore considerably lower in 6.25 x 3.125 m bin gridding, but the overall resolution is still quite similar. However, one might argue that the lateral amplitude response is slightly more continuous in the section with a bin size of 6.25 x 3.125 m. The hyperbolas and bow-tie effect related to diffraction and sharp boundaries can be seen more prominent in 6.25 x 3.125 as marked by red circles.

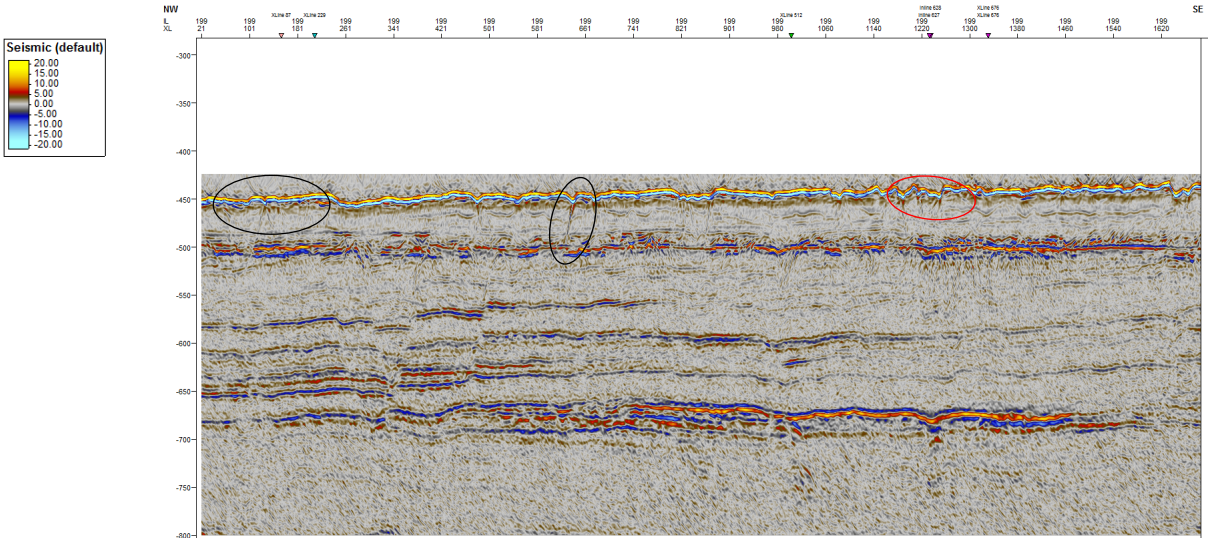

Figure 58 - Seismic section as result of Stolt migrated poststack F-XY deconvolution, Automatic gain control. Missing data interpolation, Noise expression (2 stage), in line 199, 6,25 x 3.125 bin size, x=2.85 km and y= [350,900] ms (TWT) with an increment of 100 ms.

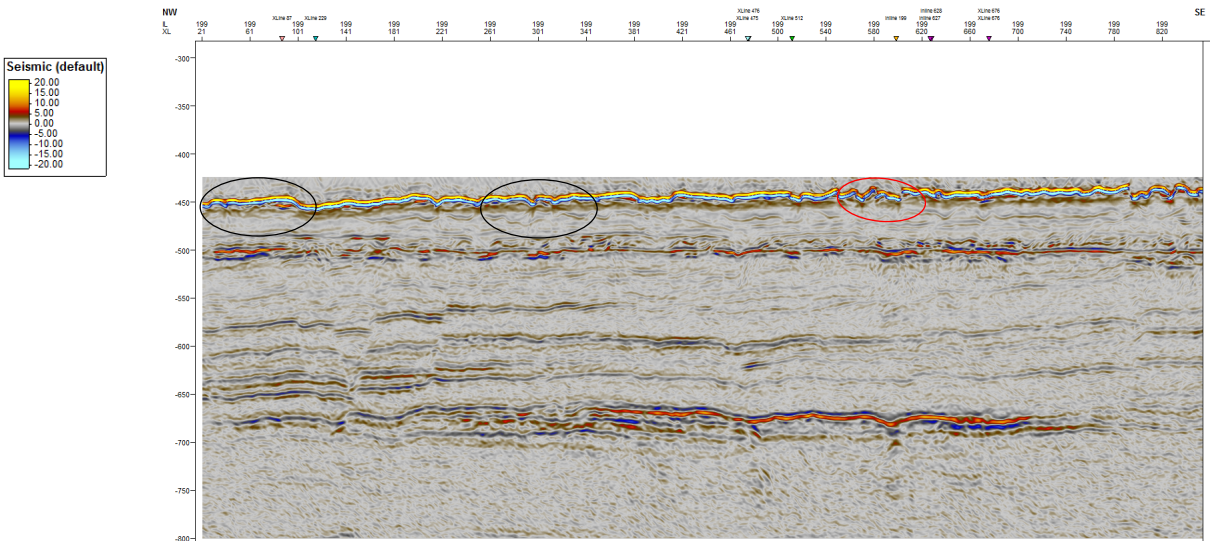

Figure 59 - Seismic section as result of Stolt migrated poststack F-XY deconvolution, Automatic gain control. Missing data interpolation, Noise expression (2 stage), in line 199, 6,25 x 6.25 bin size, x=2.85 km and y= [350,900] ms (TWT) with an increment of 100 ms.

5.2.6 Prestack time migration

Two different software (SeisSpace ProMAX, and Madagascar) were tested to perform prestack time migration due to processing efficiency. Both was based on Kirchhoff time migration, but SeisSpace ProMAX took 18 days to complete, whereas Madagascar only used 16 hours to do the same. The result of imaging in the open source software, Madagascar, can be seen in Figure 60. Compared with the result from performing Stolt migration (Figure 54 and 55), the amount of details is quite similar, with low vertical resolution, and maybe even more noise. One might also argue that the response signal of the sea floor in the prestack time migrated data is more prominent, consequently generating even weaker amplitude response of the reflectors down below, when compared to the Stolt migrated sections.

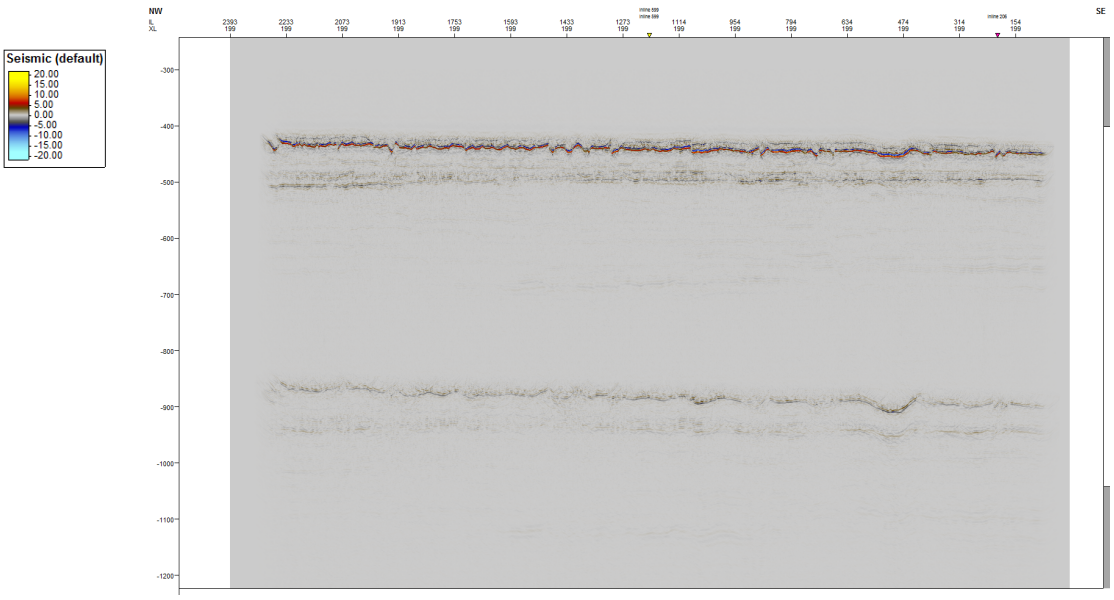

Figure 60 - Seismic section as result of prestack time migration performed in Madagascar, inline 199, 6,25 x 6.25 bin size, x=5.94 km and y= [350,1200] ms (TWT) with an increment of 100 ms.

5.2.6.1 PSTM: Automatic gain control

Automatic gain control was once again needed to obtain more details below the seafloor, to improve the amplitude scaling and allow structural interpretation. The processing in SeisSpace ProMAX was accomplished by defining the scalar to be computed as a product of mean and operator length as 100 ms (See Figure 61). In Madagascar, the scalar was set to RMS, but with the same the operator length as in ProMAX. The actual processing in both software finished within minutes, and the result from Madagascar can be seen in Figure 62. By comparing Figure 57 and 58, more details below the seafloor are imaged consequently presenting a better structural image. Something worth noticing is that the section shown in Figure 61 is covering everything from 0 - 1200 ms (TWT), including seafloor multiples at 900 ms. The presence of noise is evident by the cloud at 0 - 250 ms and as both coherent and incoherent response further down. Prestack time migration was done in SeisSpace ProMAX show more prominent migration artifacts, and less clear images of the morphology of Snøhvit compared to the same accomplished using Madagascar.

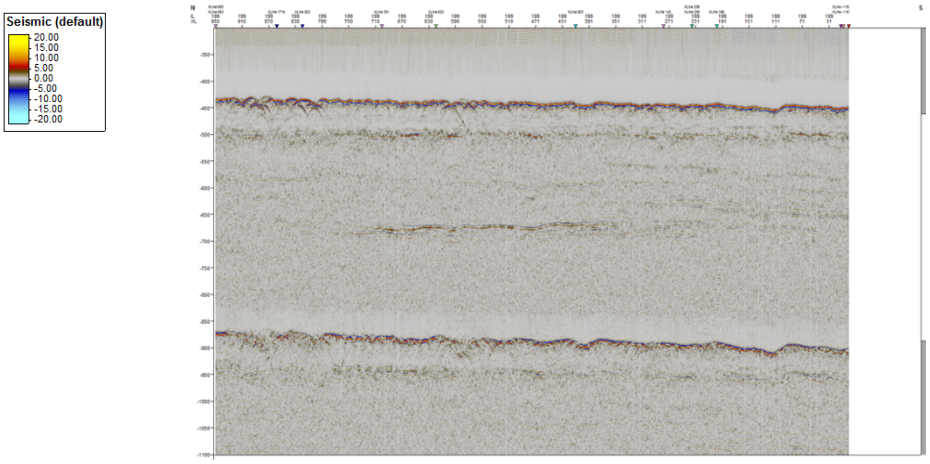

Figure 61 - Seismic section as result of prestack time migration and automatic gain control performed in SeisSpace ProMAX, inline 199, 6,25 x 6.25 bin size, x=5.94 km and y= [350,1200] ms (TWT) with an increment of 100 ms.

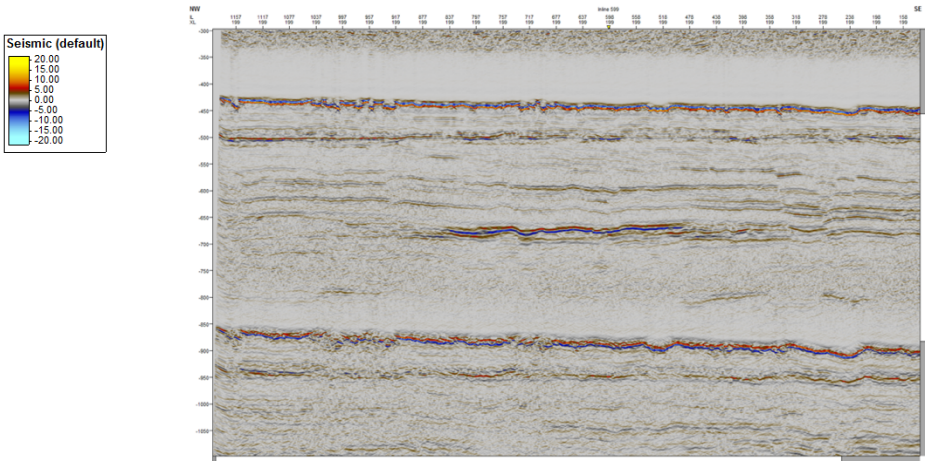

Figure 62 - Seismic section as result of prestack time migration and automatic gain control performed in Madagascar, inline 199, 6,25 x 6.25 bin size, x=5.94 km and y= [350,1200] ms (TWT) with an increment of 100 ms.

5.2.6.2 PSTM: Noise expression

Prestack time migration (PSTM) in both software generated migration artifacts and contained various kind of noise that would be beneficial to remove. The noise expression operation in GeoTeric was therefore used to remove random noise, and aggressive noise by TDiffusion and SO filters, and the results of this operation can be seen in Figure 63 (PSTM completed in SeisSpace ProMAX) and 58 (PSTM performed in Madagascar). It was also decided to cut the seismic record to focus on the time interval between 400 and 800 ms. They both show significant improvement in signal-to-noise ratio. However, Figure 63 still displays migration artifacts, and hyperbolas that were not sufficiently collapsed within the black circles. While Figure 64 show less influence by migration artifacts and better structural representation of the morphology of Snøhvit. The normal faults and graben structure marked within the red circle is more prominent in Figure 64, and the apparent number of continuous reflectors between the seafloor and Upper Regional Unconformity (red arrow) seems to be higher. In addition, dipping layers below the URU are weakly preserved by prestack time migration in SeisSpace ProMAX.

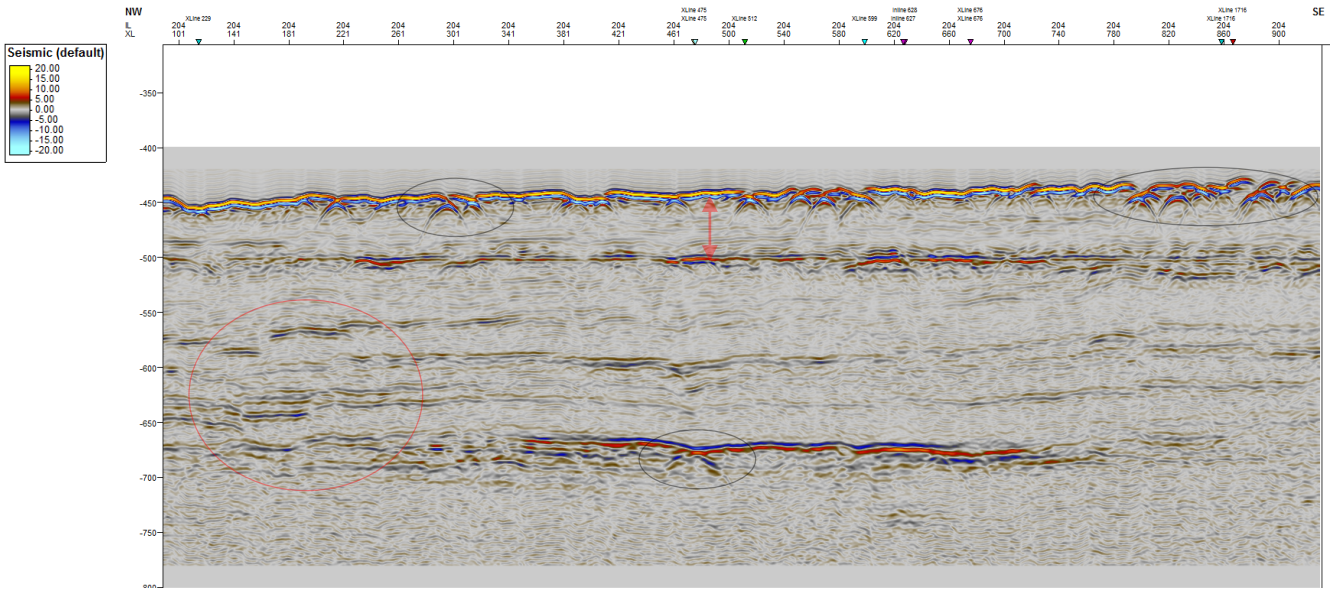

Figure 63 - Seismic section as result of prestack time migration using SeisSpace ProMAX, poststack F-XY deconvolution, Automatic gain control (mean). Missing data interpolation, Noise expression (2 stage), in line 199, 6,25 x 6.25 bin size, x=2.85 km and y= [300,800] ms (TWT) with an increment of 100 ms.

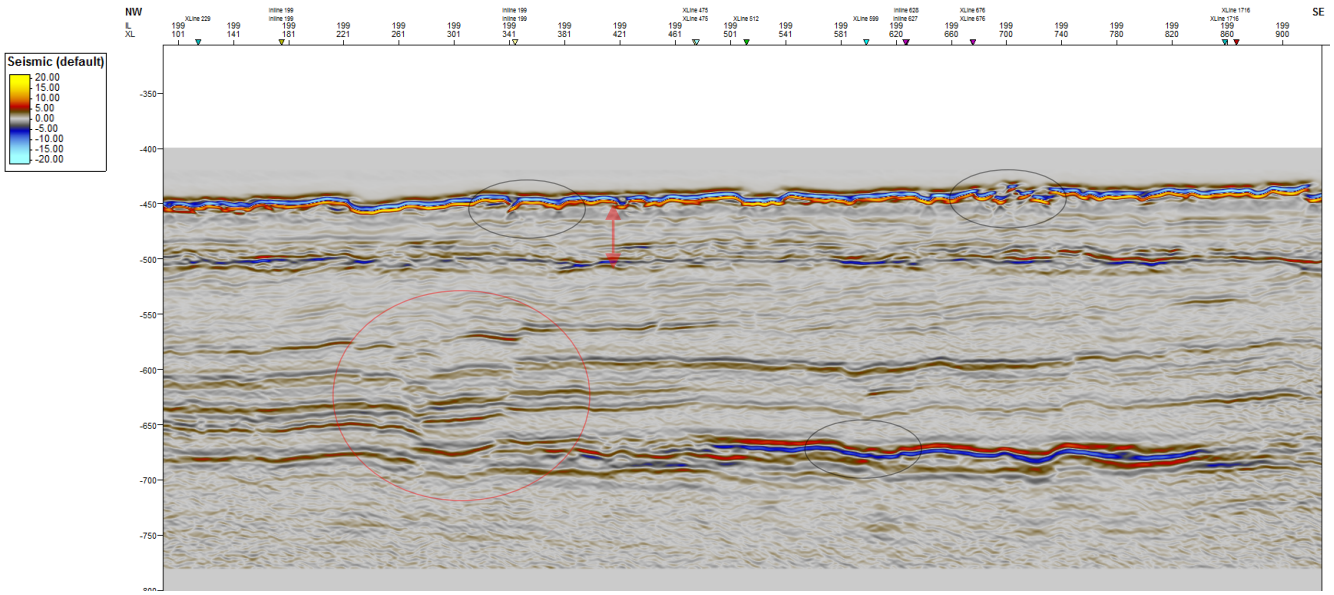

Figure 64 - Seismic section as result of prestack time migration using Madagascar, Automatic gain control (RMS), Noise expression (2 stage), in line 199, 6,25 x 6.25 bin size, x=2.85 km and y= [300,800] ms (TWT) with an increment of 100 ms

Based on this, prestack time migration completed using Madagascar show a more detailed representation of the subsurface, preserving sharper and well-defined edges, layers, and features when compared to similar processing in SeisSpace ProMAX.

5.3 Vestnesa Ridge

In the following subchapter, processing of Vestnesa Ridge 3D prestack seismic data will be presented as the preliminary result, for each main processing step. For some processes, results will be shown by two inlines; 141 and 167, which are the same inline used to make synthetic seismic data. The position of each inline can be seen in Figure 65, in relation to the interpreted seafloor in time.

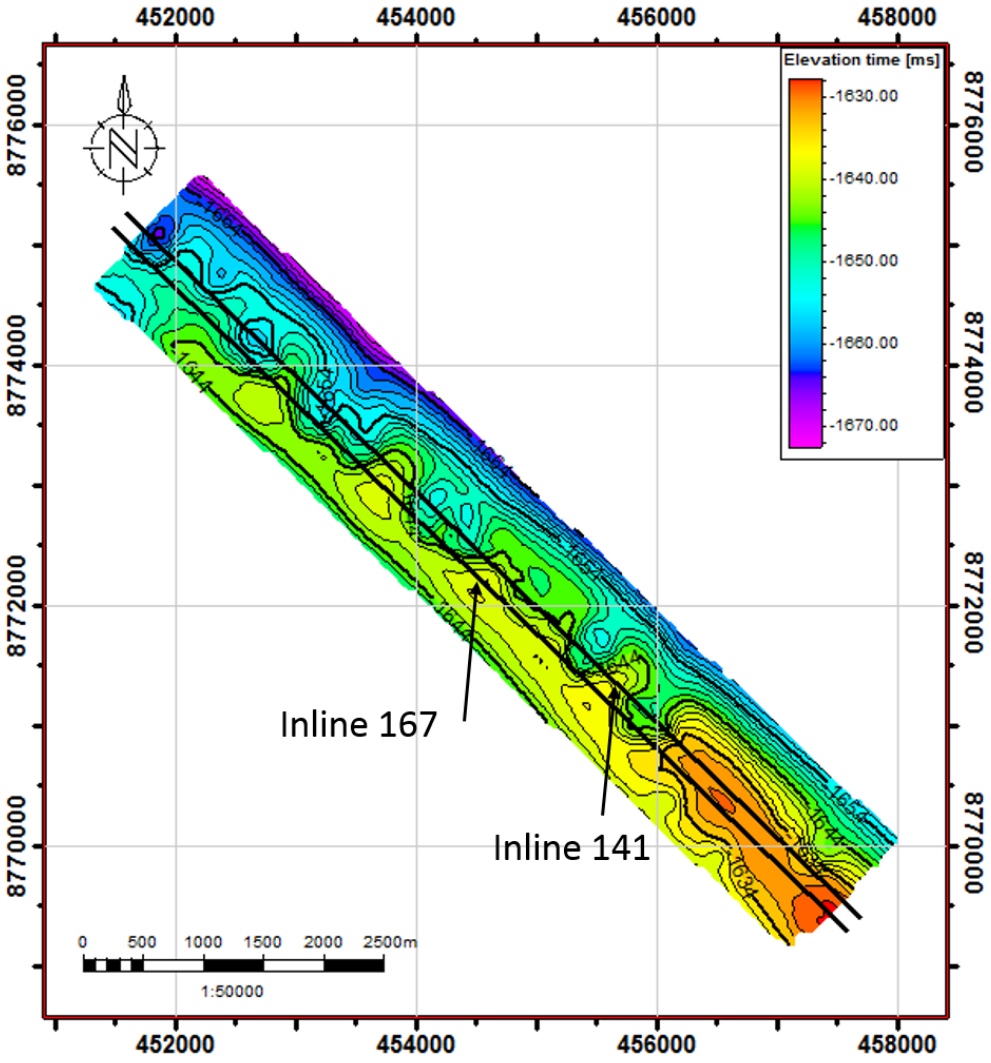

Figure 65 – Overview of the position of inline 141 and 167 in relation to the interpreted seafloor at Vestnesa Ridge in time.

5.3.1 Brute stack

The first process after applying geometry correction and binning of 6.25 x 6.25 were stacking the data, and the result of the initial brute stack of Vestnesa Ridge P-Cable 3D seismic data can be seen below in Figure 66. The two-way time interval that is of interest for this project ranges from ~ 1600 ms to 2400 ms. The brute stack was completed in SeisSpace ProMAX, which included normal moveout correction with constant velocity (1480 m/s), and ran for approximately 45 minutes on the workstation. By comparing Vestnesa Ridge and Snøhvit seismic data, one can notice that the seafloor reflector (~1650 ms) is not as sharply defined in Vestnesa Ridge, whereas Snøhvit data it is and consequently create an abnormal distribution of amplitude responses below. The bottom-simulation reflector (BSR) is weakly shown at ~1900 ms. However, Figure 65 display generally horizontal stratified section with some gas chimneys that are seen as chaotic reflectors that cause blanking effect, creating pockmarks at the seafloor and marked by the black arrows. Evidence of diffraction typically arises from the sidewall of the chimneys, marked with red arrows. Noise seen as black dots concentrated around the major reflectors may be related to as boundary-generated incoherent noise.

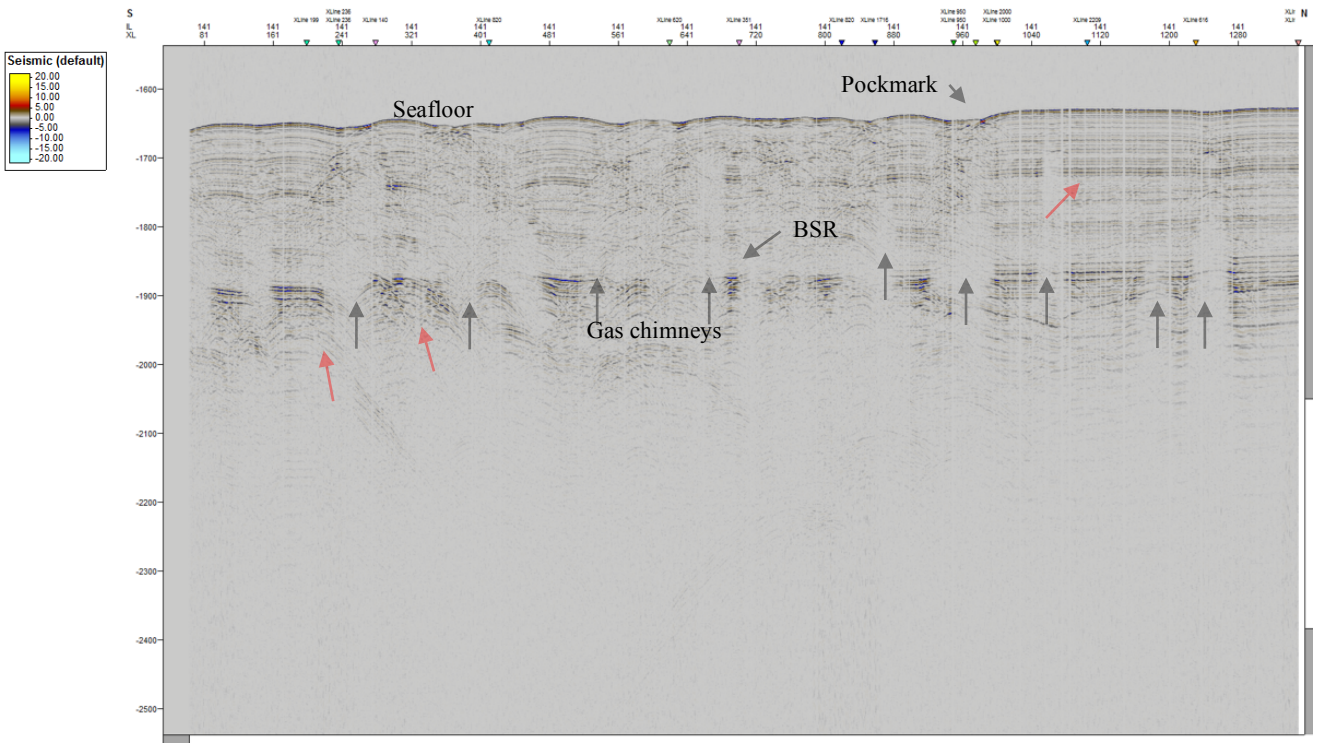

Figure 66 - Seismic section displaying the initial stack of Vestnesa Ridge, 6.25 x 6.25 m bin size, x = 8.44 km and y = [1500,2700] ms (TWT) with an increment of 100 ms, inline 141.

5.3.2 F-XY deconvolution

Next step after stacking the data was to apply F-XY deconvolution to improve the continuity of the reflections in the data and attenuate incoherent noise. This was done in SeisSpace ProMAX on the available workstation with a computing time of 45 minutes. By comparing inline 141 after F-XY deconvolution as seen in Figure 67 with the stack data (Figure 66), one can notice that the amplitude response is normalized making the seafloor reflector more continuous; it also shows slightly more details in shallow depths (1650 – 2400 ms) and generally less noise. Empty traces creating a stripy pattern and random noise are now visible as marked out. However, diffraction pattern such as hyperbolas remains visible after F-XY deconvolution.

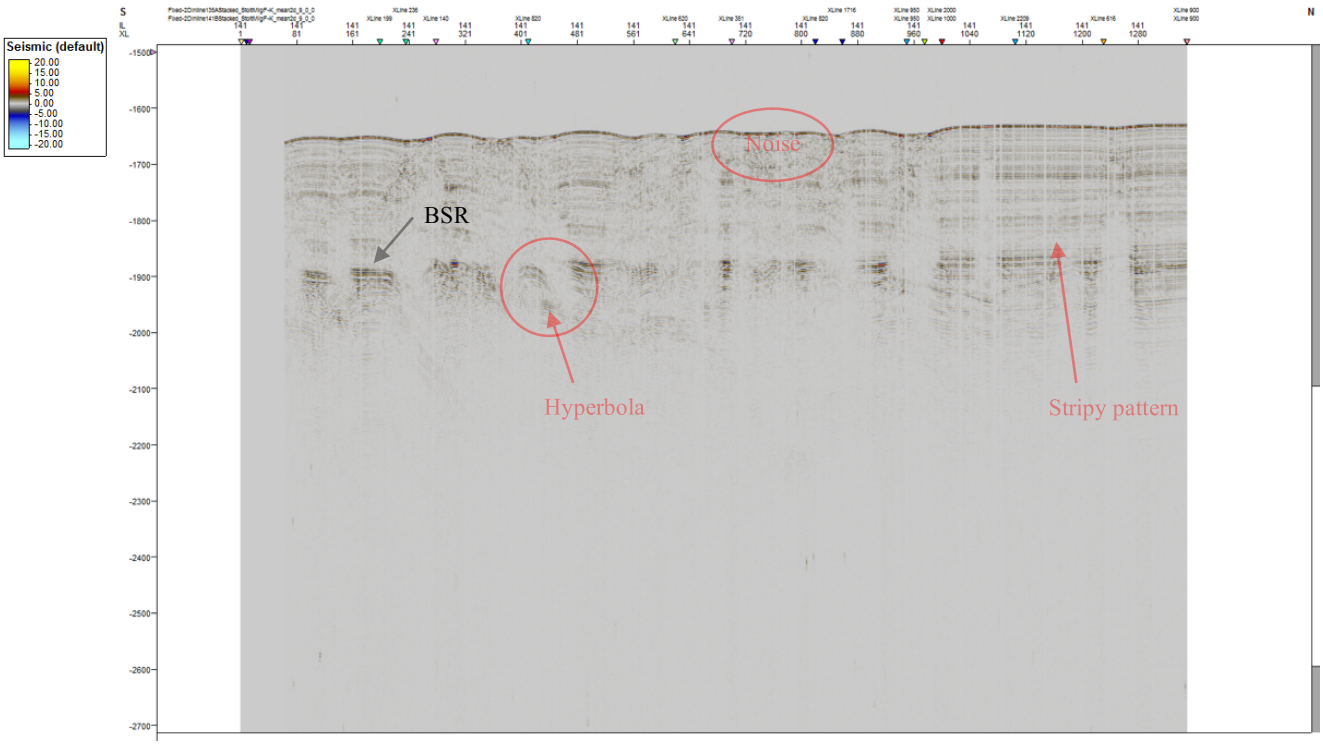

Figure 67 – Seismic inline 199 displaying data processed by poststack F-XY deconvolution, bin size of 6.25 x 6.25 m, x = 8.44 km and y = [1500,2700] ms (TWT) with an increment of 100 ms.

5.3.3 Missing data interpolation

Interpolation of Vestnesa Ridge 3D seismic data was accomplished by using the open source software, Madagascar, by utilizing the missing data interpolation technique which was based on a scons script (seen in Appendix B). As the setup of this process was not parallelized, meaning that only one core was running simultaneously, consequently leading to low processing efficiency, taking approximately 26 hours running time on 100% memory and single core. This process was surprisingly efficient as in areas with dead or missing traces most of the gaps and stripy patterns were filled, and the results can be seen in Figure 68. The white stripy pattern is now barely visible as areas with dead/ zero-fold have been interpolated.

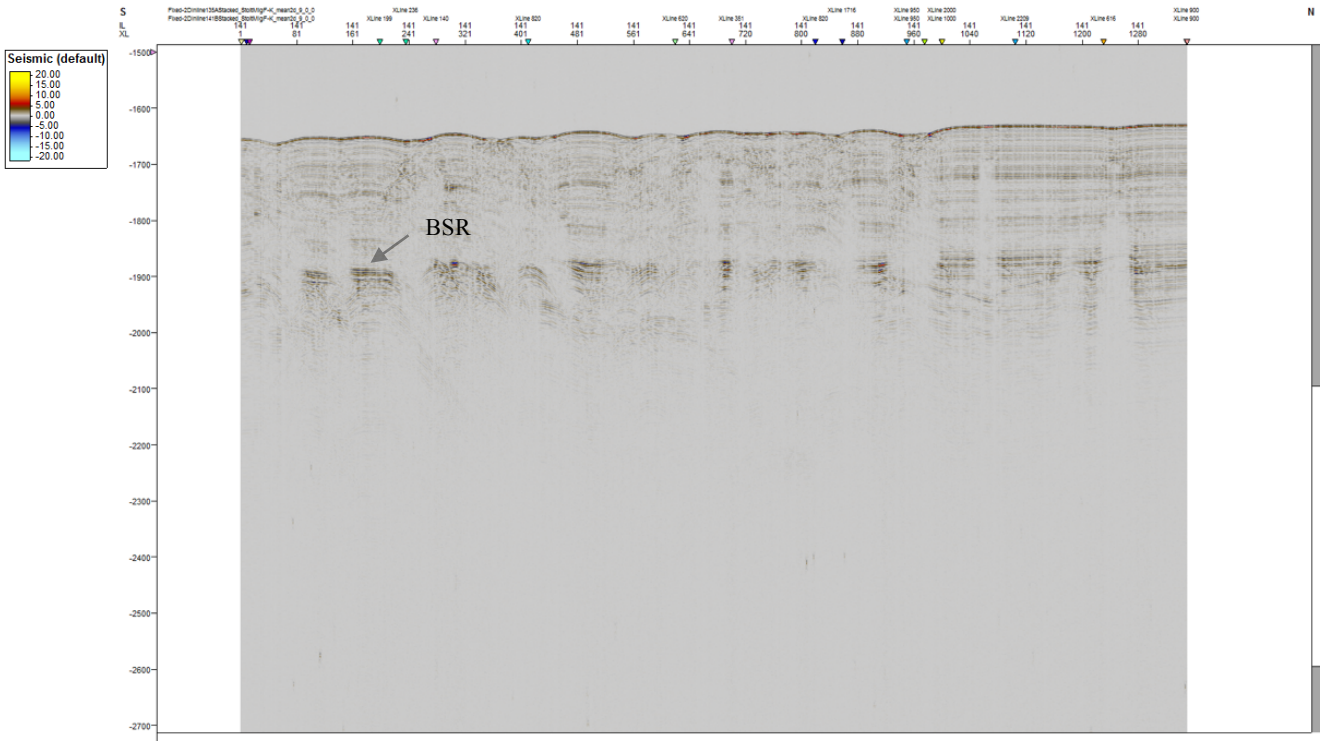

Figure 68 - Seismic section of data processed by poststack F-XY deconvolution and missing data interpolation. Inline 141, bin size of 6.25 x 6.25, x=8.44 km and y=[1500,2700] ms (TWT) with an increment of 100 ms.

5.3.4 Stolt migration

The Stolt migration was carried out with constant velocity (1480 m/s) and computed by using SeisSpace ProMAX on the available workstation. As mentioned previously, several trials were conducted with different parameters (Appendix B), with varying running time depending on bin size (~3-5 hours), although the best results obtained without gain correction can be seen in Figure 69 and 70, as migration of stack, and migrated of stacked and filtered by F-XY deconvolution respectively. By comparing the before and after (input and output) of this process, one can easily see that the migration relocates the amplitude response and collapses most of the hyperbolas as seen in the original stack, and F-XY data. The BSR is also much more evident compared to previous results (Figure 66 to 68). However, migration artifacts such as noise bursts are generated and boundary-generated noise. Reflectors proximal to the gas chimneys, which was initially shown as mostly flat signals in the stacked data are now displayed with a pull-up or push-down, most probably induced by the high-velocity variation. The migration smiles (wavefront) as highlighted within the red circle may be the result of the presence of noise bursts in previous un-migrated section (Figure 69).

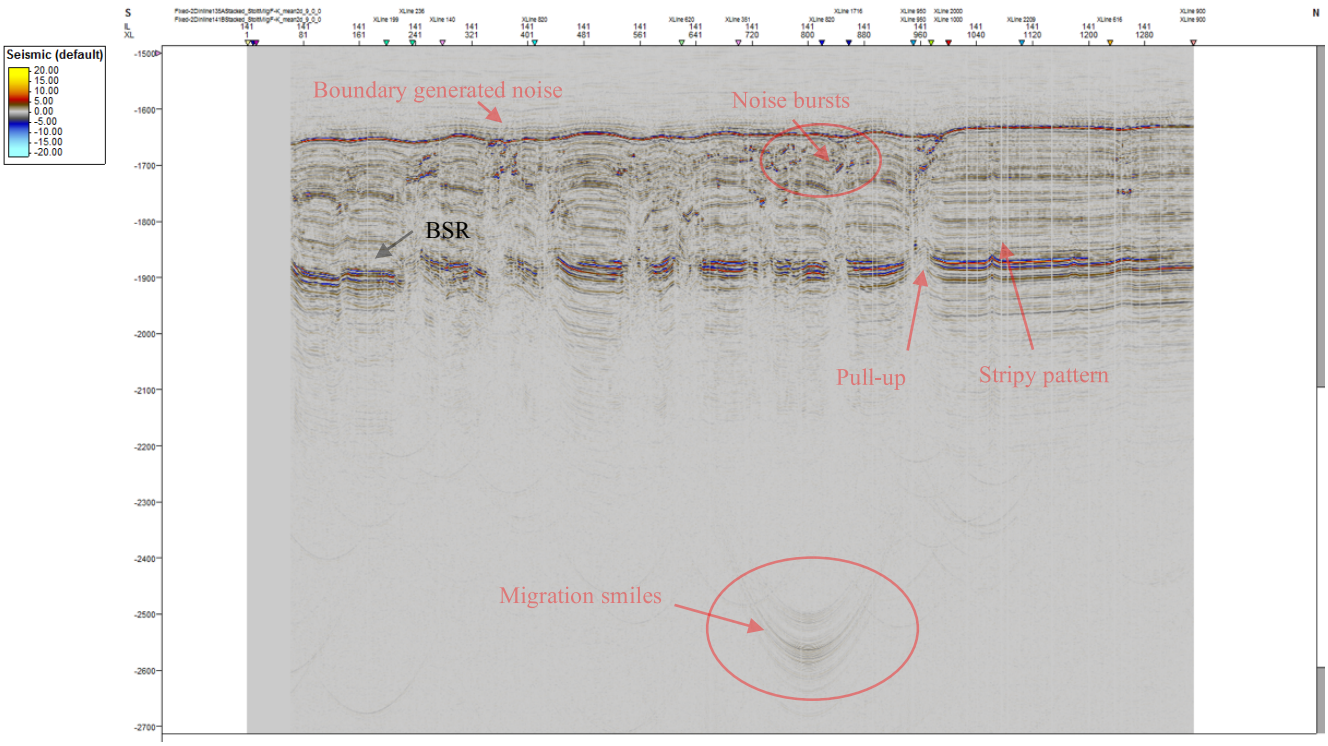

Figure 69 - Seismic section of Stolt migrated data, inline 141, bin size of 6.25 x 6.25, x = 8.44 km and y = [1500,2700] ms (TWT) with an increment of 100 ms.

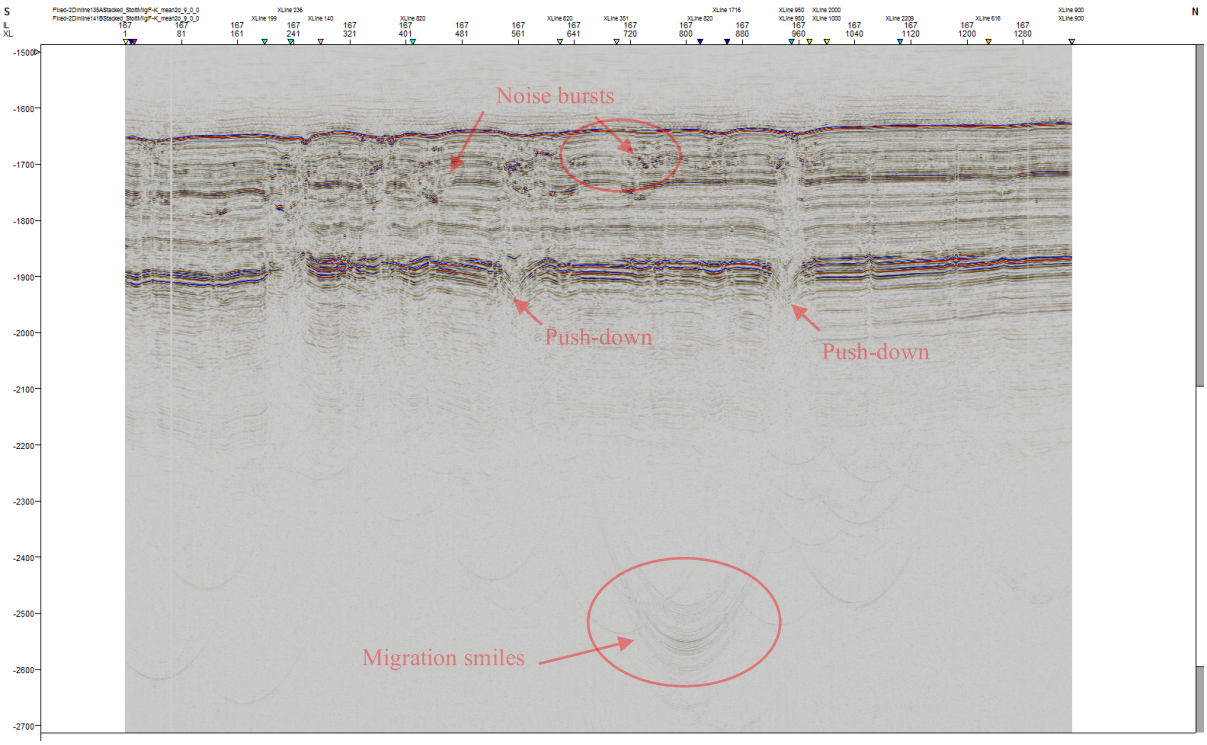

Figure 70 - Seismic section that is a result of poststack F-XY Deconvolution and Stolt migrated, inline 167, bin size of 6.25 x 6.25, x = 8.44 km and y = [1500,2700] ms (TWT) with an increment of 100 ms.

5.3.4.1 Stolt migration: Noise expression

Noise expression is an operation that is part of the GeoTeric software and used to suppress noise in a two-stages. Starting with defining the optimal filter for the available data, and applying it. For the Vestnesa Ridge 3D data, similar to Snøhvit data, random noise filter (TDiffusion; with 15 iterations) and aggressive noise attenuation (SO filter; filter size of 3, and dip azimuth filter size of 15). By comparing the results of this process (Figure 71 and 72) with the input (Figure 69 and 70), one can clearly see that there are fewer bursts (marked with black circle), random and coherent noise which are ultimately increasing the signal-to-noise ratio, and making the true reflections stand out more clearly. Finally, the migration smiles and the stripy pattern are less visible after noise filtering in Noise expression.

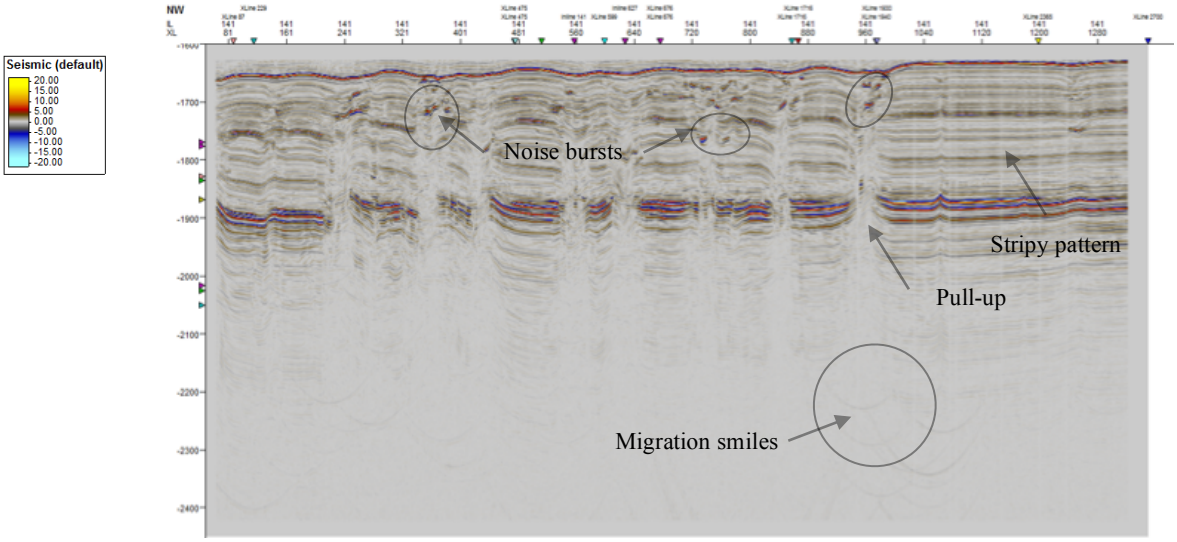

Figure 71 – Seismic section of filtered Stolt migrated data by noise expression; random noise and aggressive noise attenuation. Inline 141, bin size 6.25 x 6.25, x = 8.44 km and y = [1600,2450] ms (TWT) with an increment of 100 ms.

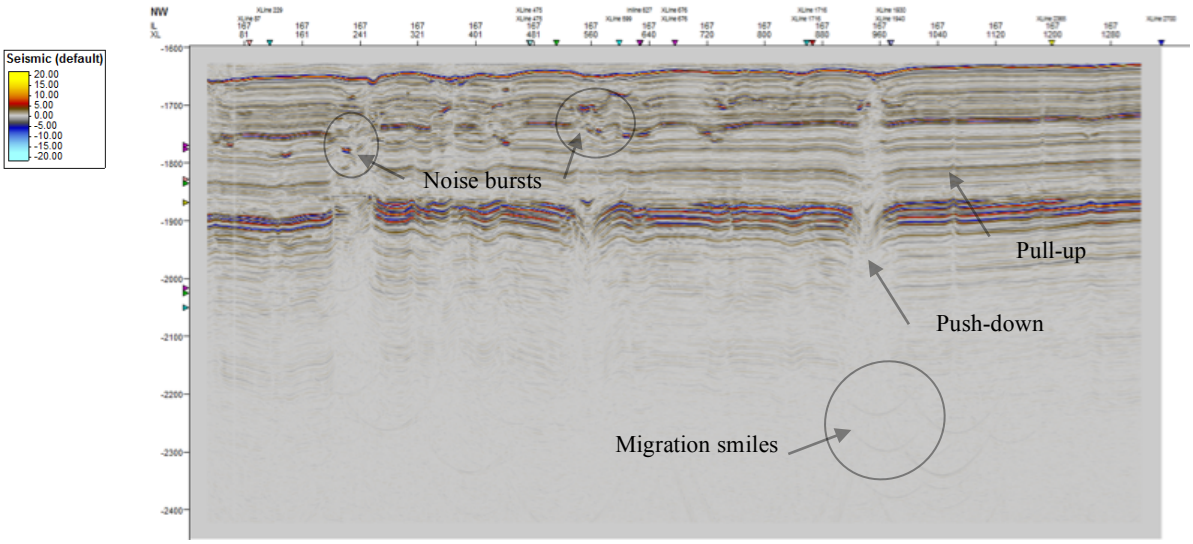

Figure 72 - Seismic section of filtered Stolt migrated data by noise expression; random noise and aggressive noise attenuation. Inline 167, bin size 6.25 x 6.25, x = 8.44 km and y = [1600,2450] ms (TWT) with an increment of 100 ms.

5.3.4.2 Stolt migration: Automatic gain control

As is it was considered necessary to apply automatic gain control to the Snøhvit seismic data to obtain a broader distribution of the signal response, and it was also decided to follow the same procedure for Vestnesa Ridge. The result is presented below in Figure 73, 74 and 75, obtained by using SeisSpace ProMAX, scalar as mean and operator length of 100 m. This was a relatively inexpensive process completed on a regular workstation within few minutes. Figure 73 shows a comparison of inline 141 with the input (A) with the output (B), and the automatic gain control rearrange the response distribution making underlying reflectors ~1950 ms more visible. This is an operation done purely with the purpose of structural visualization and could be used to improve interpretation of the morphology. However, automatic gain control would not preserve the natural amplitude response, gaining both signal and noise.

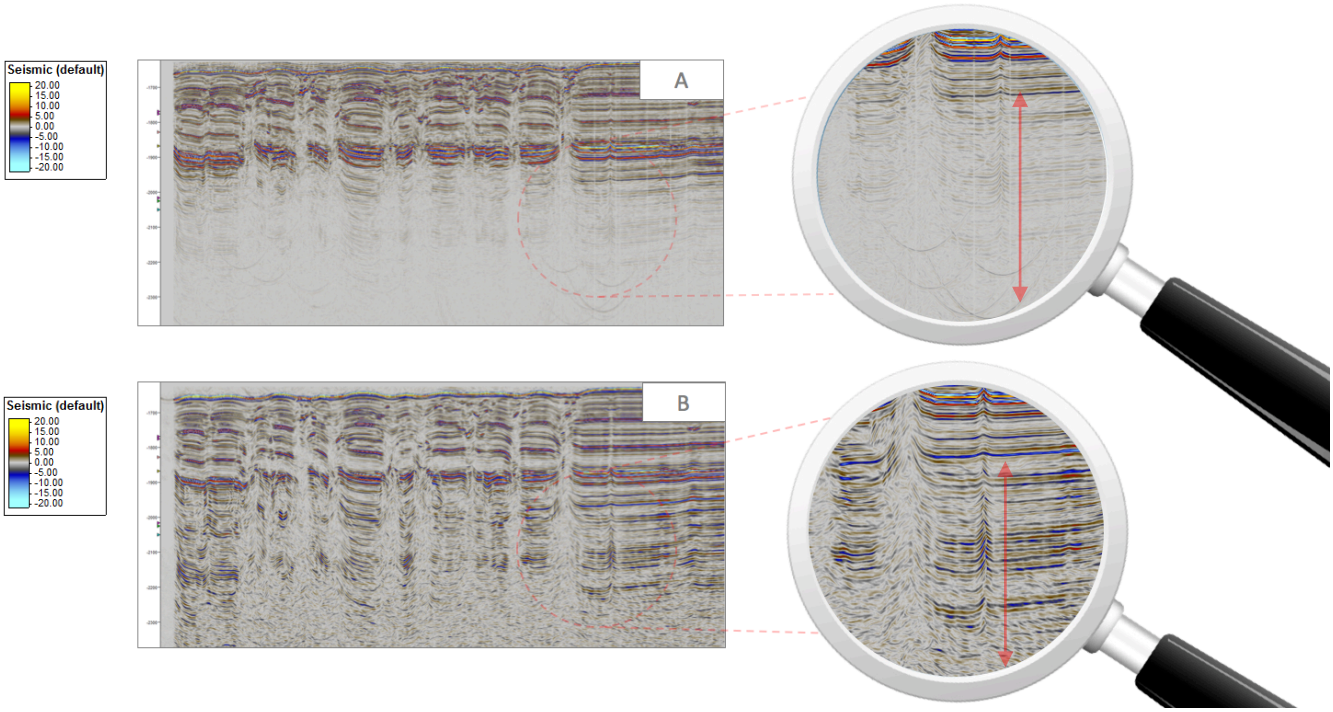

Figure 73 - Comparison of Stolt migrated, noise filtered (TDiffusion and SO filter) section (A), with same section that is corrected with automatic gain control (B), inline 141, bin size of 6.25 x 6.25 m, x = 8.44 km and y = [1600,2400] ms (TWT) with an increment of 100 ms.

By comparing the magnitude glass for A with B, one can distinctly see that automatic gain control adds value in the visualization of deeper reflectors in the interval highlighted by the red arrow (1920 – 2250 ms). The pull-up effect within the chimney are more evident in B. However, there is also more noise compared to in A.

In figure 74 and 75, inline 141 and 167 are displaying the results after applying automatic gain control and noise filtering in noise expression. By comparing these two sections with Figure 71 and 72, more details are obtained below 1950 ms, which also highlight the possible extent of the stratified section (morphology) in addition to the gas chimneys. Pull-up and pull-down and other migration artifacts are highlighted in within the black circles. The red circle is showing irregularities such as bursts that possibly are not reflecting an accurate description of the subsurface.

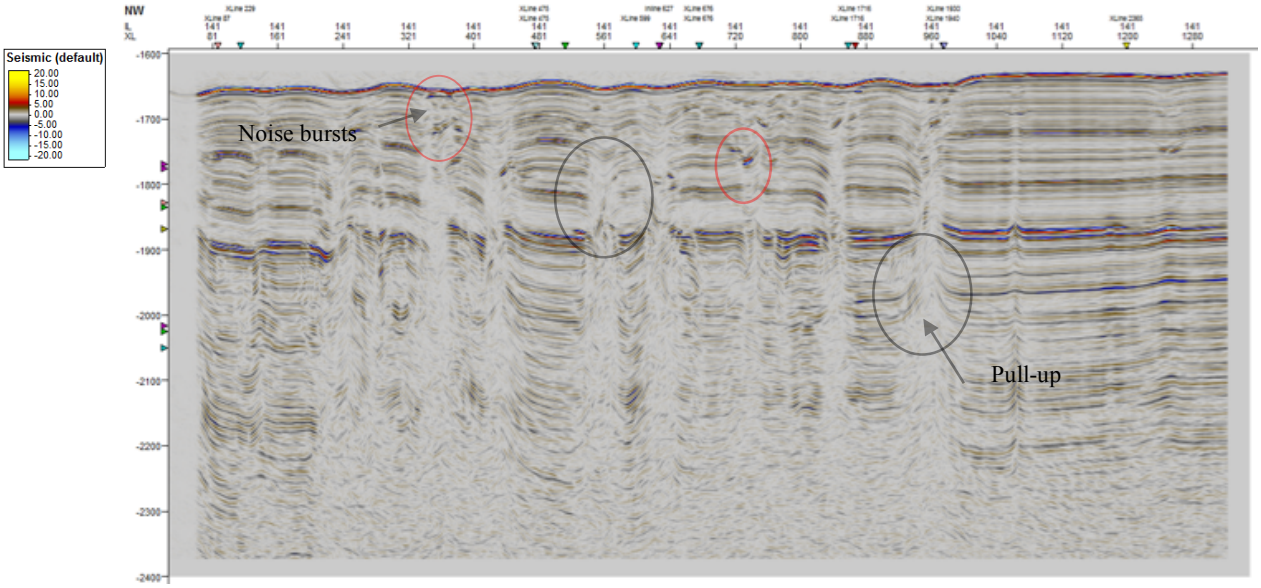

Figure 74 - Stolt migrated section after noise filtered by noise expression (random noise and aggressive noise), inline 141, bin size of 6.25 x 6.25 m, x = 8.44 km and y = [1600,2400] ms (TWT) with an increment of 100 ms.

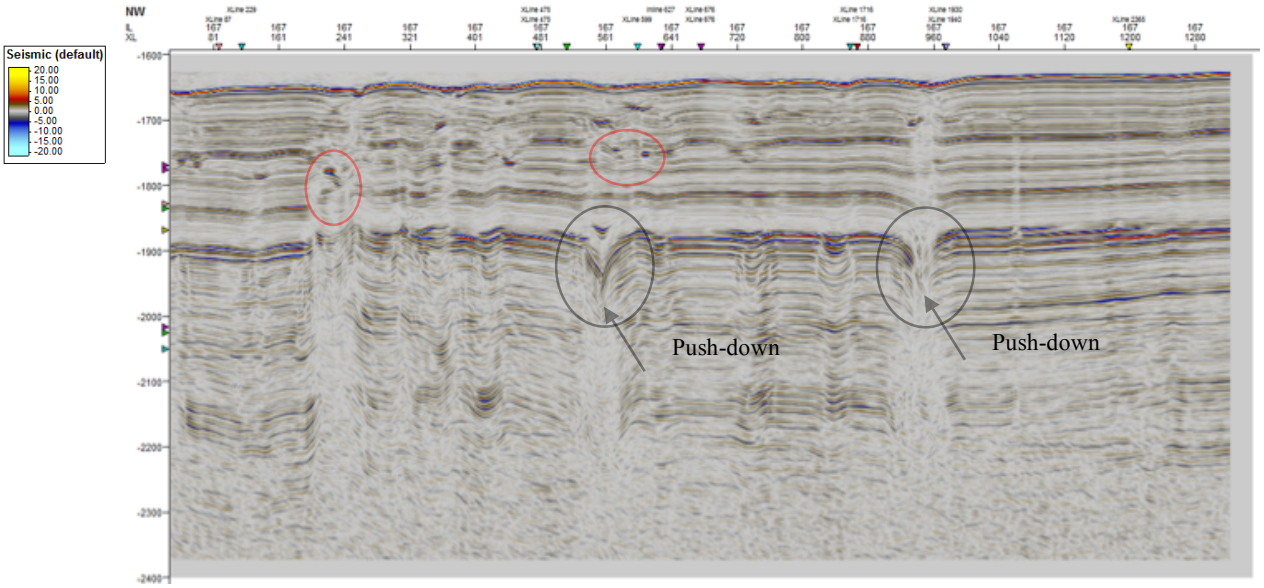

Figure 75 - Stolt migrated section noise filtered by noise expression (random noise and aggressive noise), inline 167, bin size of 6.25 x 6.25, x = 8.44 km and y = [1600,2400] ms (TWT) with an increment of 100 ms.

5.3.5 Prestack time migration

Prestack time migration of Vestnesa Ridge was performed by utilizing Madagascar, based on Kirchhoff time migration. It was decided not to do the same in SeisSpace ProMAX as it did not obtain better result or time efficiency. The migration was carried out with using constant velocity (1480 m/s), and took about 18 hours to complete. The result can be seen in Figure 76 and 77. By comparing this result with the result after applying Stolt migration (Figure 69 and 70), the amount of details is quite similar, with low vertical resolution, but with potentially more noise and blanking effect.

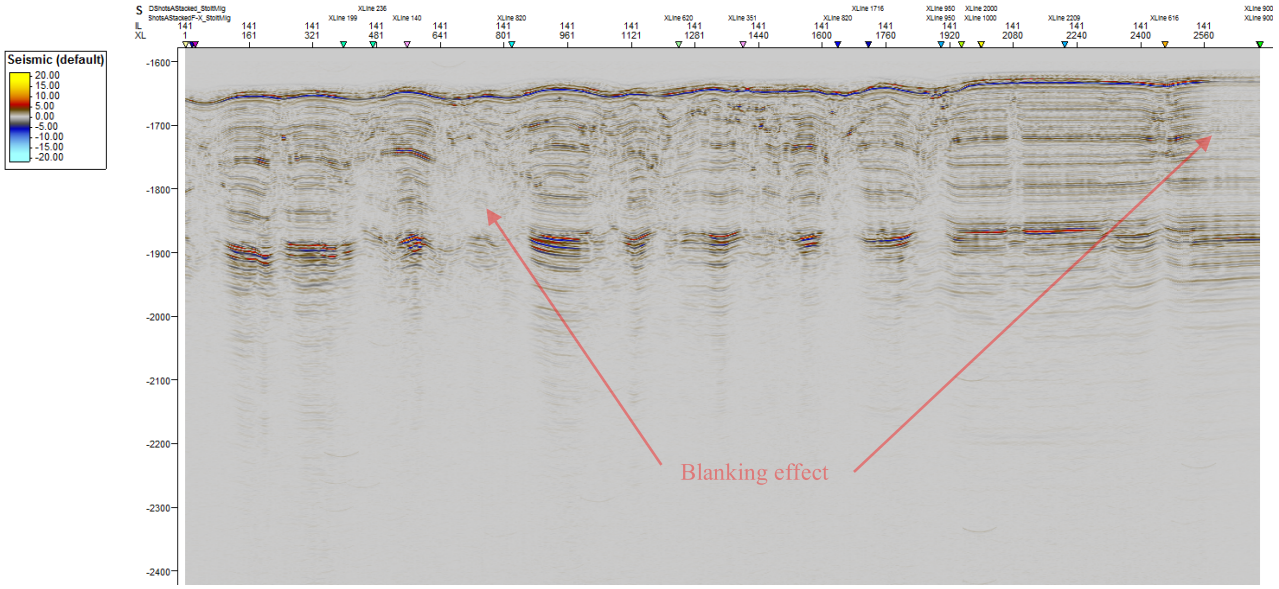

Figure 76 - Prestack time migrated seismic section, inline 141, bin size of 6.25 x 6.25, x = 8.44 km and y = [1600,2400] ms (TWT) with an increment of 100 ms.

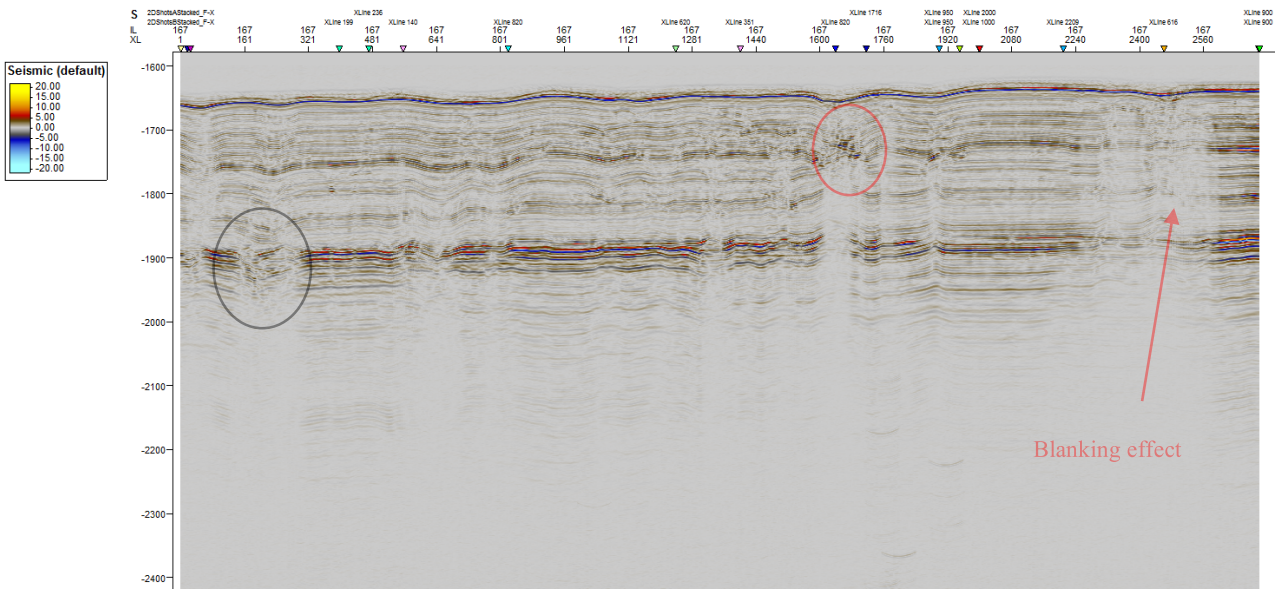

Figure 77 – Prestack time migrated seismic section, inline 167, bin size of 6.25 x 6.25, x = 8.44 km and y = [1600,2400] ms (TWT) with an increment of 100 ms.

5.3.5.1 PSTM: Noise expression

Prestack time migration completed in Madagascar generated some migration artifacts and contained various kind of noise that would be beneficial to remove. Noise expressing in GeoTeric was therefore used to remove random noise and aggressive noise by TDiffusion and SO filters, and the results of this operation can be seen in Figure 78 showing inline 141, and 79 displaying inline 167.

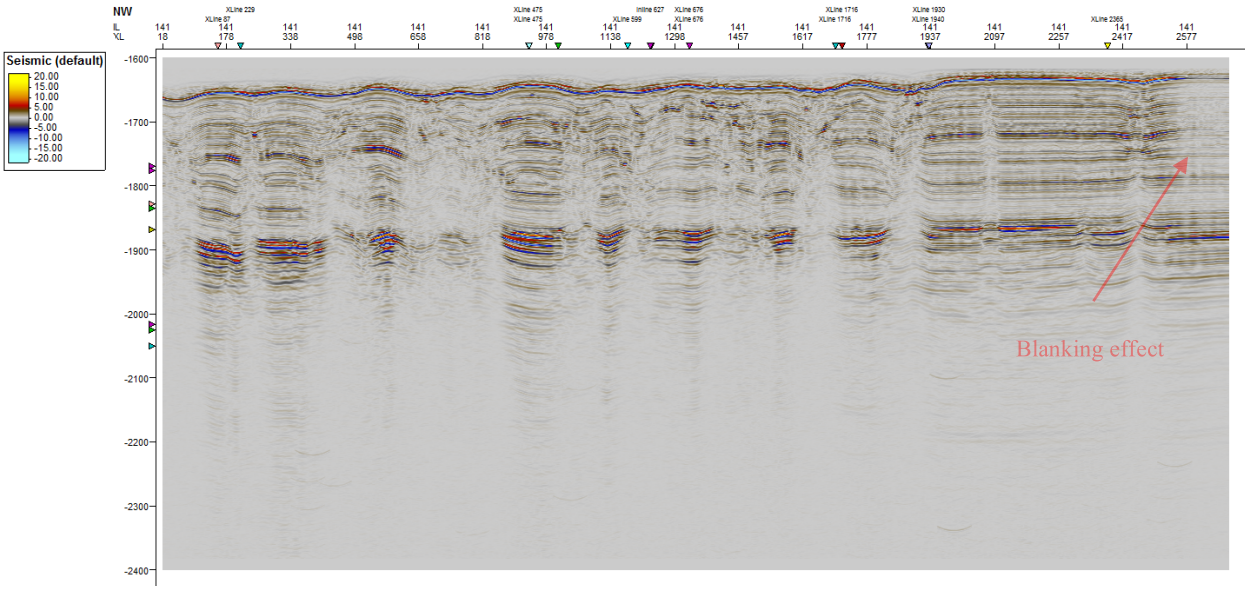

Figure 78 - Filtered noise (random noise and aggressive noise attenuation) prestack time migrated data, inline 141, bin size of 6.25 x 6.25 m, x = 8.44 km and y = [1600,2400] ms (TWT) with an increment of 100 ms.

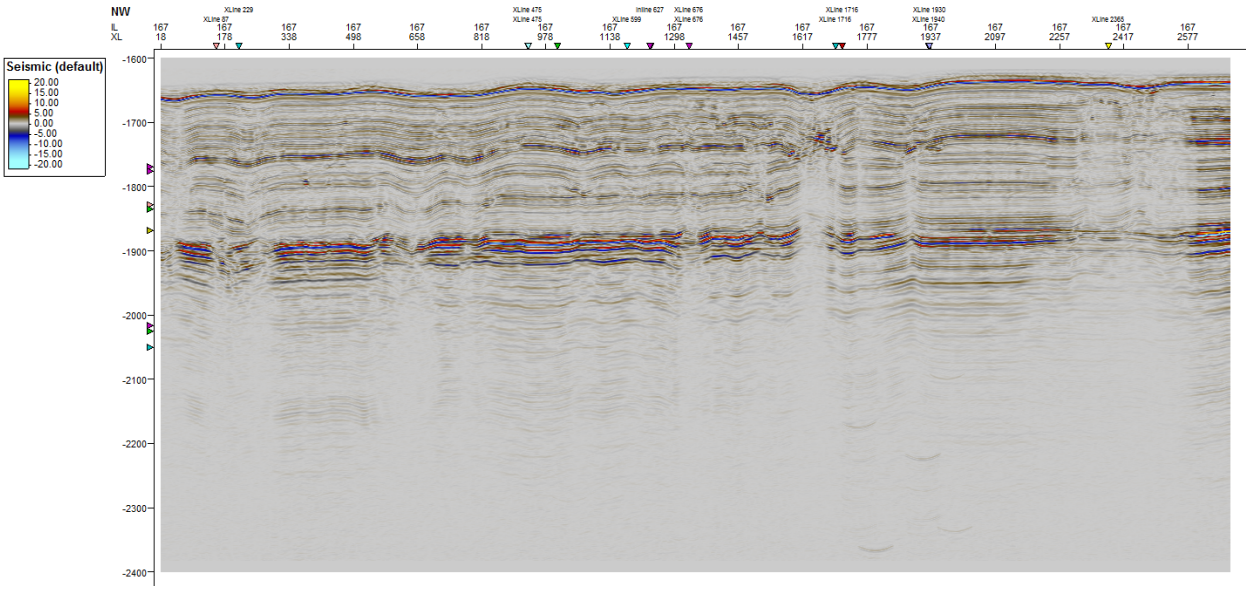

Figure 79 - Filter noise (random noise and aggressive noise attenuation) prestack time migrated seismic data, inline 141, bin size of 6.25 x 6.25 m, x = 8.44 km and y = [1600,2400] ms (TWT) with an increment of 100 ms.

5.4 Synthetic seismic data

As the construction of synthetic 3D seismic data required more computer power than was available, it was deiced to focus on the two synthetic 2D seismic inline, 141 and 167, which are the basis for creating synthetic seismic data. When the synthetic velocity model was created, two versions of it were carried out to compare the effect of adding random and/or vertical changes with some heterogeneity within the gas chimney zone. The two different velocity models, A and B, as seen in Figure 80 and 81 with corresponding inline 141 and 167, show the basis for constructing synthetic 2D seismic data.

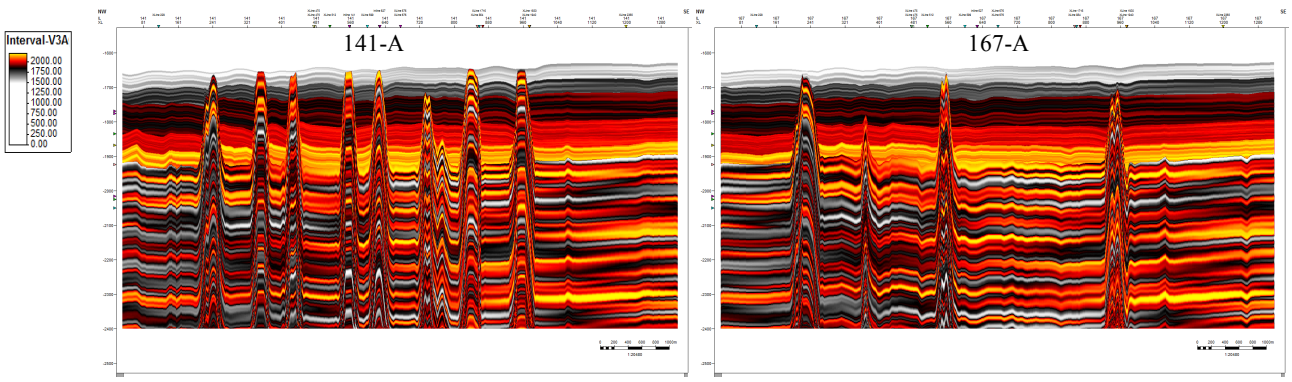

Figure 80 – 2D velocity model of 141B (inline 141) and 167B (inline 167), with vertical and lateral velocity changes, bin size of 6.25 x 6.25, x = 8.04 km and y = [1500,2400] ms (TWT) with an increment of 100 ms.

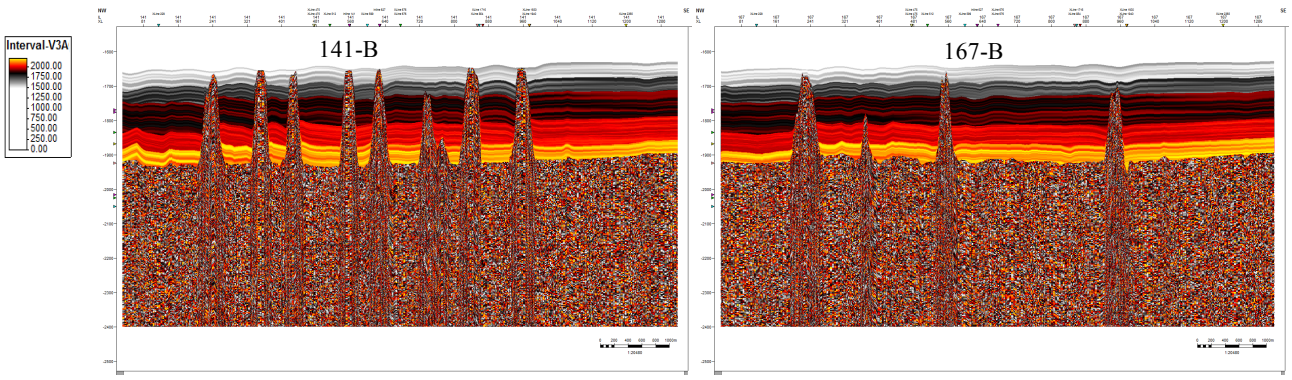

Figure 81 - 2D velocity model of 141B (inline 141) and 167B (inline 167), with random velocity distribution within the gas chimneys, bin size of 6.25 x 6.25, x = 8.04 km and y = [1500,2400] ms (TWT) with an increment of 100 ms.

However, the result of creating synthetic 2D seismic data of velocity model B compared to A did not show good correlation with the real seismic data. As seen in Figure 82 blow, the result of the brute stack corresponding to model A and B. Blow the BSR (black arrows) there are no horizontal oriented reflectors in model B, which do not match with the real seismic data. A similar mismatch can be seen within the gas chimneys as they appear heavily influence by noise bursts. For this reason, it was decided to discard velocity model B and keep working on model A.

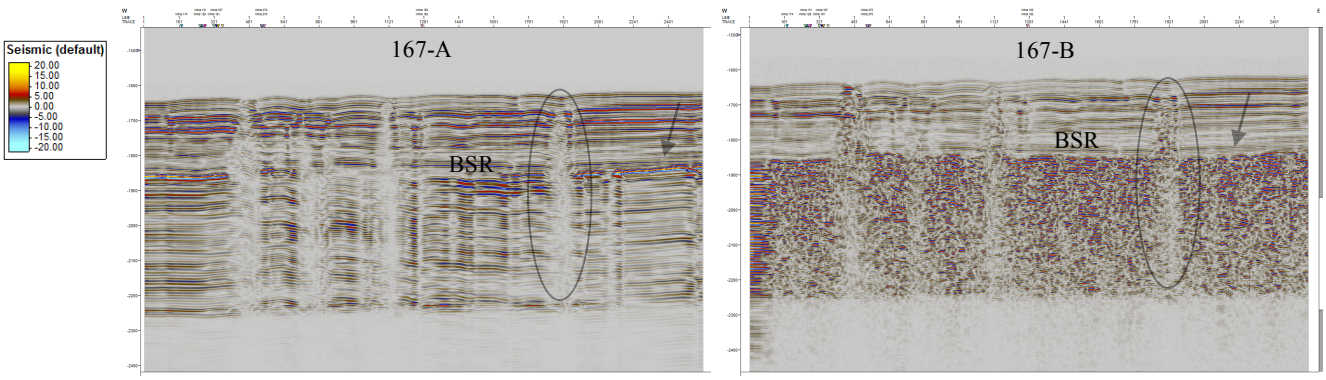

Figure 82 - Synthetic 2D seismic section of velocity model 167A compared to 167B, bin size of 6.25 x 6.25, x = 8.04 km and y = [1500,2400] ms (TWT) with an increment of 100 ms.

Something worth noticing is that all the results shown in this subchapter have to be filtered in GeoTeric by noise expression as the output of constructing the seismic inlines showed very coarse pixelated image as seen in Figure 83, A) original output of make SEG-Y, B) filtered by noise expression (random noise with 15 iteration and aggressive noise with filter size of 3), and C) image of the real prestack time migrated seismic data. The correlation between B and C is quite good, even though there is a higher density in reflectors displayed in B.

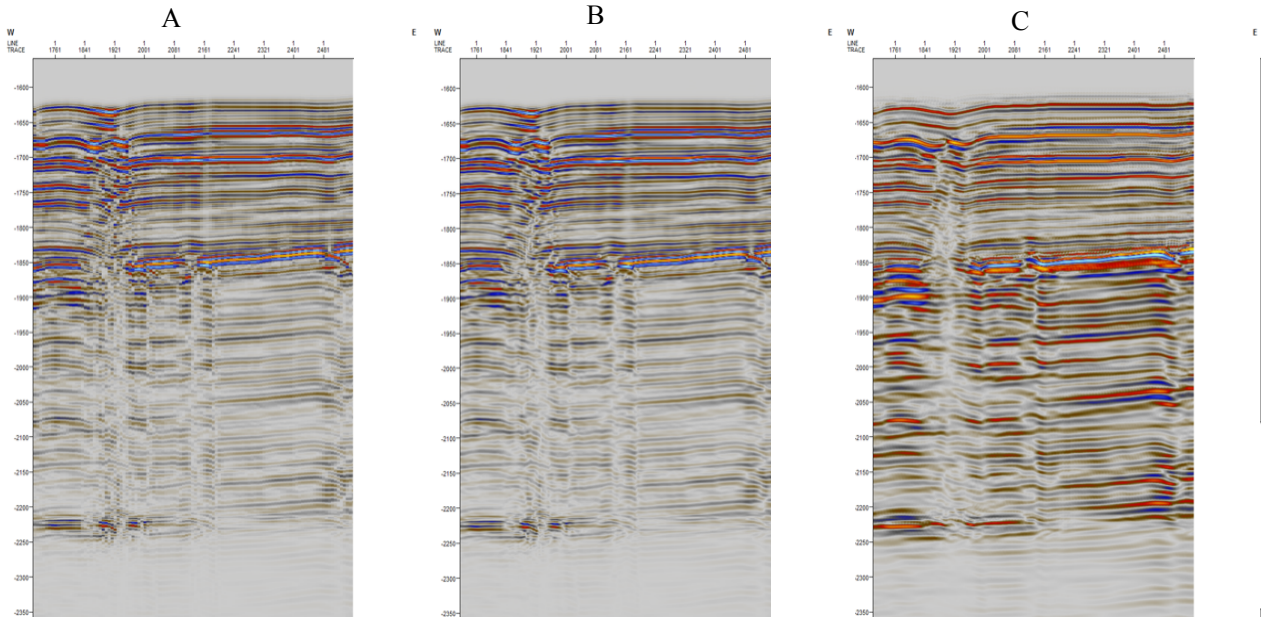

Figure 83 – Comparison of prestack time migrated synthetic seismic data with actual seismic data at the same location, A) output of make-segy in Madagascar after PSTM, B) A filtered by noise expression (Random and aggressive noise attenuation) in GeoTeric, C) actual prestack time migrated data from Vestnesa Ridge, bin size: 6.25 x 6.25 m, x = 2.34 km and y = [1550,2250] ms (TWT) with an increment of 100 ms.

5.4.1 Brute stack

The first process after applying geometry correction and binning of 6.25 x 6.25 were stacking the data and the result of the initial brute stack of synthetic representation of Vestnesa Ridge seismic data can be seen below in Figure 84 and 85, as both inline 141 and 167 respectively. This process was completed in SeisSpace ProMAX, included normal moveout correction with constant velocity (1480 m/s) and ran for approximately 3 minutes on the workstation. By comparing synthetic seismic data with the actual seismic data of Vestnesa Ridge, one can notice that there is a good correlation in regard to dimension, representation of features and overall morphology with stratified layers. However, due to extreme interval velocity variations, very prominent reflectors were also generated, which is highlighted by the red arrows, in Figure 84 and 85. The two-way time interval that is of interest for this project ranges from ~ 1600 ms to 2400 ms. These Figures also show signs of diffraction, some noise above the seafloor generated by the stacking process. Powerful amplitude response above the gas chimneys correlates to the sharp boundary between velocities.

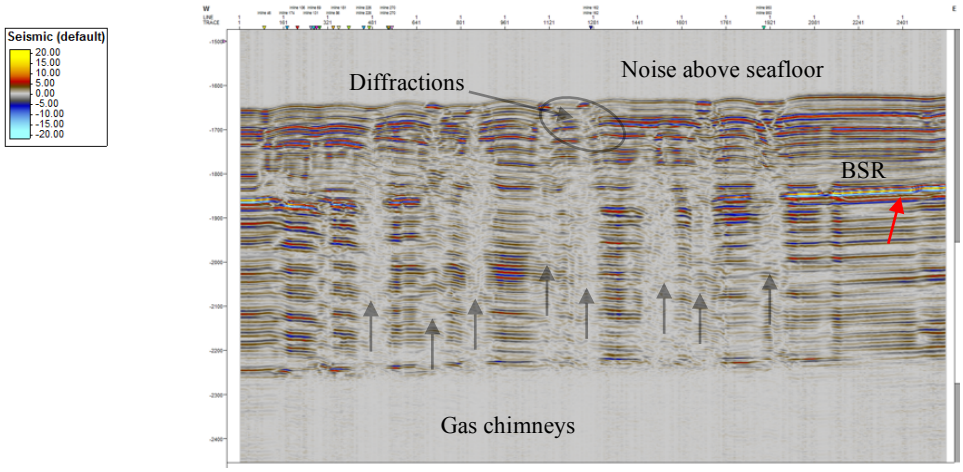

Figure 84 – Brute stacked synthetic seismic section inline 141, bin size of 6.25 x 6.25 m, x = 7.96 km and y = [1450,2400] ms (TWT) with an increment of 100 ms.

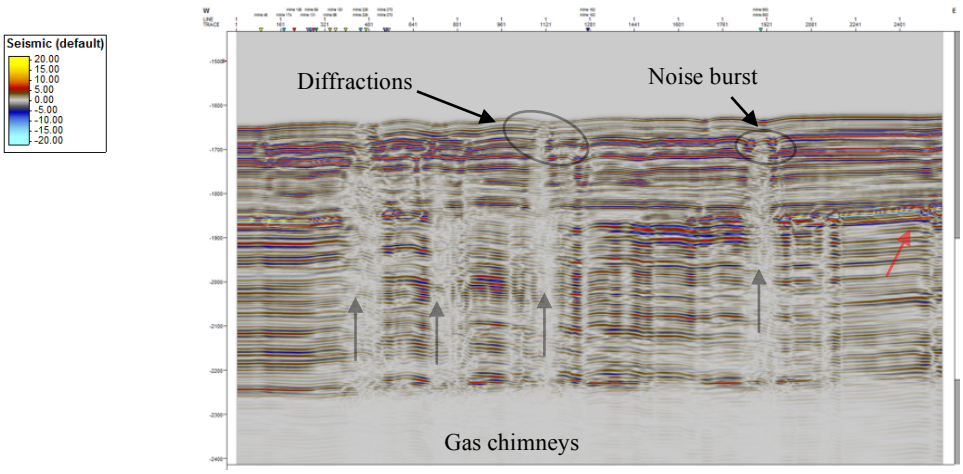

Figure 85 - Brute stacked synthetic seismic section inline 167, bin size of 6.25 x 6.25 m, x = 7.96 km and y = [1450,2400] ms (TWT) with an increment of 100 ms.

5.4.2 F-XY deconvolution

Next step after stacking the data was to apply F-XY deconvolution to improve the continuity of the reflections in the data and attenuate incoherent noise. In theory, synthetic data should not naturally contain any kind of noise. However, the effect of applying deconvolution showed better imaging than the brute stack as it removed random noise and equalized raw amplitude response shown as more coherent reflectors (see Figure 86 and 87). Deconvolution also removed bursts mainly within the chimneys, which are thought to be the result of extreme velocity changes but could be artifacts related to previous processing. This step was done in SeisSpace ProMAX on the available workstation with a computing time of 4 minutes. By closer look, one can notice that there are still diffractions as hyperbola visible in the synthetic data, highlighted within the black circles and a poor representation of what should be continuous layers seen within the red circle in Figure 87.

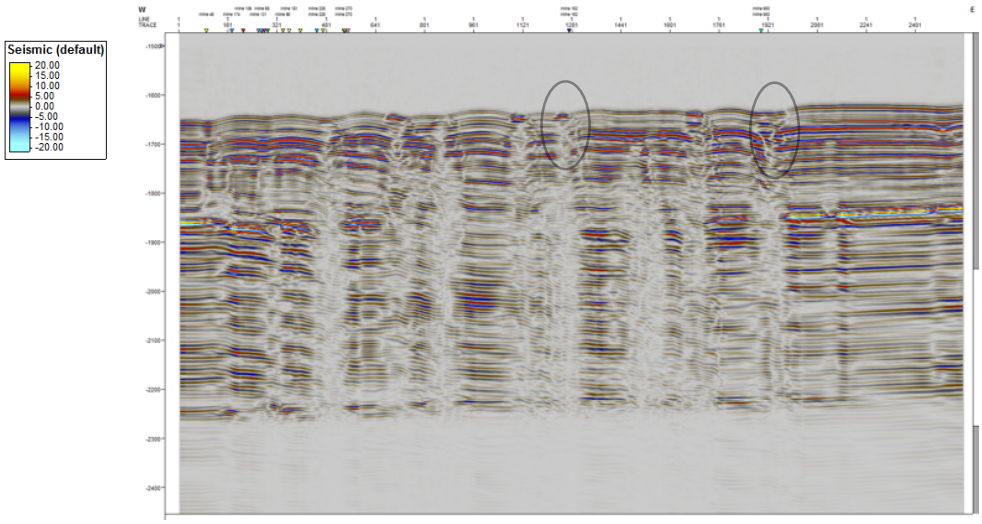

Figure 86 – F-XY deconvolution applied to synthetic seismic brute stack inline 141, bin size of 6.25 x 6.25 m, x = 7.96 km and y = [1450,2400] ms (TWT) with an increment of 100 ms.

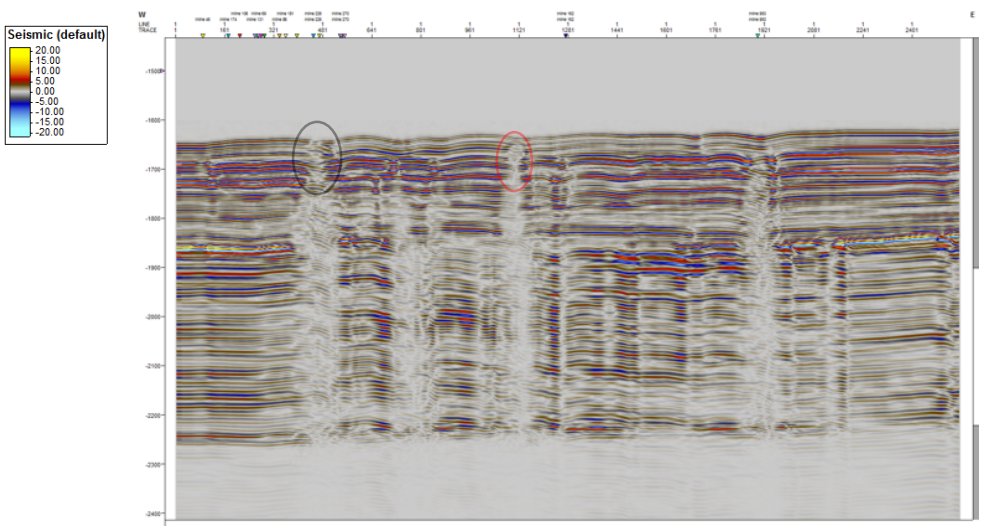

Figure 87 - F-XY deconvolution applied to synthetic seismic brute stack inline 167, bin size of 6.25 x 6.25 m, x = 7.96 km and y = [1450,2400] ms (TWT) with an increment of 100 ms.

5.4.3 Stolt migration

The Stolt migration was carried out with constant velocity (1480 m/s) and computed by using SeisSpace ProMAX on the available workstation. Several trials were conducted with different parameters (Appendix B), and with varying running times depending on bin size. Figure 88 and 89 below show the best result after applying Stolt migration on inline 141 and 167. The results indicate less influence of diffraction such as hyperbolas compared to the stacked data after F-XY deconvolution (Figure 86-87), but contain pull-up effect within the gas chimneys. In addition, migration artifacts as noise above the seafloor, poor preservation of amplitude dynamics at the far-left side, and discontinuous reflectors above the gas chimneys that do not correlate with the synthetic model are all seen in Figure 88 and 89.

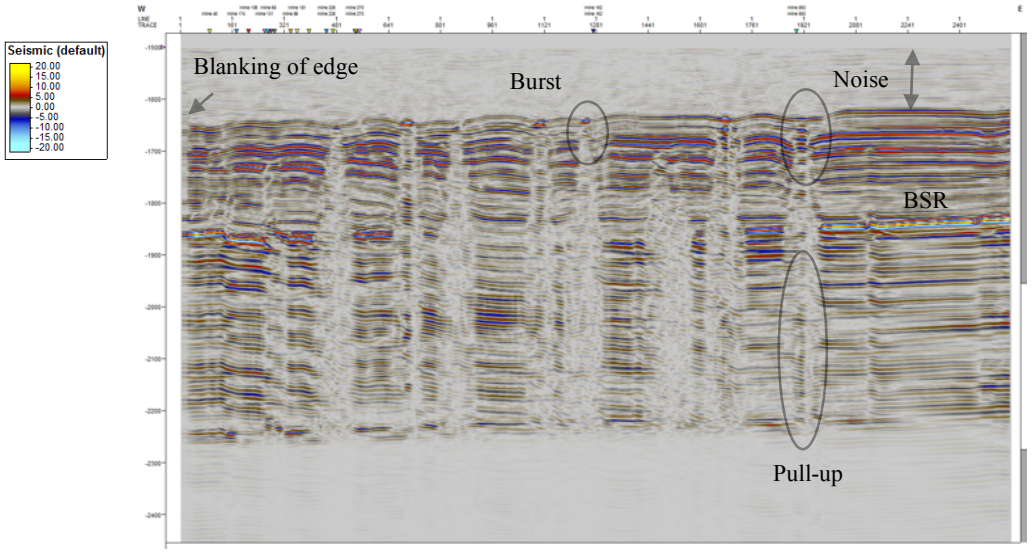

Figure 88 – Stolt migrated synthetic section inline 141, bin size: 6.25 x 6.25 m, x = 7.96 km and y = [1450,2400] ms (TWT) with an increment of 100 ms.

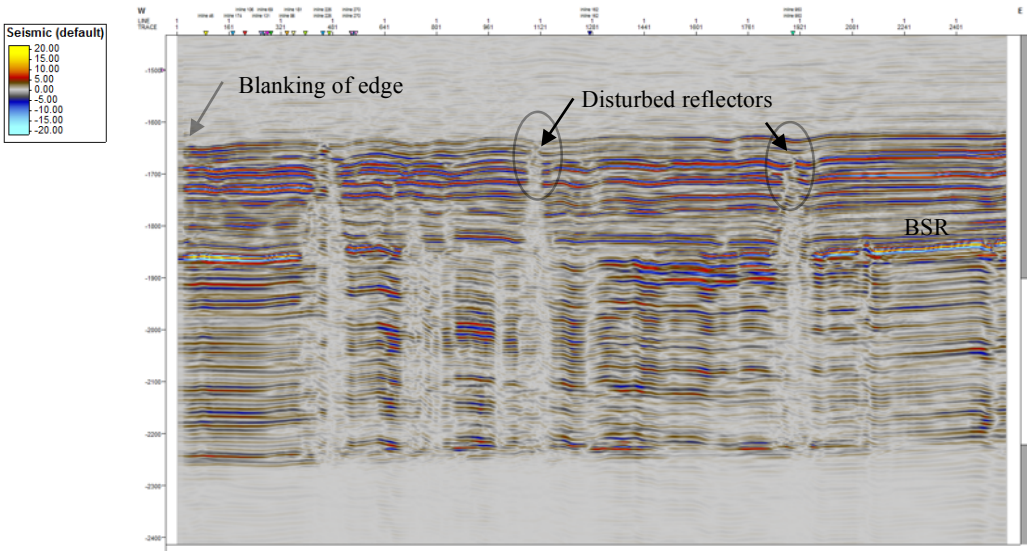

Figure 89 - Stolt migrated synthetic section inline 167, bin size: 6.25 x 6.25 m, x = 7.96 km and y = [1450,2400] ms (TWT) with an increment of 100 ms.

5.4.4 Prestack time migration

Prestack time migration of the synthetic data was performed by utilizing both, SeisSpace ProMAX and Madagascar, based on Kirchhoff time migration. The migration was carried out by constructing two versions, one migrated with constant velocity (1480 m/s) and the second calculated with the actual velocity models, which had to be converted from interval to RMS velocity (Figure 80).

5.4.4.1 Constant velocity migration

Even though SeisSpace ProMAX and Madagascar are configured the same, the results are entirely different as seen in Figure 90, 91, and 92. Figure 90 shows the PSTM processed in ProMAX and Figure 91 the same operation but done in Madagascar on Stallo super-computer. The result from ProMAX shows problems with edge preservation as highlighted with the red arrow. In addition, the outline of the gas chimneys is not as well displayed as in previous results, e.g. after Stolt migration, and the correction of dipping reflectors (hyperbolas) are not adequately, highlighted by black circles. However, by comparing it with the results obtained using Madagascar, one can clearly see how the hyperbolas are collapsed and the outline of the gas chimneys are preserved without high amplitude response within. The result from PSTM in Madagascar also shows that even though the gas chimneys contain high-velocity variation, it still does not influence the reflectors above seen within the red circle.

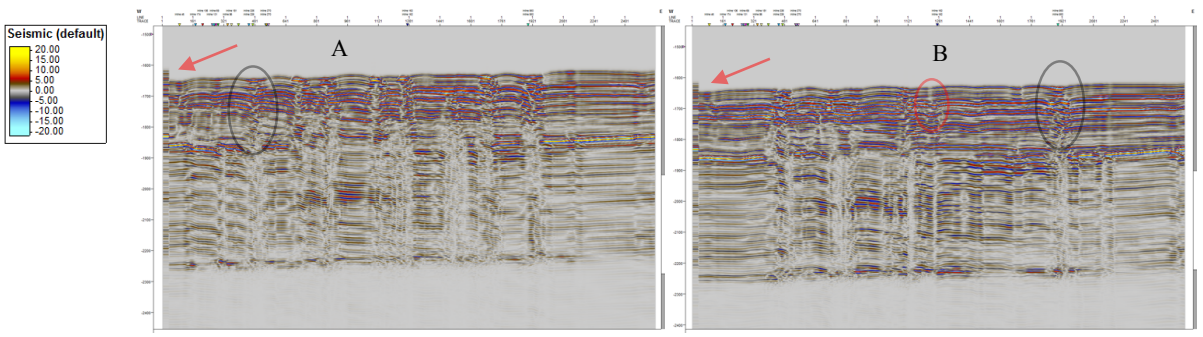

Figure 90 – Prestack time migrated synthetic section with constant velocity of 1480 m/s in ProMAX of A) Inline 141, B) inline 167, bin size: 6.25 x 6.25 m, x = 2.34 km and y = [1400,2400] ms (TWT) with an increment of 100 ms.

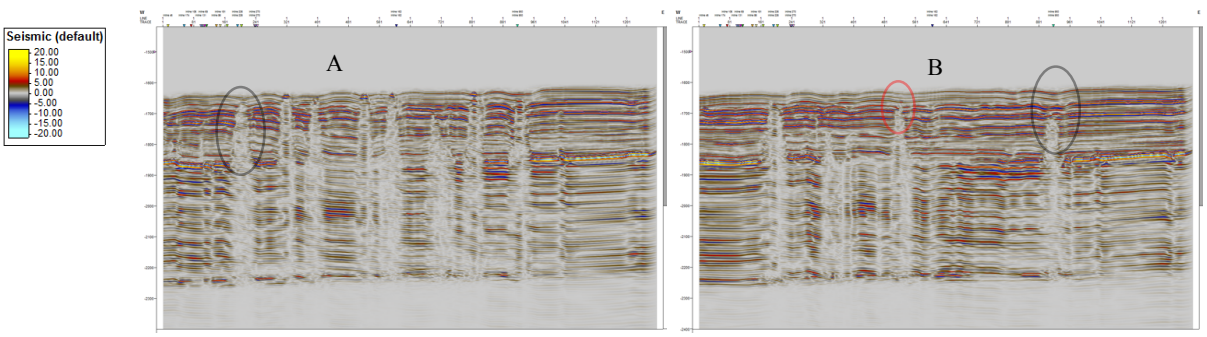

Figure 91 - Prestack time migrated synthetic section with constant velocity of 1480 m/s in Madagascar of A) Inline 141, B) inline 167, bin size: 6.25 x 6.25 m, x = 2.34 km and y = [1400,2400] ms (TWT) with an increment of 100 ms.

5.4.4.2 Actual velocity field migration

The result of prestack time migration with the velocity model (Figure 92) can be seen in Figure 93 below. By comparing this result with the result of migration with constant velocity (Figure 91), the amount of details is very similar and difficult to distinguish. There is no difference worth noting, which might indicate that the prestack time migrating is less dependent on the input velocity than previously thought.

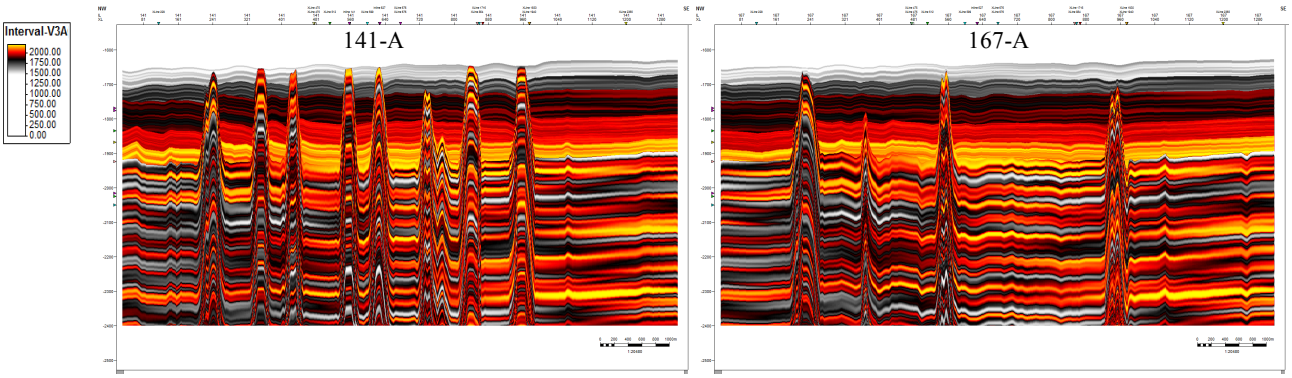

Figure 92 – 2D velocity model of 141B (inline 141) and 167B (inline 167), with vertical and lateral velocity changes, bin size of 6.25 x 6.25, x = 8.04 km and y = [1500,2400] ms (TWT) with an increment of 100 ms.

The correlation between the velocity models and the synthetic seismic data in Figure 93 is convincingly good, with more accurate representation as the continuous reflectors above the gas chimneys in B are unaffected by the extreme velocity variation below compared to the result of Stolt migration (Figure 89).

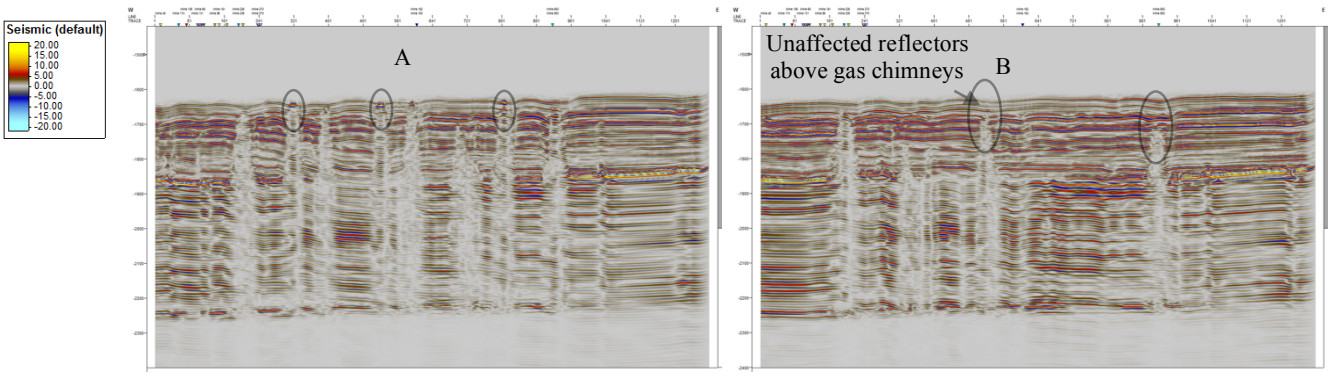

Figure 93 - Prestack time migrated synthetic section with the actual 2D velocity model in Madagascar of A) Inline 141, B) inline 167, bin size: 6.25 x 6.25 m, x = 2.34 km and y = [1400,2400] ms (TWT) with an increment of 100 ms.

5.4.5 Reverse time migration (RTM)

Two runs of reverse time migration were conducted using the open source Madagascar software with the help of Stallo super-computer. This process took approximately 30 minutes for each run, one with constant interval velocity (1480 m/s) and the second one with the actual velocity model (interval velocity). For each version, two seismic section corresponding to inline 141 and 167 were made.

5.4.5.1 Constant velocity migration

The result of reverse time migration with constant velocity (1480 m/s) can be seen in Figure 94 and 95, as inline 141 and 167 respectively. Compared to the previous result, e.g. Stolt migrated and prestack time migrated data, one can notice that the reflectors below 1900 ms are getting weaker through depth. The seafloor reflector appears to be time shifted down, approximated 10-12 ms, which is not the case. However, this can be explained due to very similar velocity (low impedance) at the interface of the seafloor, which does not generate any strong amplitudes. This makes sense as the water velocity is very similar to at shallow depth below the seafloor (10-15 ms), and tells us that RTM is honoring the input velocity model. There is also fewer details within the gas chimneys. However, this result shows good correlation with the synthetic model and the actual seismic data. Artifacts related to migration can be seen as blanking from the seafloor and too shallow depth below (highlighted as blanking). There is also a considerable lower amount of burst few sign if diffraction.

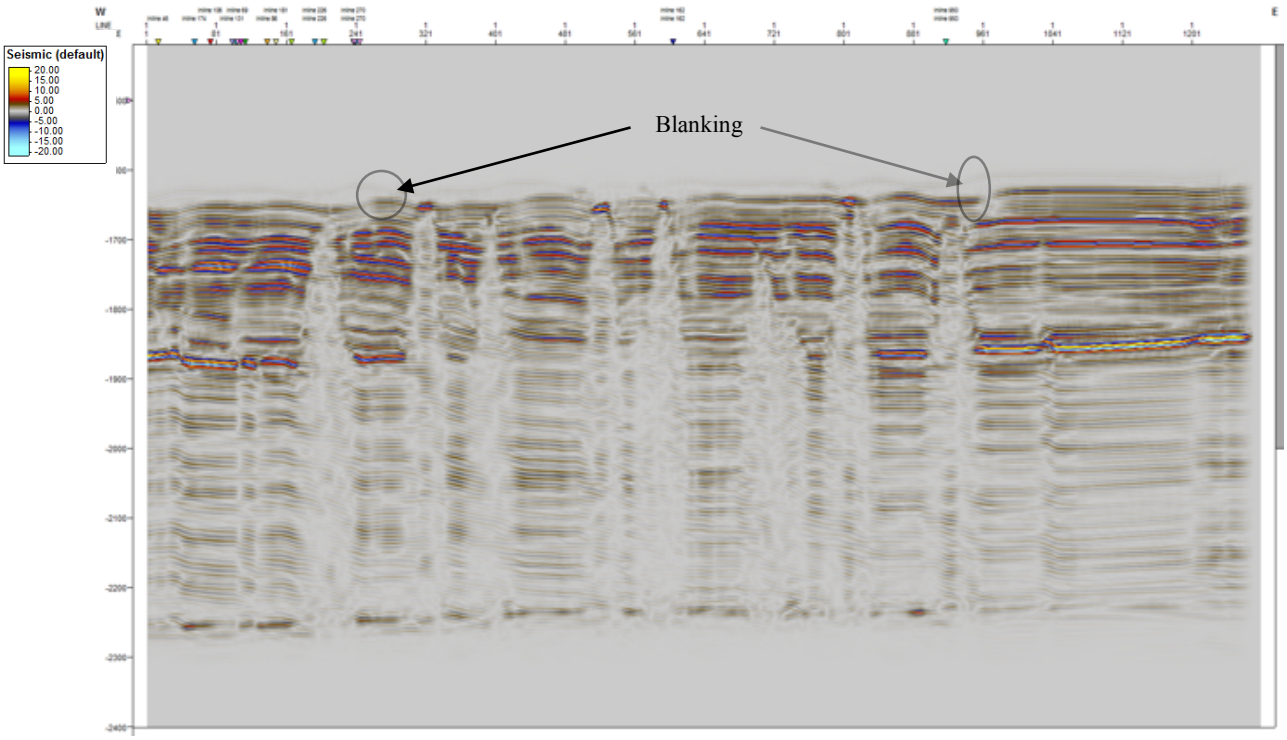

Figure 94 – Reverse time migrated synthetic section with constant velocity of 1480 m/s in Madagascar of inline 141, bin size: 6.25 x 6.25 m, x = 2.34 km and y = [1400,2400] ms (TWT) with an increment of 100 ms.

Figure 95 below show within the red circle RTM is doing a better job in preserving the horizontal reflectors above the gas chimneys.

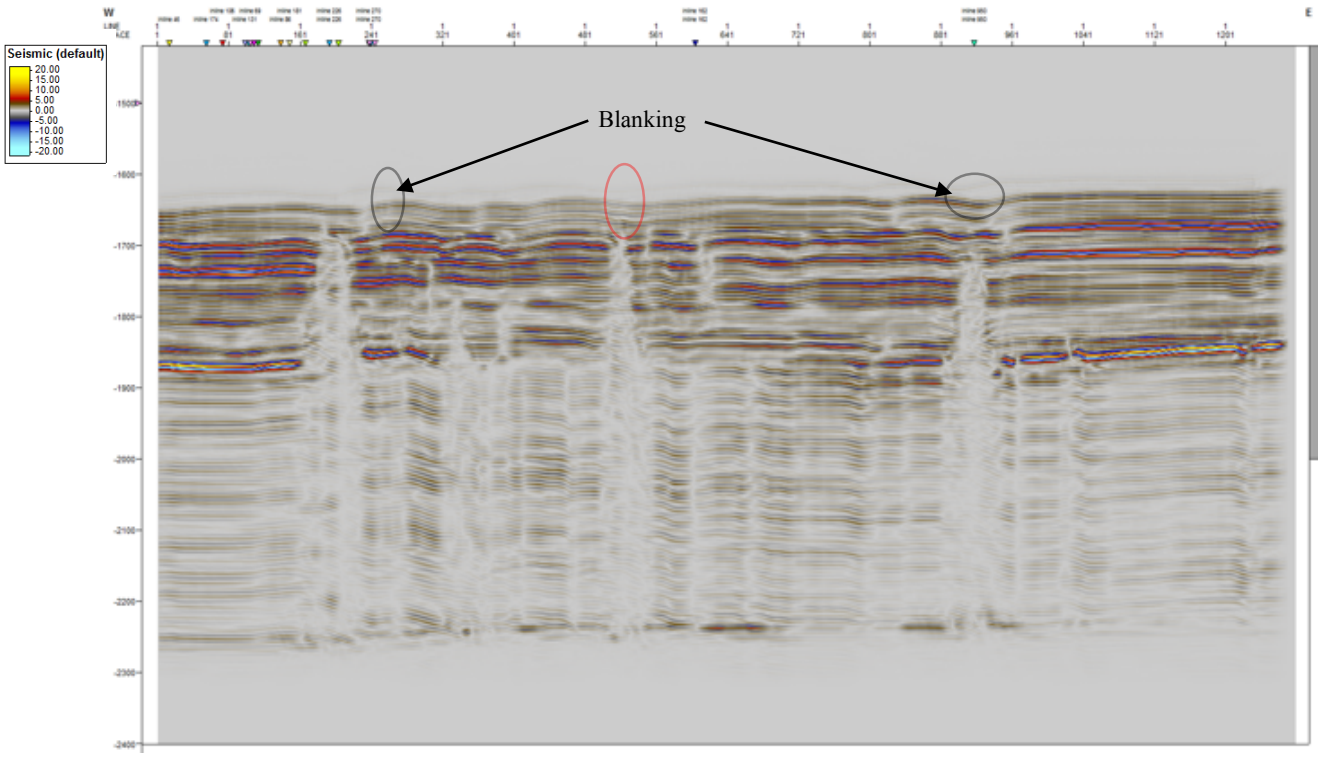

Figure 95 - Reverse time migrated synthetic section with constant velocity of 1480 m/s in Madagascar of inline 167, bin size: 6.25 x 6.25 m, x = 2.34 km and y = [1400,2400] ms (TWT) with an increment of 100 ms.

5.4.5.2 Actual velocity field migration

The reverse time migration with the actual velocity model (Figure 96) can be seen in Figure 97. By comparing them, one can see that the synthetic seismic data is accurately imaging the high dip velocity layers at the edges of the chimneys. The correlation is surprisingly precise, however similar effect as in the prestack time migrated data (Figure 91-93), showing increasing attenuation of the amplitude response from 1900 ms and below. This result is without a doubt the most promising, as the accuracy is almost spot on, which would add significant value in reducing uncertainties related to the imaging and positioning of features, in this example the gas chimneys. However, the representation of the synthetic models is not flawless, for instance, the blanking effect recorded at shallow depth below the seafloor marked with black arrows. Reflectors proximal to the gas chimneys appears to be horizontal with slightly pull-up effect, in which correlates with the synthetic velocity model.

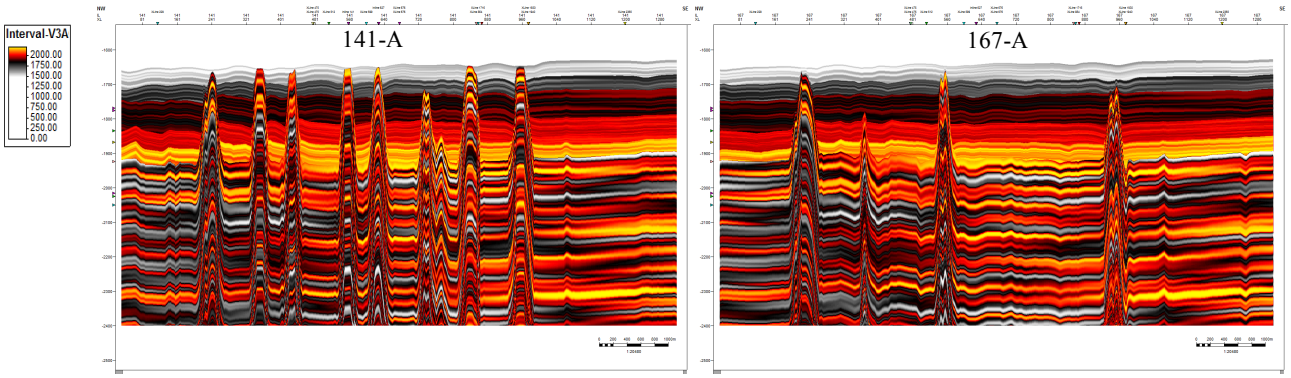

Figure 96 – 2D velocity model of 141B (inline 141) and 167B (inline 167), with vertical and lateral velocity changes, bin size of 6.25 x 6.25, x = 8.04 km and y = [1500,2400] ms (TWT) with an increment of 100 ms.

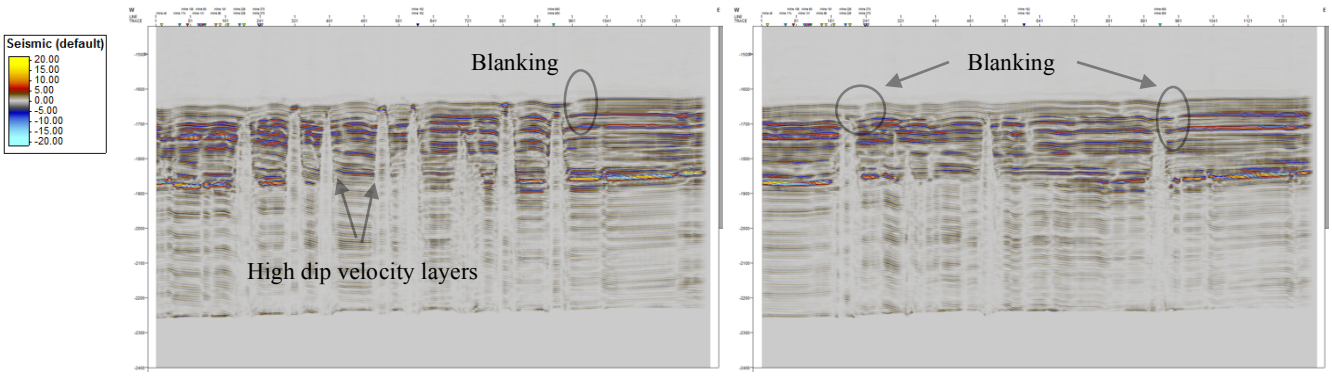

Figure 97 - Reverse time migrated synthetic section with the actual 2D velocity model in Madagascar of A) Inline 141, B) inline 167, bin size: 6.25 x 6.25 m, x = 2.34 km and y = [1400,2400] ms (TWT) with an increment of 100 ms.

6. Discussion

This chapter will be focusing on discussing the main results, which show the ultimate imaging accomplished during this investigation. Further, it will elaborate on the implication of P-Cable technology associated with seismic processing and the three main aspects: time efficiently, resolution and geological reasoning will be the main theme of this chapter.

Previous work has been conducted on P-Cable seismic data by mainly applying Stolt migration (Petersen et al., 2010), whereas this thesis has the aim of testing different time migration methods, as well as investigating the effect on the final imaging result. This includes recreation of the morphology and geological setting at Vestnesa Ridge by constructing a synthetic seismic model to analyze the effect and accuracy of velocity models on the results of migration. This is done using two different migration methods, prestack time migration and prestack reverse-time migration. Similar work has been done by (Arntsen et al., 2007), but this project will focus on the general imaging and not only the gas chimneys.

6.1 Final image of Snøhvit

The processing of Snøhvit P-Cable 3D seismic data has shown rather interesting results. Figure 98 shows the results of Stolt migration, with (A) and without (B) automatic gain control. The result of adding AGC significantly improved the structural representation of the subsurface at Snøhvit, which coincides with the objective of this thesis. Worth noting is that this operation does not preserve the original amplitude response of the data, which would impact any investigation of amplitude distribution and attributes related to it. Further, even though the different migration techniques have been processed with the same parameters and velocity field, the results have shown inequalities in resolution and geological representation. The final result of the Snøhvit data was finalized by using two different migration techniques with constant velocity approximation seen in Figure 99, a Stolt migrated section, and Figure 100 a prestack time migrated section. They both show a simple structural interpretation to highlight the differences.

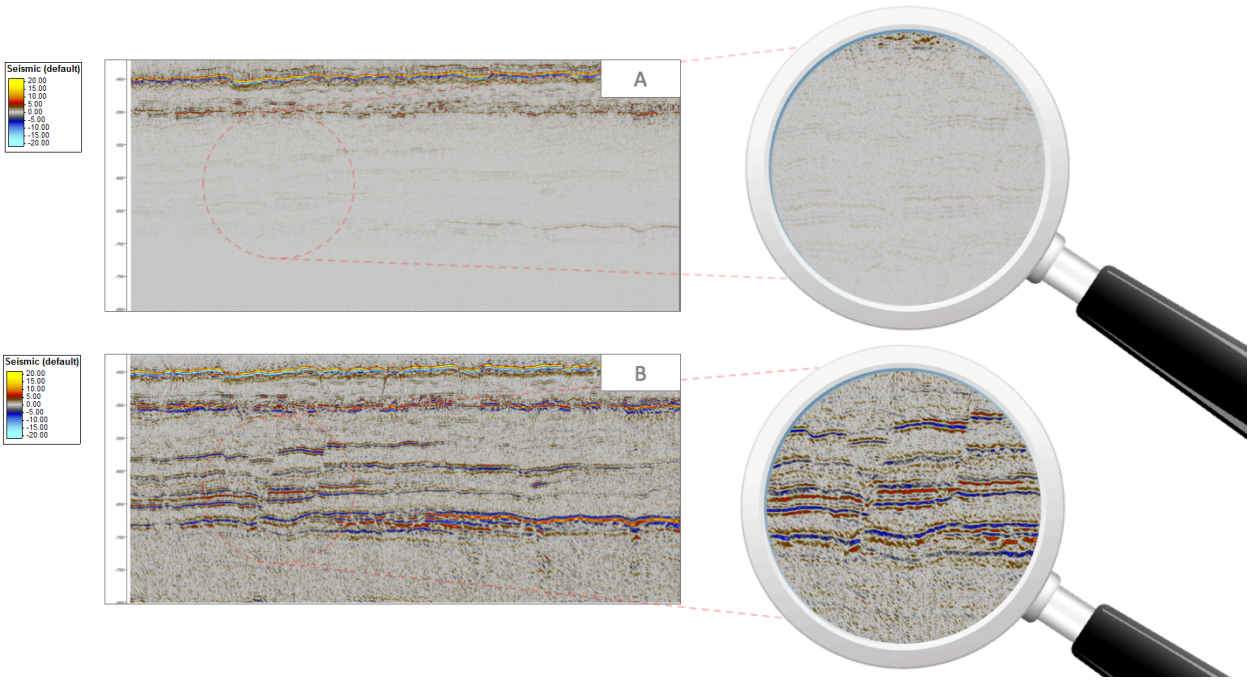

Figure 98 – Comparison of Stolt migrated with (A), and without (B) automatic gain control. Inline 199, 6,25 x 6.25 bin size, x=2.85 km and y= [300,800] ms (TWT) with an increment of 100 ms.

The seismic section in Figure 99 shows the results after applying brute stack, F-XY deconvolution, missing data interpolation, automatic gain control, Stolt migrated and finally noise suppression in Noise expression. It displays well defined and continuous representation of the seafloor with structures similar to iceberg plough-marks, but more discontinuous further below as seen in a black circle. There is also noise above the seafloor, which is a migration artifact. The resolution seems to be of higher magnitude than in the results of prestack time migrated after automatic gain control (100 ms RMS scalar) in Figure 99. However, the results in Figure 100 show a more continuous representation of reflectors in the interval between 550 to 800 ms, with less diffraction seen as full and half hyperbolas in Figure 99. Consequently, the image in Figure 100 includes less sharply defined discontinuities, which would likely result in a different structural interpretation compared to Figure 99. Moreover, there is less noise, such as bursts related to the Quaternary glaciogenic sediments, above URU in Figure 100, but more continuous and sharply defined URU compared to in Figure 99.

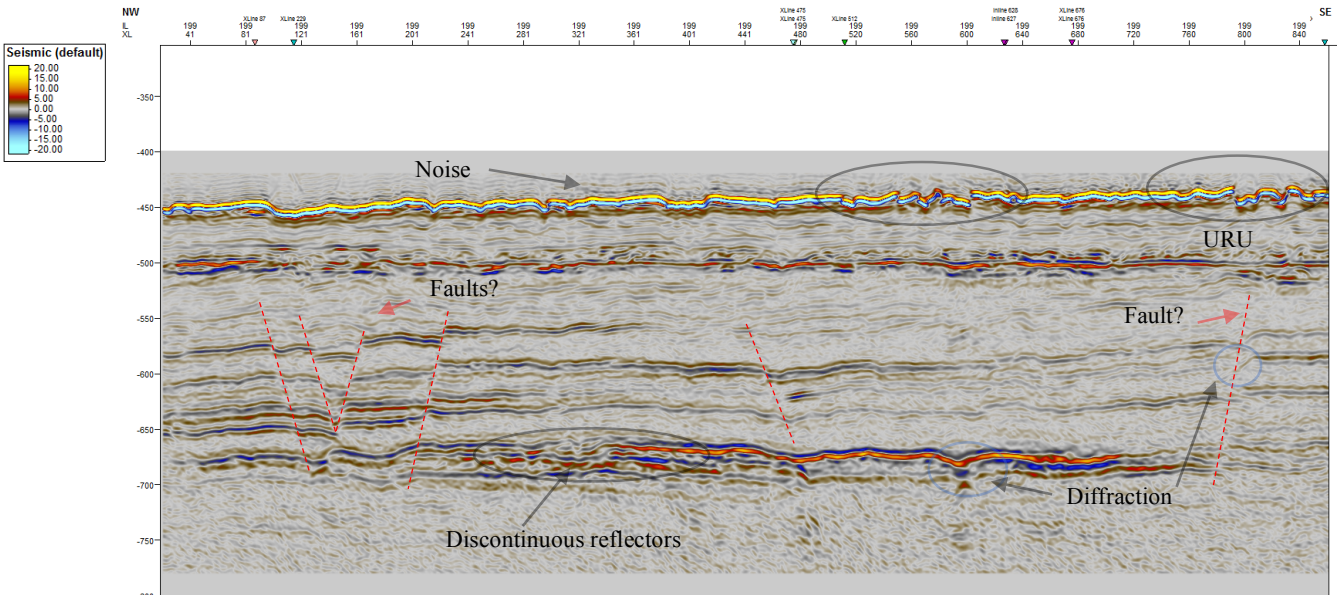

Figure 99 - Seismic section as result of Stolt migrated poststack F-XY deconvolution, Automatic gain control. Missing data interpolation, Noise expression (2 stage), in line 199, 6,25 x 6.25 bin size, x=2.85 km and y= [300,800] ms (TWT) with an increment of 100 ms. Noise, diffractions, and a simple interpretation are highlighted in this section.

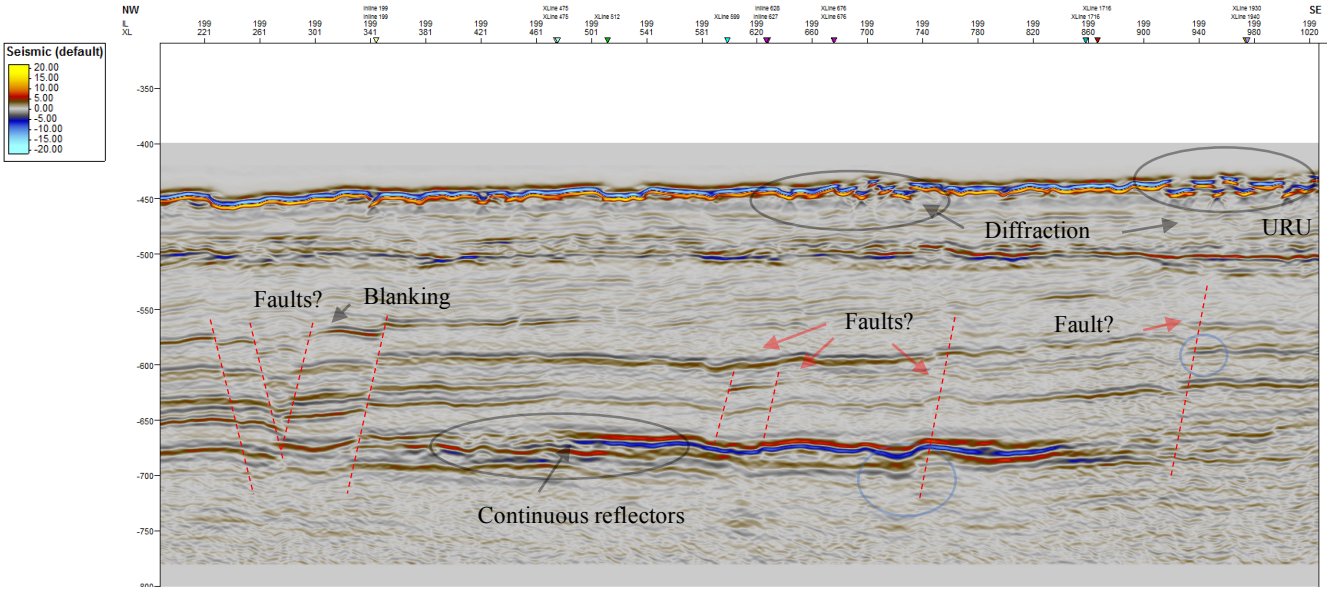

Figure 100 – Seismic section as result of prestack time migration using Madagascar, Automatic gain control (RMS), Noise expression (2 stage), in line 199, 6,25 x 6.25 bin size, x=2.85 km and y= [300, 800] ms (TWT) with an increment of 100 ms. Noise, diffractions, and a simple interpretation are highlighted in this section.

It may seem that Stolt migration is representing the morphology at Snøhvit with a higher degree of artifacts, and higher resolution, while the prestack time migration shows a lower number of artifacts, an image with higher coherence, and consequently displaying lower resolution. These differences make it more likely that interpretation of the subsurface will vary and without precise knowledge of morphology at Snøhvit, it is hard to conclude which process that presents the better imaging in the sense of displaying geological setting.

When considering the cost efficiency, prestack time migration has an advantage of fewer individual processes, even though the process that takes the longest time to finish. Stolt migration is by far the most cost-efficient migration technique, but as this is a poststack process, it depends on all the pre-migration processes, which in total take the longest time, thereby lowering cost-efficiency.

6.2 Final image of Vestnesa Ridge

The imaging of P-Cable 3D seismic data from Vestnesa Ridge has been conducted with the same aim as for the Snøhvit data, to increase the resolution, keep the cost efficiency high, and to obtain a reasonable representation of the subsurface. To obtain this results, different migration techniques was applied for various parameters, and the final results can be seen in Figure 101, 102, and 103. To determine the quality of the results, it is important to use observations to compare pros and cons.

The seismic section shown in Figure 101 was obtained by poststack Stolt Migration after F-XY deconvolution and missing data interpolation, with noise filtering by Noise Expression post migration. Figure 102 however, shows the results of prestack time migration and noise filtering by Noise Expression in GeoTeric software. By comparing these results, worth noting is that there is more acoustic blanking and consequently fewer details within the gas chimneys in Figure 102. However, there are more migration smiles possibly related to its higher number of bursts in Figure 101 compared to 102. Both sections show pull-up effect within the chimney structures, while the Stolt migrated section is the only one that also shows reflectors affected by the push-down effect. The amplitude response (reflections) in Figure 101 shows better lateral continuity with the stronger signature of the BSR. This figure also show improved quality in displaying the geological records in the vertical domain, seen as regressive surface as pinch out structures, highlighted by the red circle.

The choice of migration method can significantly impact the imaging result, even if the input data and velocity model are the same. Overall the image obtained with Stolt migration has a higher resolution, better lateral continuity and is also cleaner. This can be clearly seen when comparing Figures 101 and 102. However, it is not clear which image better represents the true geological setting. Both images have artifacts in the form of pull-ups across the seismic chimneys and blanking effects over some areas (see, for example, the top right corner in Figure 102). These migration artifacts can be easily misinterpreted as false structures. One example of an artifact that can be mistaken for a real geological feature is shown in Figure 103, where the seismic chimney shows a pull-up effect. This pull up is not real, but it is a mere artifact of migration. In this case, this artifact appears in both images, however, it is exacerbated in the Stolt migration.

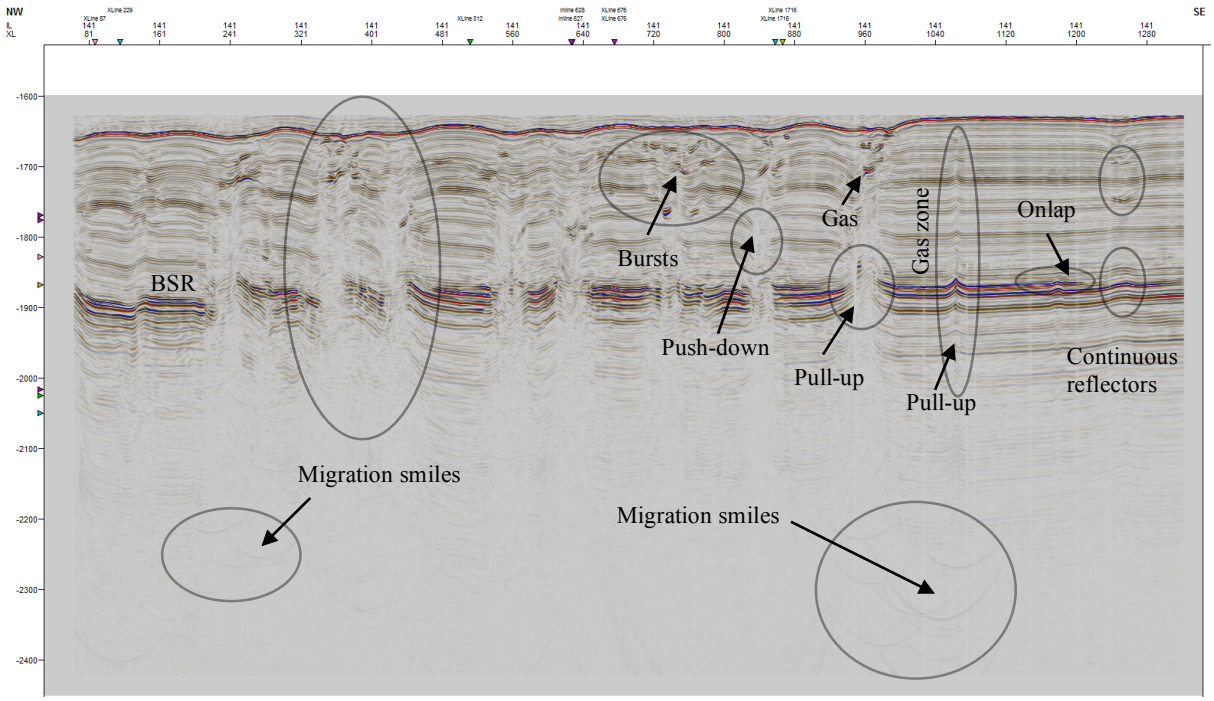

Figure 101 - Seismic section of filtered Stolt migrated data by noise expression; random noise and aggressive noise attenuation. Inline 141, bin size 6.25 x 6.25, x = 8.44 km and y = [1600,2450] ms (TWT) with an increment of 100 ms.

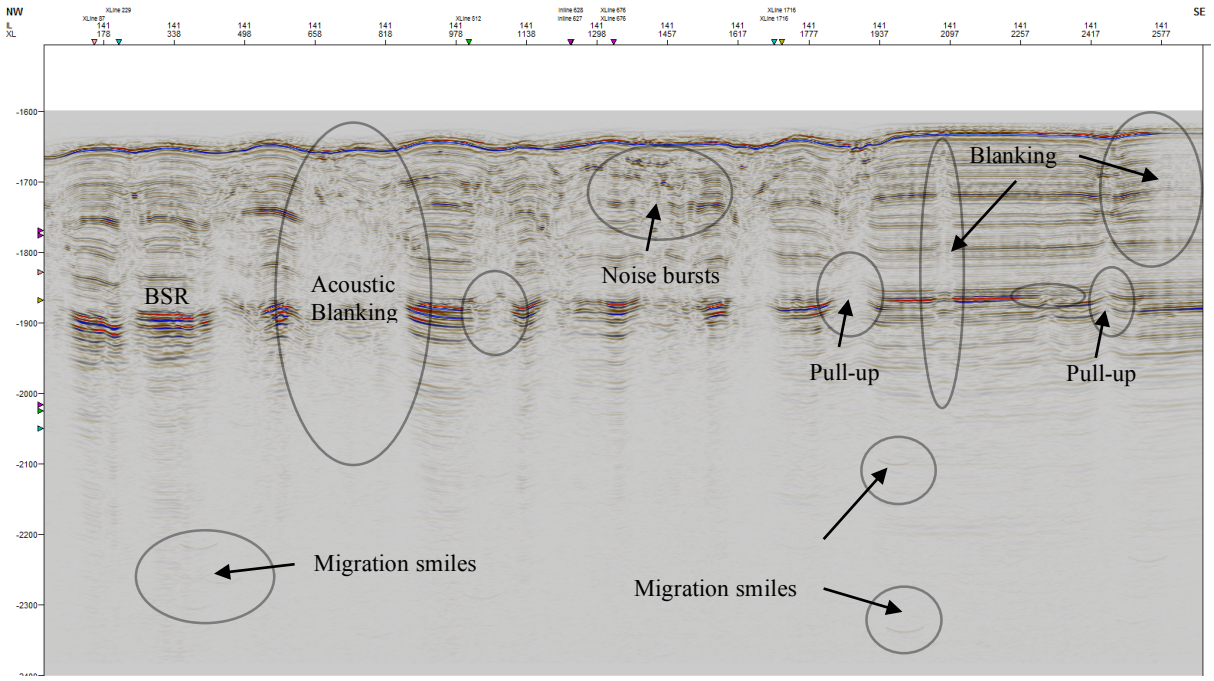

Figure 102 - Seismic section of filtered prestack time migrated data by noise expression; random noise and aggressive noise attenuation. Inline 167, bin size 6.25 x 6.25, x = 8.44 km and y = [1600,2450] ms (TWT) with an increment of 100 ms.

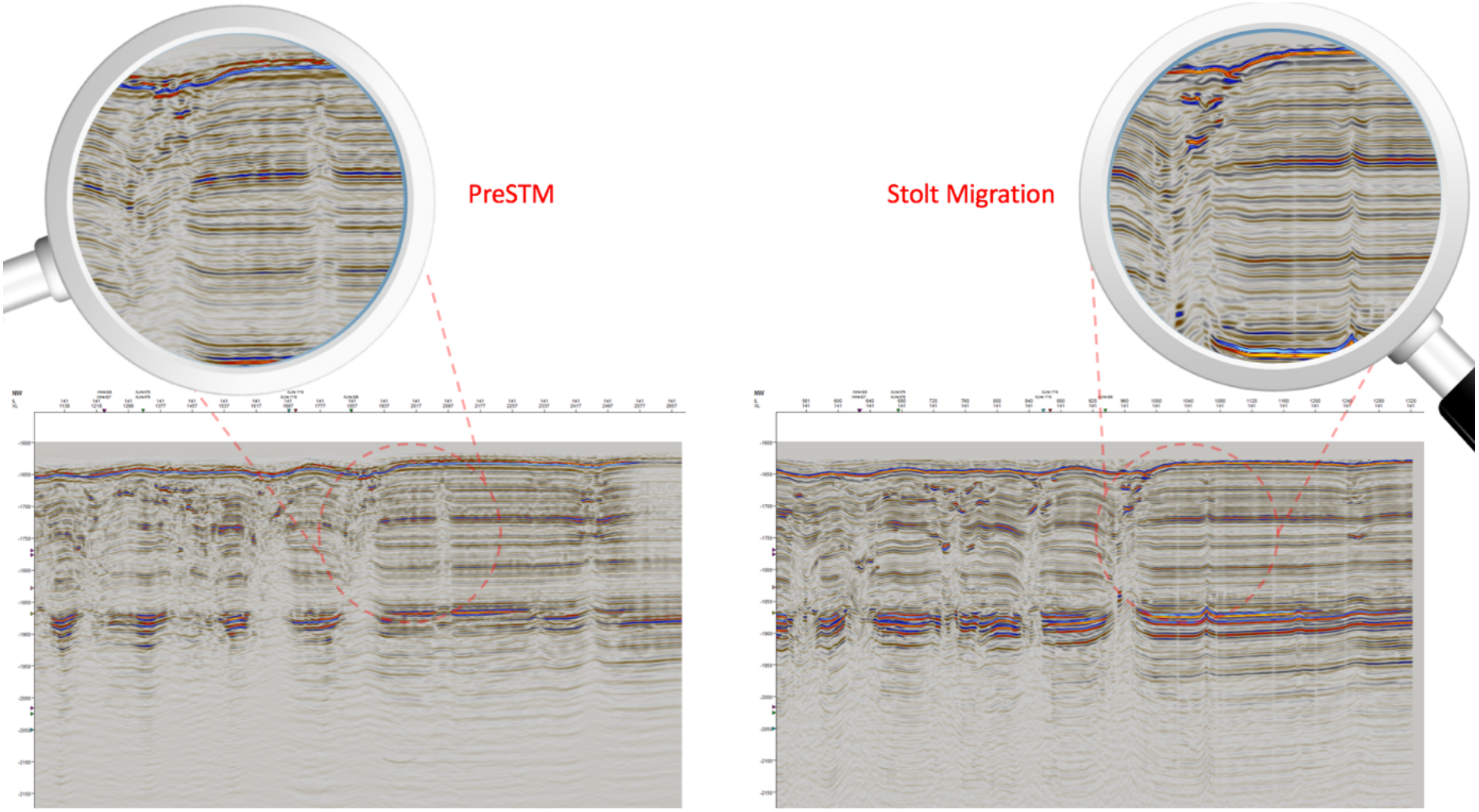

Figure 103 - Comparison of Stolt migrated, noise filtered (TDiffusion and SO filter) section (A), inline 141, bin size of 6.25 x 6.25 m, x = 8.44 km and y = [1600,2400] ms (TWT) with an increment of 100 ms.

As the Snøhvit seismic data had to be corrected by the automatic gain control to improve structural imaging, Vestnesa Ridge did not need the same. Although, AGC was also tested on Vestnesa Ridge data, and the result of Stolt migration with AGC (operator length of 100 ms, mean scalar) can be seen in Figure 104, part B. This was done mainly to see if valuable information could be obtained, by comparing the results one can clearly see that more details of the deeper part are obtained (marked by red arrows). However, wheter this adds value and represent the actual morphology is up for discussion.

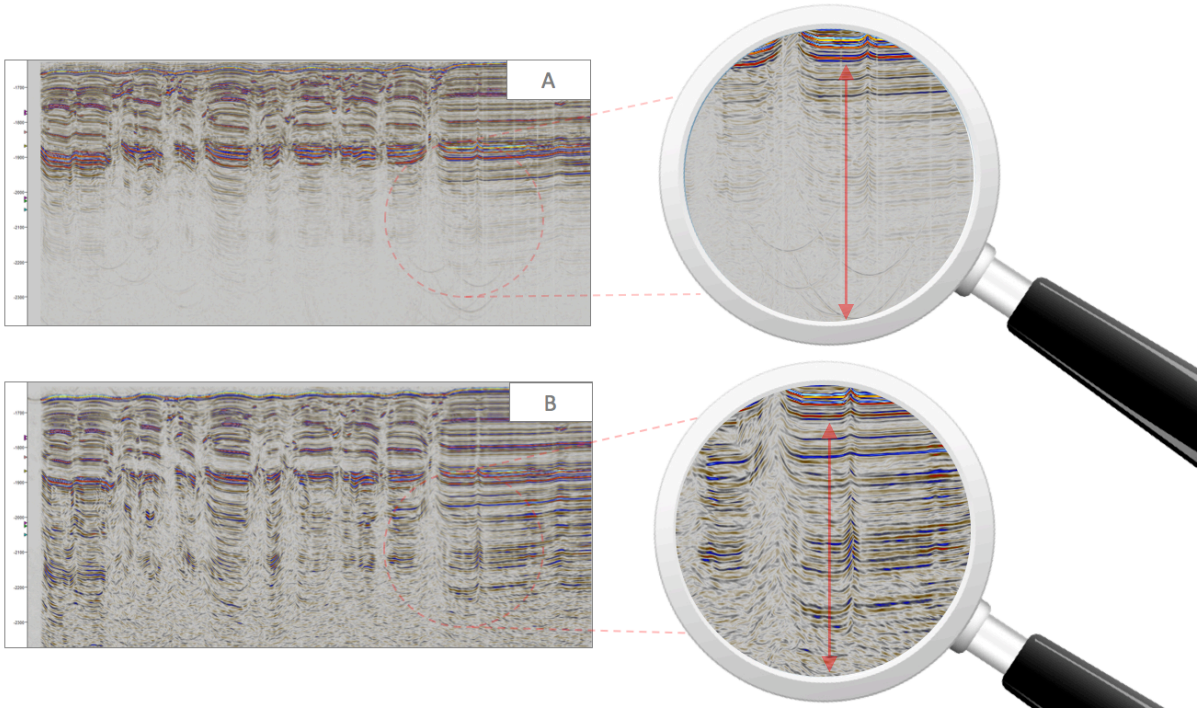

Figure 104 - Comparison of Stolt migrated, noise filtered (TDiffusion and SO filter) section (A), with same section that is corrected with automatic gain control (B), inline 141, bin size of 6.25 x 6.25 m, x = 8.44 km and y = [1600,2400] ms (TWT) with an increment of 100 ms.

The processing cost-efficiency related to Figure 101 and 102 are not that different. The prestack time migration is by far the most costly process, using up to 24 hours, while the Stolt Migration step could be done within a couple of hours. However, the Stolt migrated data is the result of several stages, such as F-XY deconvolution and missing data interpolation, which in total made up for the time difference, consequently realizing both results with very similar cost-efficiency. With that said, the possibility of errors forcing a redo of prestack time migration would further lower the cost-efficiency considerably.

6.3 Synthetic seismic data

Based on literature (e.g. Bünz et al, 2012; Plaza-Faverola et al., 2011; Petersen et al., 2010), generation of synthetic P-cable seismic data has not been done previously. Thus, the creation of synthetic models were conducted with the aim of confirming the behavior and effect of applying different migration techniques, with or without the actual velocity field. This section will highlight and discuss the final results of Stolt migration, prestack time migration and reverse time migration on the synthetic seismic data displayed as inline 141 and 167.

The result of applying Stolt migration with a constant velocity can be seen in Figure 106, with the aim of representing the morphology and physics of the model in Figure 105 as detailed as possible. By comparing the synthetic seismic data in Figure 106, with the synthetic seismic data after prestack time migration (Figure 107), one can notice that they are quite similar with equal amounts of detail making them difficult to distinguish. However, the prestack time migrated section shows similar imaging as the real seismic data, as it displays the result with more coherency, smoothened reflector, while the Stolt migrated section include more abrupt changes capturing more resolution. Further, the seismic section in Figure 106 shows more migration artifacts as noise bursts above the seafloor and possibly diffractions.

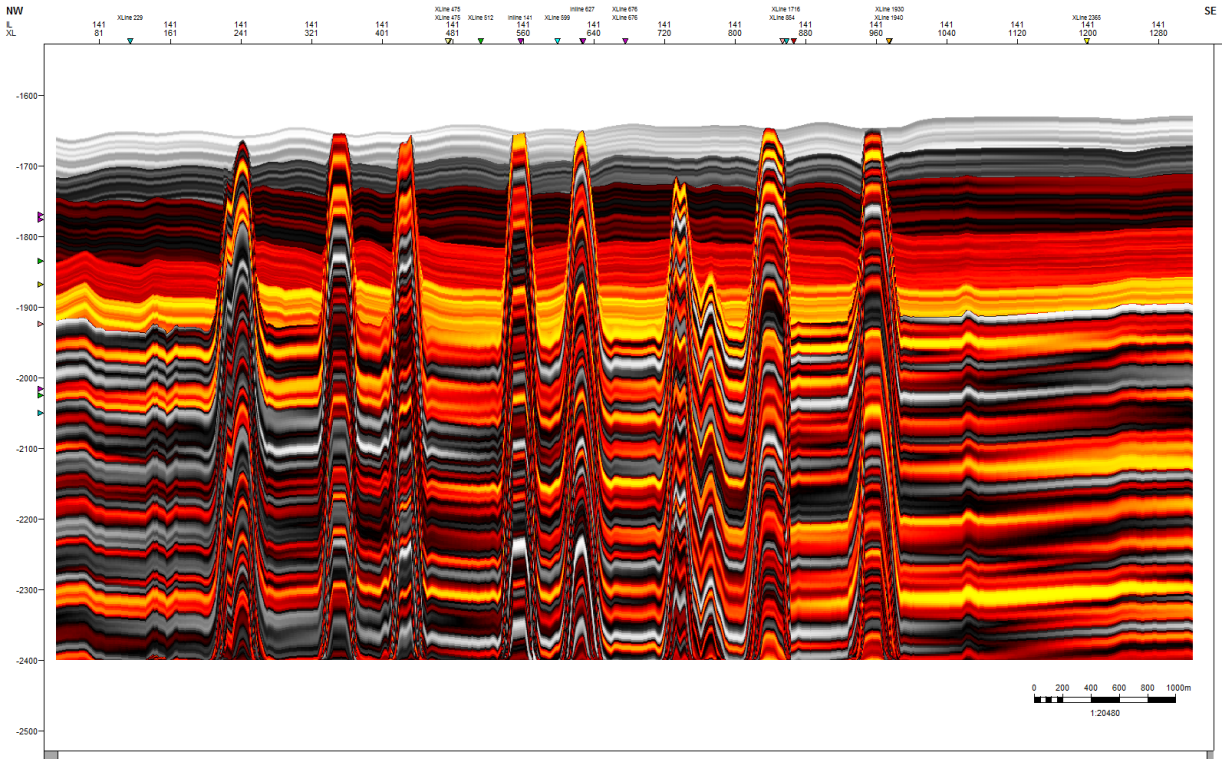

Figure 105 - 2D velocity model of 141B, with vertical and lateral velocity changes, bin size of 6.25 x 6.25, x = 8.04 km and y = [1500,2400] ms (TWT) with an increment of 100 ms.

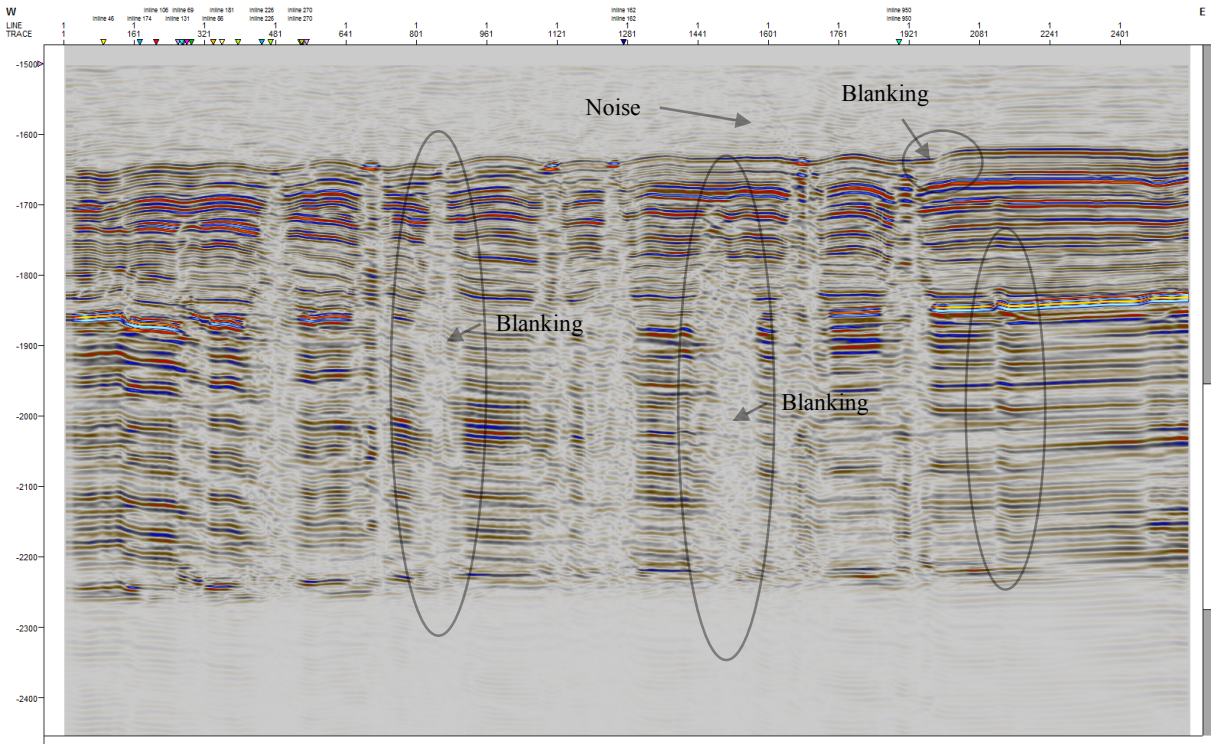

Figure 106 - Stolt migrated synthetic section inline 141, bin size: 6.25 x 6.25 m, x = 7.96 km and y = [1450,2400] ms (TWT) with an increment of 100 ms.

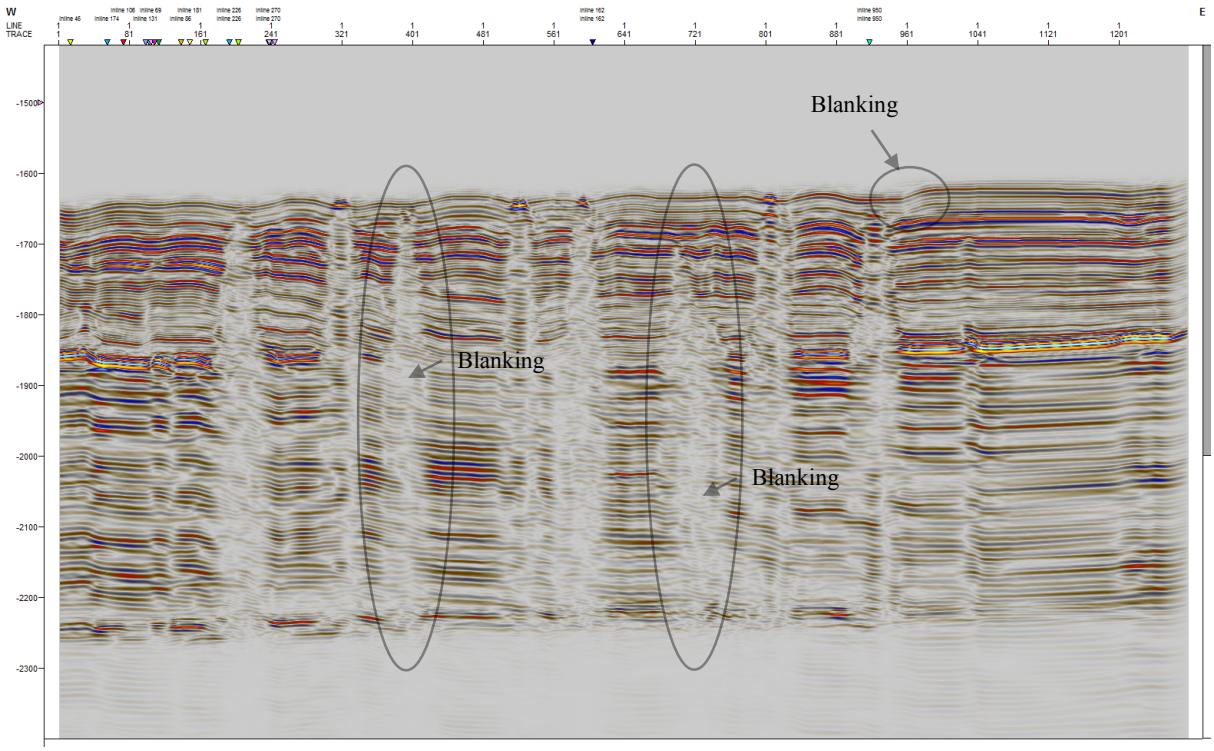

Figure 107 - Prestack time migrated synthetic section with constant velocity of 1480 m/s in ProMAX of A) Inline 141, bin size: 6.25 x 6.25 m, x = 2.34 km and y = [1400,2400] ms (TWT) with an increment of 100 ms.

The result of reverse time migration (Figure 108) correlates with the synthetic velocity model with a higher degree of accuracy, by capturing the steep angle “layers” at the edges of the chimneys and more accurately display the boundaries between the features, consequently a more precise measure of the structures and other features. However, RTM shows that it is the most sensitive migration technique to abrupt changes in the vertical domain (anticline and syncline) as is result in acoustic blanking at spots in the section, which are marked in all the Figures.

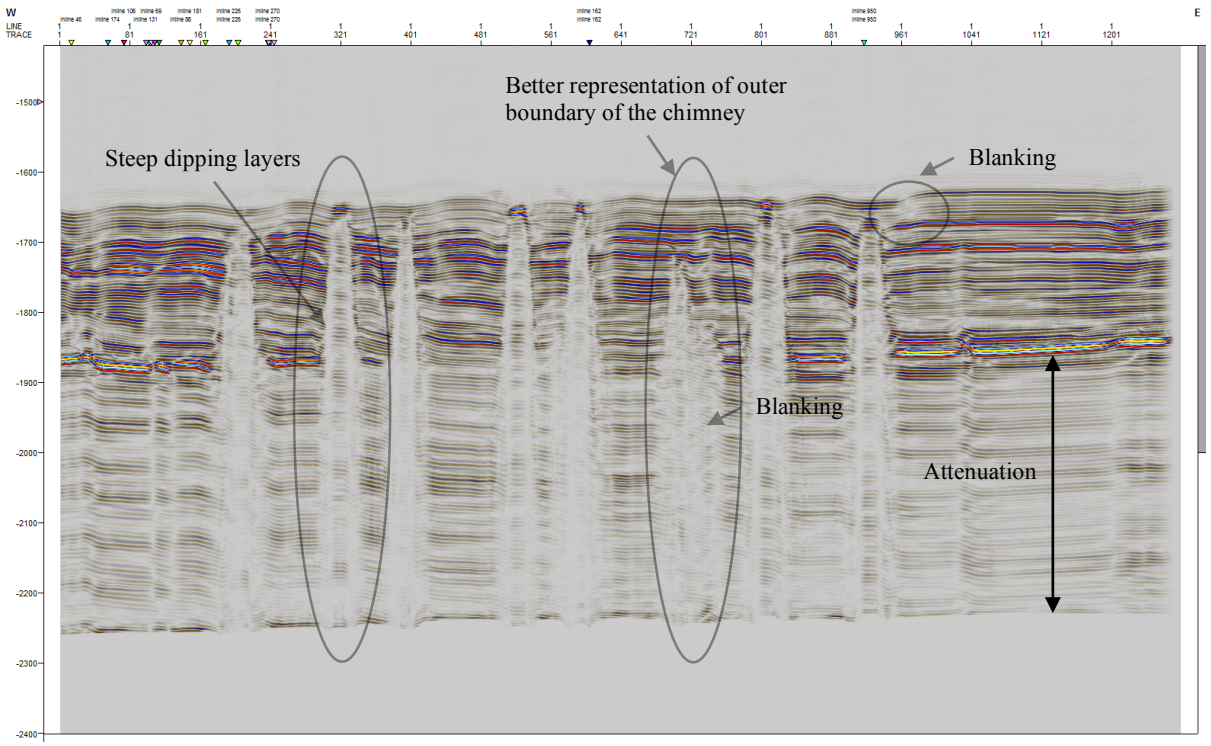

Figure 108 - Reverse time migrated synthetic section with the actual 2D velocity model in Madagascar of, inline 141, bin size: 6.25 x 6.25 m, x = 2.34 km and y = [1400,2400] ms (TWT) with an increment of 100 ms.

The following Figures: 110, 111, and 112 show the results of processing inline 167, Stolt migration, prestack time migration, and reverse time migration accordingly.

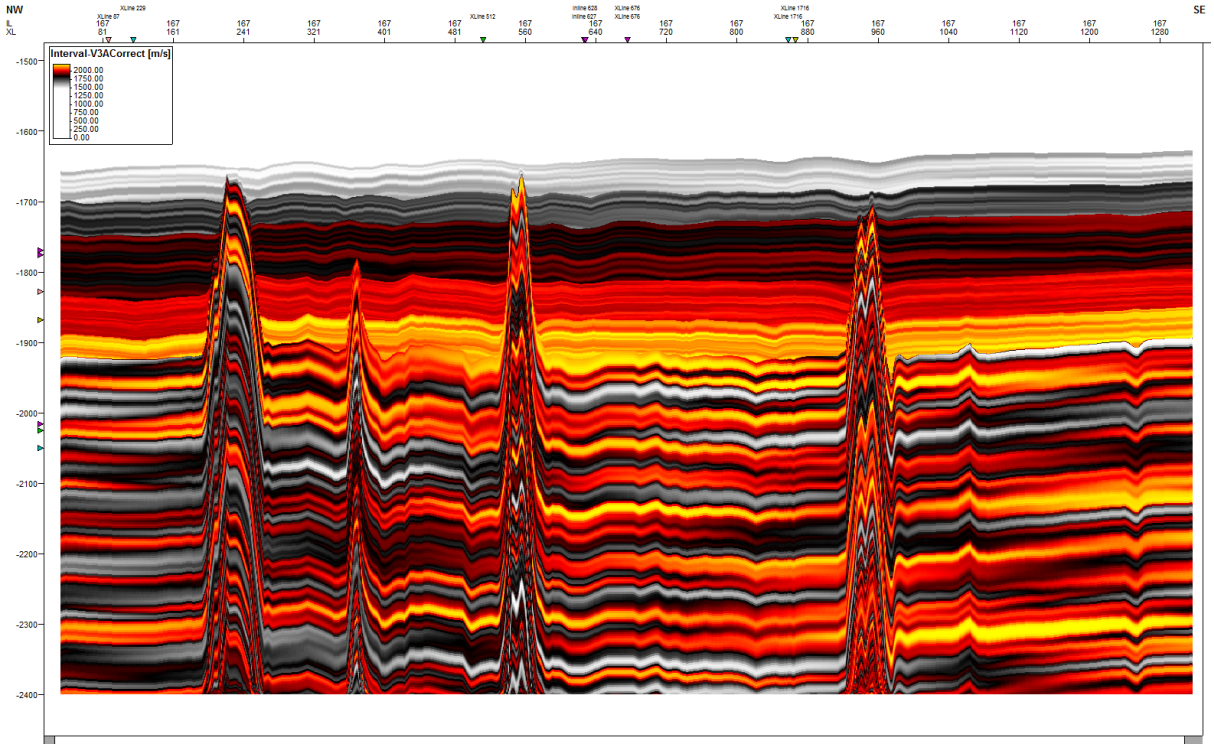

Figure 109 - 2D velocity model of 167B, with vertical and lateral velocity changes, bin size of 6.25 x 6.25, x = 8.04 km and y = [1500,2400] ms (TWT) with an increment of 100 ms.

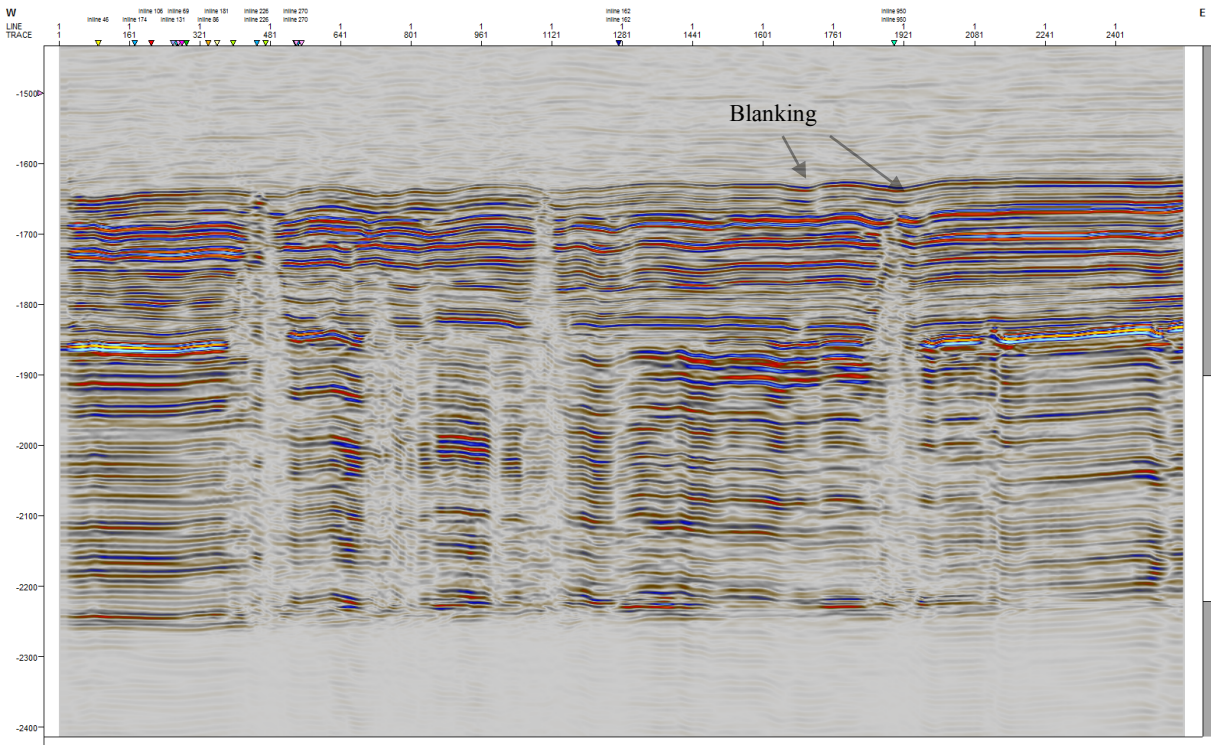

Figure 110 - Stolt migrated synthetic section inline 167, bin size: 6.25 x 6.25 m, x = 7.96 km and y = [1450,2400] ms (TWT) with an increment of 100 ms.

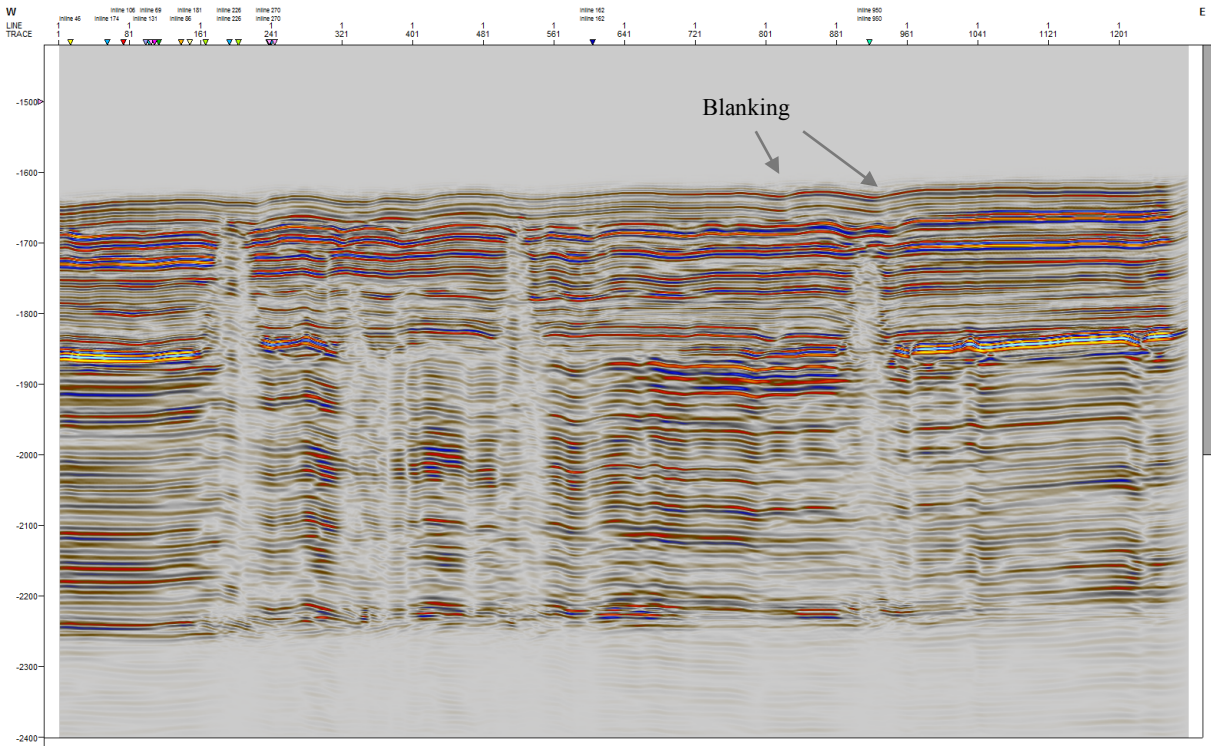

Figure 111 - Prestack time migrated synthetic section with the actual 2D RMS velocity model in Madagascar of inline 167, bin size: 6.25 x 6.25 m, x = 2.34 km and y = [1400,2400] ms (TWT) with an increment of 100 ms.

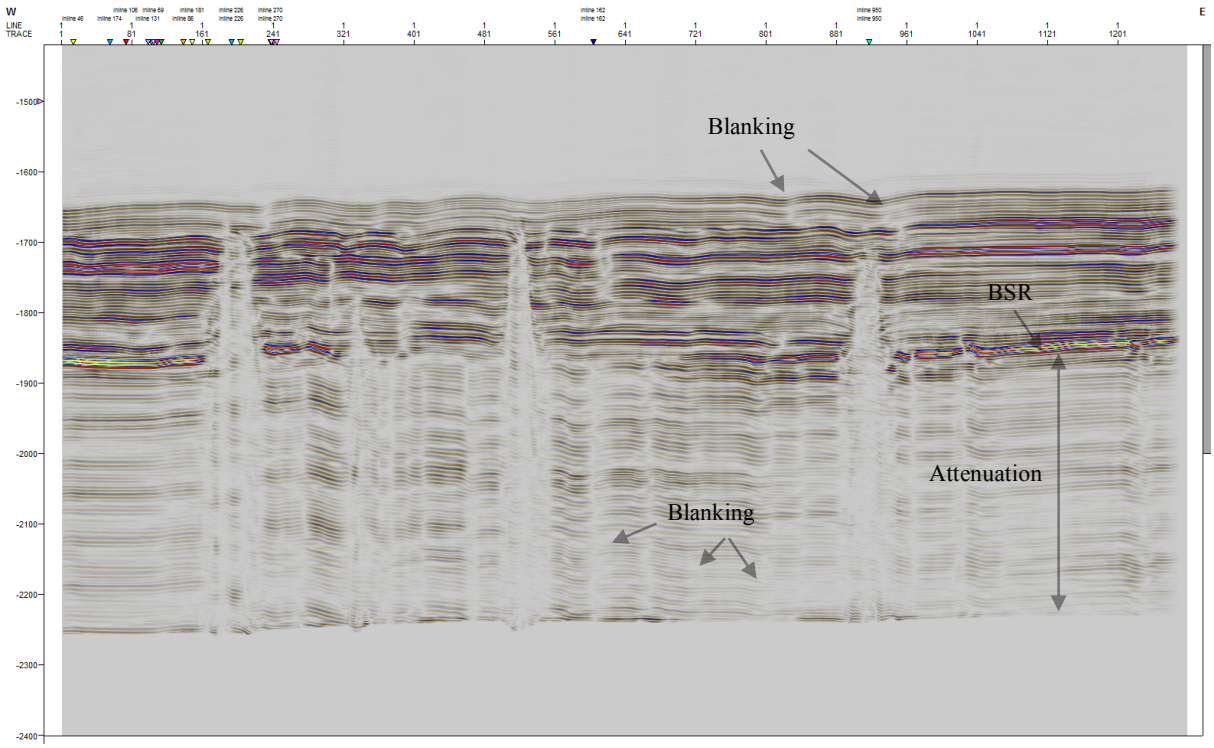

Figure 112 - Reverse time migrated synthetic section with the actual 2D RMS velocity model in Madagascar of inline 167, bin size: 6.25 x 6.25 m, x = 2.34 km and y = [1400,2400] ms (TWT) with an increment of 100 ms.

Processing of the synthetic model (Figure 108) as seen in previous Figures (109, 110, and 111) reviled that applying Stolt migration resolve higher resolution than prestack time and reverse time migration. However, in representing the actual model, the result of Stolt migration do not show as accurate structural representation as both others. The results after reverse time migration still show the best correlation with the synthetic model, even though this migration technique is the most sensitive to abrupt changes; seen as acoustic blanking, and decreasing amplitude response through depth, practically below the BSR. To make sense of the extensive acoustic blanking effect, one should keep in mind that the acquisition geometry of P-Cable system acquire data with very short offset, which means that it will only capture the ray-path with small dip (close to vertical). Consequently, small dip variation in the subsurface would change the ray spreading, which might not be recorded by small offset geometry. Migration operations, in general, does not preserve the amplitude distribution, which is evident by comparing Figure 110 and 111 with Figure 112. For structural interpretation, the result of reverse time migration might benefit from applying automatic gain control to highlight the deeper part of the seismic section.

As mentioned in the previous section, the results of prestack time migration and reverse time migration based on constant velocity versus the actual velocity model did not show any significant differences. This might indicate that P-Cable seismic data is less dependent on correct velocities when migrated, and migth relate to the acquisition geometry as the data was acquired with short offset and narrow azimuth.

The resolution associated with the results, as shown above, are after Stolt migration, prestack time and reverse time migration are not that different. They all present the geology of synthetic model sufficiently, however, the imaging of Stolt migration seems sharper, but do not correlate as well with the synthetic model as the result of prestack time migration and reverse time migration. By considering the cost-efficiency, the RTM was more expensive than Stolt migration and PSTM, running for approximately 30 minutes in the Stallo super-computer, even though they were all processed fairly quickly. The difference of applying the same processing steps on synthetic 3D seismic data would be that the processing time would increase exponentially and should therefore be picked carefully based on resolution in relation to geological reasoning.

7. Conclusions

This study was set with the aim of investigating different processing techniques for P-cable 3D seismic data, which was done by testing various approaches with the goal of constructing a workflow to enhance the seismic imaging. However, the workflow proposed has been investigated for different methods, arrangements, and parameters to clearly define the benefits and draw conclusions. Besides, the results were discussed with emphasis on aspects such as seismic resolution, geological reasoning, and cost-efficiency.

Results shown how different approaches can lead to completely different results regarding signal-to-noise ratio, resolution, overall precision in presenting accurate imaging of the subsurface, and cost-efficiency. However, this study has been partly separated into two studies, which include processing and examining of real P-Cable 3D seismic data acquired at Snøhvit field and Vestnesa Ridge, and secondly, modeling, processing and analyzing of synthetic seismic data. Compared to previous studies working with P-Cable seismic data, this project differs as it has focused on examining the behavior of different processing techniques applied to the synthetic models.

The results of processing P-Cable 3D seismic data have shown that noise filtered (Noise expression) Stolt migrated data, including pre-migration operation; brute stack, F-XY deconvolution, missing data interpolation, and automatic gain control, obtains excellent imaging with the benefit of resolving high spatial resolution and increased signal-to-noise ratio. Compared to prestack time migration, Stolt migration presented imaging of Snøhvit and Vestnesa Ridge with more continuous reflectors and resolution sufficient to confidently separate features, such as onlap and pinch out sequences. On the other hand, prestack time migration presented images of less diffraction imprint, such as migration smiles and bow-tie effect but contained more extensive acoustic blanking and noise bursts, which are most likely related to migration artifacts and short offset acquisition geometry. Automatic gain control was useful to enhance structural visualization, but not recommended for any other purposes, as it does not preserve the original nature of the amplitude response.

Initially, the aim of constructing synthetic seismic data was to resolve questions related to the impact of applying different seismic processing techniques. However, results have shown that processing of synthetic seismic data is helpful in diagnosing properties of the various

migration methods and for eliminating uncertainties related to velocity variation. To conclude, the main conclusions drawn from this study are:

1. Processing of P-Cable 3D seismic data utilizing pre-migration operation such as; brute stack, F-XY deconvolution, missing data interpolation, automatic gain control, Stolt migration and post migration noise filtering in Noise Expression gave the best imaging result regarding resolution and signal-to-noise ratio compared to prestack time migration.

2. The cost-efficiency of the processing is highly dependent on which method is utilized and the computer hardware available. As the result of Stolt migration is composed of different steps, the total cost (processing hours) is not that different to prestack time migration, even though this is assumed to be the most expensive single process. The benefits of stacking, and applying poststack processes are that they allow imaging step-by-step, which makes it easy to compare and gain knowledge of optimal parameterization.

3. Even though the result of Stolt migration obtained higher resolution than prestack time migration, it still is not enough to argue that it presents a correct representation of geological setting. Prestack time migration might introduce more acoustic blanking within areas of high-velocity variation, while Stolt migration tends to show more evident pull-up, or push down effect, of which neither represents the actual morphology. However, it is important to keep in mind that both display a simplification of the actual morphology of the subsurface. Nevertheless, events such as pull-up and push-down might be more misleading than acoustic blanking would be for a geologist that with the aim of interpreting the seismic data. Thus, it is therefore concluded that neither of the methods are perfect, but for an interpreter, one could argue that the Stolt migrated data is less accurate by highlighting nonexistent features.

4. The investigation of varying the bin size has shown that the optimal gridding parameters differ from the theoretical, idealized bin size (6.25 x 3.125 m), which is 6.25 x 6.25 m. The conclusion was based on image quality related to changes in bin size, as 6.25 x 6.25 captured similar resolution without significant noise bursts associated with the seafloor and diffractions in shallow depth.

5. By testing reverse-time and prestack time migration on the synthetic seismic data with two different velocity models, one could compare the results and the influence of computing with constant velocity versus actual velocity model. The result showed practically no changes as they displayed almost the same image, which confirms the assumption of an independent relationship between migration of P-Cable seismic data with a specific velocity field. Moreover, this implies that whether P-Cable seismic data is migrated with constant velocity or a more detailed velocity model will not add any value as the results did not show major differences. This is related to the short offset and narrow acquisition azimuth. In this case, short offset does not only limit the ability to construct a velocity model based on the seismic data, but also the dependency of migrating data with a proper velocity function.

8. Recommendation for future work

For future work, possibilities exist of reaffirming the relationship between the result of migration of P-Cable seismic data and particular velocity model. This could be done by a statistical comparison to investigate the difference by computing the correlation and dependence. It would also add value and confidence to constructing synthetic 3D seismic model of both Vestnesa Ridge and Snøhvit field to further confirm the processing behavior as presented in this project.

9. Appendices

9.1 Appendix: A - Nomenclature

NMO: Normal moveout

URU: Upper Regional Unconformity

FFID: Field file ID

NW – Northwest

SE – Southeast

RTM: Reverse time migration

PSTM: Prestack time migration

9.2 Appendix: B – Processing steps

(see separate file: Appendix B – Processing steps)

Reference list

Andreassen, K., Laberg, J.S., Vorren, T.O., 2008. Seafloor geomorphology of the SW Barents Sea and its glaci-dynamic implications. Geomorphology, 97(1): 157-177.

ArcGIS, 2017. ArcMap.

Arntsen, B., Wensaas, L., Løseth, H., Hermanrud, C., 2007. Seismic modeling of gas chimneys. Geophysics, 72(5): SM251-SM259.

Bahorich, M., Farmer, S., 1995. 3-D seismic discontinuity for faults and stratigraphic features: The coherence cube. The leading edge, 14(10): 1053-1058.

Baysal, E., Kosloff, D.D., Sherwood, J.W., 1983. Reverse time migration. Geophysics, 48(11): 1514-1524.

Berndt, C., Bünz, S., Mienert, J., 2003. Polygonal fault systems on the mid-Norwegian margin: a long-term source for fluid flow. Geological Society, London, Special Publications, 216(1): 283-290.

Bohling, G., 2005. Stochastic simulation and reservoir modeling workflow. Australian Journal of Basic and Applied Sciences, 3: 330-341.

Bratvold, R.B., Begg, S., Engineers, S.o.P., 2010. Making Good Decisions. Society of Petroleum Engineers.

Bünz, S., Polyanov, S., Vadakkepuliyambatta, S., Consolaro, C., Mienert, J., 2012. Active gas venting through hydrate-bearing sediments on the Vestnesa Ridge, offshore W-Svalbard. Marine Geology, 332-334: 189-197.

Cahill, S.V., 1992. Automatic gain control apparatus and method. Google Patents.

Canales, L.L., 1984. Random noise reduction, SEG Technical Program Expanded Abstracts 1984. Society of Exploration Geophysicists, pp. 525-527.

Cavanagh, A.J., Di Primio, R., Scheck-Wenderoth, M., Horsfield, B., 2006. Severity and timing of Cenozoic exhumation in the southwestern Barents Sea. Journal of the Geological Society, 163(5): 761-774.

Christopher, L.L., 2003. Elements of 3D Seismology, 2. PennWell, 608 pp.

Claerbout, J.F., Green, C., Green, I., 1985. Imaging the earth's interior, 6. Blackwell scientific publications Oxford.

Crane, K., Sundvor, E., Buck, R., Martinez, F., 1991. Rifting in the northern Norwegian-Greenland Sea: Thermal tests of asymmetric spreading. J. geophys. Res, 96(14): 529-14550.

Directorate, N.P., 2016. Exploration on the NCS, Exploration activity is essential if undiscovered resources are to contribute to production and create value both for the industry and for society.

Eiken, O., Hinz, K., 1993. Contourites in the Fram Strait.

Elverhøi, A., Solheim, A., Kristoffersen, Y., 1985. Physical Environment Western Barents Sea, 1: Western Barents Sea. Norsk polarinstitutt.

Engen, Ø., Faleide, J.I., Dyreng, T.K., 2008. Opening of the Fram Strait gateway: A review of plate tectonic constraints. Tectonophysics, 450(1): 51-69.

Faleide, J.I. et al., 2008. Structure and evolution of the continental margin off Norway and the Barents Sea. Episodes, 31(1): 82.

Fichtner, A., 2010. Full seismic waveform modelling and inversion. Springer Science & Business Media.

Fomel, S., 2001. Plane wave prediction in 3-D. STANFORD EXPLORATION PROJECT: 101.

Fomel, S., Clapp, R., Claerbout, J., 1997. Missing data interpolation by recursive filter preconditioning. SEP-95: Stanford Exploration Project: 15-25.

Games, K., Self, E., 2017. HRS 3D data—a fundamental change in site survey geohazard interpretation. First Break, 35(3): 39-47.

Green, P., Duddy, I., 2010. Synchronous exhumation events around the Arctic including examples from Barents Sea and Alaska North Slope, Geological Society, London, Petroleum Geology Conference series. Geological Society of London, pp. 633-644.

Gülünay, N., 2000. Noncausal spatial prediction filtering for random noise reduction on 3-D poststack data. Geophysics, 65(5): 1641-1653.

Halliburton, 2017. SeisSpace ProMAX.

Howe, J.A., Shimmield, T.M., Harland, R., Eyles, N., 2008. Late Quaternary contourites and glaciomarine sedimentation in the Fram Strait. Sedimentology, 55(1): 179-200.

Hustoft, S., Bünz, S., Mienert, J., Chand, S., 2009. Gas hydrate reservoir and active methane-venting province in sediments on< 20 Ma young oceanic crust in the Fram Strait, offshore NW-Svalbard. Earth and Planetary Science Letters, 284(1): 12-24.

Kelly, K., Ward, R., Treitel, S., Alford, R., 1976. Synthetic seismograms: A finite-difference approach. Geophysics, 41(1): 2-27.

Lavergne, M., 1989. Seismic methods. Editions OPHRYS.

Lee, O., Elghorori, A., Bisset, A., 2013. The Effect of Noise Attentuation on Data Driven Interpreter Guided Fault Analysis, SPE Middle East Oil and Gas Show and Conference. Society of Petroleum Engineers.

Liner, C.L., 2003. Elements of 3D seismology. Society of Exploration Geophysicists.

Linjordet, A., Olsen, R.G., 1992. The Jurassic Sntfhvit Gas Field, Hammerfest Basin, Offshore Northern Norway, Giant Oil and Gas Fields of the Decade 1978-1988. Memoir, pp. 349-370.

Madagascar, 2017.

Mohammedyasin, S., Lippard, S., Omosanya, K., Johansen, S., Harishidayat, D., 2016. Deep-seated faults and hydrocarbon leakage in the Snøhvit Gas Field, Hammerfest Basin, Southwestern Barents Sea. Marine and Petroleum Geology, 77: 160-178.

Ostanin, I., Anka, Z., di Primio, R., Bernal, A., 2012. Identification of a large Upper Cretaceous polygonal fault network in the Hammerfest basin: Implications on the reactivation of regional faulting and gas leakage dynamics, SW Barents Sea. Marine Geology, 332: 109-125.

Ostanin, I., Anka, Z., Primio, R.D., Bernal, A., 2013. Hydrocarbon plumbing systems above the Snøhvit gas field: Structural control and implications for thermogenic methane leakage in the Hammerfest Basin, SW Barents Sea. Marine and Petroleum Geology, 43: 127-146.

P-Cable, 2017. Technology.

Parkes, G., Hatton, L., 2013. The marine seismic source, 4. Springer Science & Business Media.

Petersen, C.J., Bünz, S., Hustoft, S., Mienert, J., Klaeschen, D., 2010. High-resolution P-Cable 3D seismic imaging of gas chimney structures in gas hydrated sediments of an Arctic sediment drift. Marine and Petroleum Geology, 27(9): 1981-1994.

Planke, S. et al., 2013. P-Cable 3D High-Resolution Seismic Site Survey Technology.

Plaza-Faverola, A. et al., 2015. Role of tectonic stress in seepage evolution along the gas hydrate-charged Vestnesa Ridge, Fram Strait. AGU Publications.

Rafaelsen, B., 2006. Seismic resolution and frequency filtering. Univ. Tromso Lecture Series, Tromso, Norway.

Rajan, A., Mienert, J., Bünz, S., 2011. Acoustic evidence for a gas migration and release system in Arctic glaciated continental margins offshore NW-Svalbard. Marine and Petroleum Geology, 32: 36-49.

Ritzmann, O. et al., 2004. A deep seismic transect from Hovgård Ridge to northwestern Svalbard across the continental-ocean transition: A sheared margin study. Geophysical Journal International, 157(2): 683-702.

Robein, E., 2010. Seismic Imaging - A review of the Technigues, their Principles, Merits and Limitations. EAGE.

Rodrigues, E., di Primio, R., Anka, Z., Stoddart, D., Horsfield, B., 2011. Leakage of hydrocarbons in a glacially influenced marine environment: Hammerfest Basin (Southwestern Barents Sea.), Geophysical Research Abstracts.

Sheriff, R.E., Geldart, L.P., 1995. Exploration seismology. Cambridge university press.

Stolt, R., 1978. Migration by Fourier transform. Geophysics, 43(1): 23-48.

Vadakkepuliyambatta, S., Hornbach, M.J., Bünz, S., Phrampus, B.J., 2015. Controls on gas hydrate system evolution in a region of active fluid flow in the SW Barents Sea. Marine and Petroleum Geology, 66: 861-872.

VBPR AS, V.B.P.R., 2017. P-Cable Data.

Weibull, W.W., 2014. Seismic Processing and Velocity Analysis Using Reverse-Time Migration.

Westbrook, G.K. et al., 2009. Escape of methane gas from the seabed along the West Spitsbergen continental margin. Geophysical Research Letters, 36(15).

Yoon, K., Shin, C., Suh, S., Lines, L.R., Hong, S., 2003. 3D reverse-time migration using the acoustic wave equation: An experience with the SEG/EAGE data set. The Leading Edge, 22(1): 38-41.